Journal of Alloys and Compounds 905 (2022) 164208

Contents lists available at ScienceDirect

Journal of Alloys and Compounds

journal homepage: www.elsevier.com/locate/jalcom

Lattice dynamics of high-pressure hydrides studied by inelastic neutron scattering

Vladimir E. Antonov[a,b,*], Vladimir K. Fedotov[a], Alexandre S. Ivanov[c], Alexander I. Kolesnikov[d], Mikhail A. Kuzovnikov[a,e], Marek Tkacz[f], Volodymyr A. Yartys[g,**]

[a] Institute of Solid State Physics RAS, Chernogolovka, 142432 Moscow, Russia
[b] National Research University Higher School of Economics, 20 Myasnitskaya ul., 101000 Moscow, Russia
[c] Institut Laue-Langevin, 71 avenue des Martyrs CS 20156, 38042 Grenoble Cedex 9, France
[d] Neutron Scattering Division, Oak Ridge National Laboratory, Oak Ridge, TN 37831, USA
[e] Centre for Science at Extreme Conditions and School of Physics and Astronomy, University of Edinburgh, Edinburgh EH9 3FD, United Kingdom
[f] Institute of Physical Chemistry PAS, 44/52 Kasprzaka, 01-224 Warsaw, Poland
[g] Institute for Energy Technology, P.O. Box 40, Kjeller NO-2027, Norway

ARTICLE INFO

Article history:
Received 21 December 2021
Received in revised form 3 February 2022
Accepted 10 February 2022
Available online 12 February 2022

Keywords:
Metal hydrides
High-pressure
Inelastic neutron scattering
Phonons
Heat capacity

ABSTRACT

Due to the small mass and anomalously large neutron scattering cross-section of proton (about 80 barns compared to a few barns for other nuclei), inelastic neutron scattering is considered as one of the most effective tools in studying optical vibrations of hydrogen atoms in metal hydrides. The current review is focused on the binary hydrides of 3d- and 4d-metals of groups VI–VIII, which were produced at high hydrogen pressures of several gigapascals in relatively large quantities of hundreds of mg, quenched to low temperature and studied by INS *ex situ* at ambient pressure with high statistical accuracy. One of the unusual effects revealed by INS is a strong increase in the strength of the metal-hydrogen interactions with decreasing atomic number of the d-metal accompanied by an increase in the Me-H distance. Based on the available experimental results, the spectra $g(E)$ of the phonon density of states and temperature dependencies $C_V(T)$ of the heat capacity at constant volume at T up to 1000 K have been derived in this paper and presented both in the figures and in digital form. This provides the reference data for the theoretical investigations of the crystal structures and compositions of new practically important hydrides giving the opportunity to validate calculation methods by comparing the calculated $g(E)$ and $C_V(T)$ with the accurate experimental dependencies for the binary hydrides. Recent INS studies showed [R.A. Klein et al., J. Alloy. Compd. 894 (2022) 162381] that the fingerprints of anomalously short H-H separations of 1.6 Å violating the "2 Å rule" can be easily and unambiguously identified in the complex INS spectra of quaternary hydrides (La,Ce)NiInH$_{1+x}$. This makes neutron spectroscopy an attractive means for obtaining valuable data in the search for novel hydrides with a record high hydrogen capacity.

1. Introduction

Inelastic neutron scattering (INS) is a powerful method in the study of atomic dynamics in metal hydrides owing to the extraordinarily large scattering cross-section of hydrogen. The neutron scattering intensity is also inversely proportional to the mass of the vibrating atom, which gives additional benefits to distinguish contributions from hydrogen with respect to any metal. Therefore, the INS spectra of metal hydrides well represent vibrations of the H atoms.

Furthermore, the INS intensity is roughly proportional to $(\boldsymbol{Q}\cdot\boldsymbol{e})^{2n}$, where $\boldsymbol{Q}$ is the momentum transfer and $\boldsymbol{e}$ is the polarisation vector of the n hydrogen vibrations created by the scattered neutron. In contrast to the inelastic light scattering, in the INS method there are no selection rules, and all modes of H vibrations are equally active. This simplifies the interpretation of the INS spectra and makes it possible to reliably derive the one-phonon scattering contribution from the spectra of powder samples and further convert it to the phonon density of states, $g(E)$, where E is the phonon energy. The "experimental" $g(E)$ spectra obtained in such a way can be directly

* Corresponding author at: Institute of Solid State Physics RAS, Chernogolovka, 142432 Moscow, Russia.
** Corresponding author.
E-mail addresses: antonov@issp.ac.ru (V.E. Antonov), volodymyr.yartys@ife.no (V.A. Yartys).

https://doi.org/10.1016/j.jallcom.2022.164208
0925-8388/

Table 1
Crystal structures and vibrational properties of some metal hydrides. The hydrides are listed in ascending order of the atomic number of the metal, that is, from left to right along the rows of the periodic table. "O" and "T" indicate H atoms occupying octahedral and tetrahedral interstices, respectively. FM = ferromagnetic; AFM = antiferromagnetic; SC = superconductor.

Phase	Metal lattice	Hydrogen coordination	Me-H distance, Å	Magnetic order/ superconductivity	Structure ref.	Fundamental INS features, meV	INS ref.
LiH	fcc a = 4.072 Å (T = 300 K)	O	2.04	no	[1]	98, 130	[2]
NaH	fcc a = 4.881 Å (T = 300 K)	O	2.44	no	[3]	77, 109	[2]
α-MgH_2	$tI2$ ($P4_2/mnm$) a = 4.501 Å c = 3.010 Å (T = 300 K)	Trigonal planar	1.95	no	[4]	Complex bands at 40–105 and 105–190 (see Fig. 1)	[5]
α-AlH_3	distorted primitive simple cubic ($R\bar{3}c$) a = 4.449 Å c = 11.804 Å (T = 300 K)	Linear bent	1.72	no	[6]	Complex bands at 60–135 and 175–265	[7]
KH	fcc a = 5.71 Å (T = 300 K)	O	2.86	no	[8]	Complex band at 58–101	[9]
CaH_2	distorted hcp ($Pnma$) a = 5.948 Å b = 3.593 Å c = 6. 801 Å (T = 298 K)	O+T	2.39 (O) 2.26 (T)	no	[10]	Complex band at 70–145	[10]
$ScH_{2.9}$	hcp a = 3.373 Å c = 6.121 Å (T = 95 K)	T + trigonal planar	2.07 (T) 1.96 (trigonal planar)	no	[11]	Complex band at 40–190	[11]
χ-$TiH_{0.71}$	distorted fcc ($Fmmm$) a = 4.34 Å b = 4.18 Å c = 4.02 Å (T = 80 K)	O	2.01	SC	[12]	75 (the lowest optical peak in the INS spectrum)	[13]
γ-TiH	distorted fcc ($Cccm$) a = 4.168 Å b = 4.234 Å c = 4.577 Å (T = 300 K)	T	1.88	no	[12]	153, 167	[14]
ε-TiH_2	distorted fcc ($I4/mmm$) a = 3.20 Å c = 4.27 Å (T = 80 K)	T	1.92	no	[15]	Bimodal peak at 139, 153	[16]
V_2H	distorted bcc ($C2/m$) a = 4.457 Å b = 3.002 Å c = 4.476 Å β = 95.6° (T = 300 K)	O	1.77	no	[17]	50, 223	[18]
$VH_{1.92}$	fcc a = 4.27 Å (T = 300 K)	T	1.85	no	[19]	165	[20]
γ-CrH	fcc a = 3.854 Å (T = 8 K)	O	1.93	no	[21]	118 (see Fig. 6a)	[21]
ε-CrH	hcp a = 2.719 Å c = 4.433 Å (T = 8 K)	O	1.92	no	[21]	122 (see Fig. 6a)	[21]
ε-$MnH_{0.86}$	hcp a = 2.692 Å c = 4.355 Å (T = 120 K)	O	1.90	AFM	[22]	112 (see Fig. 6a)	[23]
γ-$MnH_{0.41}$	fcc a = 3.776 Å (T = 300 K)	O	1.89	AFM	[24]	111 (see Fig. 6a)	[25]
α-$MnH_{0.073}$	$cI58$ ($I\bar{4}3m$) a = 8.940 Å (T = 300 K)	O	1.83	AFM	[26]	6, 73, 106, 131	[27]

(*continued on next page*)

Table 1 (*continued*)

Phase	Metal lattice	Hydrogen coordination	Me-H distance, Å	Magnetic order/ superconductivity	Structure ref.	Fundamental INS features, meV	INS ref.
ε′-FeH	dhcp a = 2.679 Å c = 8.77 Å (T = 90 K)	O	1.90	FM	[28]	103 (see Fig. 6a)	[29]
γ-CoH	fcc a = 3.712 Å (T = 95 K)	O	1.86	FM	[30]	102 (see Fig. 6a)	[30]
γ-NiH	fcc a = 3.740 Å (T = 120 K)	O	1.87	no	[31]	89 (see Fig. 6a)	[32]
RbH	fcc a = 6.05 Å (T = 300 K)	O	3.02	no	[8]	Complex band at 55–95	[9]
SrH_2	distorted hcp (*Pnma*) a = 6.371 Å b = 3.872 Å c = 7.302 Å (T = 300 K)	O+T	2.58 (O) 2.43 (T)	no	[33]	Complex band at 66–136	[34]
YH_2	fcc a = 5.205 Å (T = 300 K)	T	2.25	no	[35]	Bimodal peak at 117, 127	[36]
YH_3	distorted hcp ($P\bar{3}c1$) a = 6.358 Å c = 6.607 Å (T = 95 K)	T + trigonal planar	2.27 (T) 2.14 (trigonal planar)	no	[37]	Complex band at 40–180	[37]
γ-ZrH	distorted fcc ($P4_2/ncm$) a = 4.583 Å c = 4.945 Å (T = 300 K)	T	2.04	no	[38]	145	[39]
ε-ZrH_2	distorted fcc ($I4/mmm$) a = 3.518 Å c = 4.455 Å (T = 300 K)	T	2.08	no	[40]	Bimodal peak at 137, 143	[41]
$NbH_{0.82}$	distorted bcc (*Cccm*) a = 4.83 Å b = 3.44 Å c = 4.89 Å (T = 300 K)	T	1.92	no	[42]	119, 167	[43,44]
NbH_2	fcc a = 4.53 Å (T = 300 K)	T	1.96	no	[45]	148	[20]
ε-$MoH_{1.1}$	hcp a = 2.931 Å c = 4.745 Å (T = 100 K)	O+T	2.07 (O) 1.75 (T)	SC	[31]	114(O) (see Fig. 6b)	[46]
γ-RhH	fcc a = 4.010 Å (T = 120 K)	O	2.01	no	[31]	73 (see Fig. 6b)	[47]
γ-$PdH_{0.63}$	fcc a = 4.022 Å (T = 85 K)	O	2.01	no	[48], this paper	57.5	This paper
γ-PdH	fcc a = 4.090 Å (T = 77 K)	O	2.05	SC	[48,49]	56 (see Fig. 6b)	[50,51]
CsH	fcc a = 6.39 Å (T = 300 K)	O	3.19	no	[8]	Complex band at 52–91	[9]
BaH_2	distorted hcp (*Pnma*) a = 6. 803 Å b = 4.170 Å c = 7.860 Å (T = 300 K)	O+T	2.83 (O) 2.57 (T)	no	[52]	Complex band at 62–125	[34]
$LaH_{1.94}$	fcc a = 5.652 Å (T = 300 K)	T	2.45	no	[53]	103	[54]
LaH_3	fcc a = 5.622 Å (T = 300 K)	O+T	2.81 (O) 2.43 (T)	no	[55]	60 (O), 120 (T)	[56]
CeH_2	fcc a = 5.581 Å (T = 300 K)	T	2.42	AFM	[57]	Bimodal peak at 102, 113	[58]

(*continued on next page*)

Table 1 (*continued*)

Phase	Metal lattice	Hydrogen coordination	Me-H distance, Å	Magnetic order/ superconductivity	Structure ref.	Fundamental INS features, meV	INS ref.
$CeH_{2.72}$	fcc a = 5.549 Å (T = 300 K)	T + O	2.40 (T) 2.77 (O)	FM	[59]	65 (O), 110 (T)	[60]
$PrH_{1.94}$	fcc a = 5.518 Å (T = 298 K)	T	2.39	AFM	[61]	108	[20]
$PrH_{2.8}$	fcc a = 5.46 Å (T = 300 K)	T + O	2.36 (T) 2.73 (O)	no	[62]	64 (O), 85 (O), 130 (T)	[62]
$NdH_{2.62}$	fcc a = 5.43 Å (T = 300 K)	T + O	2.35 (T) 2.72 (O)	AFM	[62]	75 (O), 100 (O), 137 (T)	[62]
$HoH_{1.98}$	fcc a = 5.165 Å (T = 295 K)	T	2.24	AFM	[61]	126	[20]
ErH_2	fcc a = 5.129 Å (T = 298 K)	T	2.22	AFM	[61]	128	[20]
$DyH_{2.15}$	fcc a = 5.193 Å (T = 90 K)	T + O	2.25(T) 2.60 (O)	AFM	[61]	82 (O); broad bands at 117, 149 (T)	[62]
$TbH_{2.25}$	fcc a = 5.231 Å (T = 90 K)	T + O	2.27 (T) 2.62 (O)	AFM	[61]	Bimodal peak at 77, 84 (O); broad bands at 111, 146 (T)	[63]
YbH_2	distorted hcp (Pnma) a = 5.900 Å b = 3.576 Å c = 6.776 Å (T = 300 K)	O+T	2.23 (T) 2.38 (O)	no	[64]	Complex band at 70–150	[65]
$TaH_{0.89}$	distorted bcc ($P\bar{4}$) a = 4.816 Å c = 24.17 Å (T = 100 K)	T	1.91	no	[66]	129, 168	[66]
$TaH_{2.2}$	hcp a = 3.223 Å c = 5.143 Å (T = 100 K)	O+T	1.97 (O) 1.96 (T)	no	[67]	80 (O), 166 (O), 134 (T), 178 (T)	[67]
$ReH_{0.09}$	hcp a = 2.769 Å c = 4.456 Å (T = 90 K)	O	1.95	no	[68]	100, 130	[68]
ThH_2	distorted fcc ($I4/mmm$) a = 4.10 Å c = 5.03 Å (T = 300 K)	T	2.41	no	[40]	125	[69]
Th_4H_{15}	distorted bcc ($I\bar{4}3d$) a = 9.11 Å (T = 92 K)	T, trigonal planar	2.46 (T) 2.27 (trigonal planar)	SC	[70]	50–200	[69]
UH_3	A15 a = 6.643 Å (T = 10 K)	T	2.26	FM	[71]	80–155	[72]
$NpH_{2.65}$	distorted fcc ($I4/mmm$) a = 5.334 Å c = 10.64 Å (T = 90 K)	T + O	2.31 (T) 2.67 (O)	no	[73]	50–160	[73]

compared with the results of the computer calculations and are traditionally used to establish the main features of the vibrational spectra of the studied hydrides, such as the peak positions and cut-offs of the vibrational bands.

The available experimental data on the chemical composition, structure of the metal lattice and peak positions in the energy-loss INS spectrum for the binary hydrides, which have already been studied by inelastic neutron scattering, are summarized in Table 1. The compositions of the hydrides considered in the present paper are printed in bold.

The $g(E)$ spectrum derived from the INS data can also be used to calculate the contribution from lattice vibrations to the heat capacity $C_V(T)$ at constant volume and, consequently, to every thermodynamic potential value of the hydride. INS measurements are usually carried out at low temperatures. This reduces the effect of the Debye-Waller factor, $\exp(-u_H^2Q^2)$, where u_H^2 is a mean-squared displacement of the hydrogen atom, and also reduces the contribution from multiphonon neutron scattering, which rapidly grows up with increasing momentum and, correspondingly, energy transfers of the scattered neutrons, and significantly distorts the intensity distribution in the bands of optical vibrations, which is difficult to quantify accurately. Nevertheless, the $g(E)$ spectrum derived from INS measurements at low temperatures allows calculating the $C_V(T)$ dependence up to the very high temperatures, much exceeding the temperature of thermal decomposition of the hydride at ambient pressure. This is a definite advantage of applying the INS technique

to hydrides because the high-energy modes of H vibrations in hydrides make the standard Debye model inapplicable for the quantitative description and any extrapolations of their $C_V(T)$ dependences. Meanwhile, the thermodynamic properties of hydrides above the decomposition temperature are usually most interesting for constructing the *T-P* phase diagrams, which is important for the hydrogen storage applications (an overview of the production, storage, distribution and end-use of renewable energy can be found in Ref. [74]).

INS investigations of a large variety of hydrides revealed many interesting and frequently unexpected phenomena (see, *e.g.*, review papers [75–77] and references therein). At the same time, the INS spectra which are accurate enough to construct detailed spectra of phonon density of states for both acoustic and optical vibrations, have only been obtained for the densest modifications of α-AlH_3 and α-AlD_3 [7] and for the conventional α-modification of MgH_2 [5]. In the case of α-AlH_3 and α-AlD_3, the $C_V(T)$ dependences based on these $g(E)$ spectra well agreed with the experimental data at temperatures up to 320–350 K [78]. Applying the corrections converting the heat capacity C_V at constant volume to the heat capacity C_P at constant pressure, which became significant at temperatures above 400 K, the $C_P(T)$ dependencies for α-AlH_3 and α-AlD_3 were continued to T = 1000 K [78] and the dependence for α-AlH_3 was further used to calculate the equilibrium line of the Al + (3/2)H_2 = AlH_3 reaction at pressures up to 9 GPa and temperatures up to 870 K [6,79]. Here again, the calculations turned out to be in good agreement with the experiments.

A unique feature of α-MgH_2, which in vacuum decomposes to Mg and H_2 at ~550 K, is that its heat capacity has earlier been determined up to a temperature as high as 2000 K [80] using the analogy with a more thermally stable and thoroughly studied MgF_2 compound. A comparison with the results of Ref. [80] gave a rare opportunity to check the accuracy of calculations of the heat capacity of α-MgH_2 based on the INS data. The agreement between the $C_P(T)$ dependences from Refs. [5,80] was perfect and the difference between them proved to be less than 2.5% throughout the whole studied temperature interval up to 2000 K.

Thus, using neutron spectroscopy for the investigation of metal hydrides, one can obtain reliable spectra $g(E)$ of their phonon density of states. However, this requires rather large and homogeneous samples thermally stable at room temperature, like those of aluminum trihydride and magnesium dihydride, which can be prepared in any desirable quantity. The present review mostly deals with the samples of high-pressure hydrides synthesized at ISSP RAS at hydrogen pressures of up to 9 GPa and elevated temperatures in Toroid-type high-pressure chambers [81] using AlH_3 or NH_3BH_3 as an internal hydrogen source [82]. A pure hydrogen gas is obtained *in situ* by thermal decomposition of these precursors in the high-pressure chamber; the hydrogenated sample is rapidly cooled (quenched) to the liquid N_2 temperature together with the chamber; recovered from the chamber after the pressure was lowered to atmospheric pressure and further stored in liquid N_2 to prevent hydrogen loss. The samples to be measured by INS were usually prepared in a series of high-pressure synthesis runs performed under identical conditions; these samples contained from several hundred milligrams up to several grams of the material in maximum. In addition, most of the samples rapidly decomposed to the metal and H_2 gas at ambient conditions and should be mounted onto the sample holder in liquid nitrogen, and the sample and its holder often appeared to be covered with a noticeable amount of condensed ice deposited from the air while loading the sample into the helium cryostat of the neutron spectrometer.

To collect the INS spectra with a good statistical accuracy, almost all hydrides considered in this paper were measured with the high-luminosity IN1-BeF inverted geometry spectrometer installed at the hot source of the high-flux reactor at the Institute Laue-Langevin in Grenoble, France. This spectrometer combined the highest luminosity among the spectrometers operating in a wide energy-transfer range (25–450 meV) with a rather good resolution (6–8%). Most samples were ground in an agate mortar under liquid nitrogen to reduce the texture. A background from the cryostat without the sample, but with the sample holder and ice condensed on it while loading, was measured separately under the same conditions and subtracted from the experimental INS spectrum.

Regretfully, the IN1-BeF spectrometer could only be used for studying the high-energy optical part of the vibrational spectra of the hydrides. The reason was that the spectrometer worked with a monochromated beam of incoming neutrons, and the beam was slightly contaminated with neutrons of half the selected wavelength, and one-, two- and three-phonon scattering of the λ/2 neutrons gave spurious intensity at energies below the optical band. Consequently, the low-energy "lattice" part of the spectra of the studied hydrides was either measured with another neutron spectrometer or calculated using the Born-von-Kármán fit or Density Functional Theory (DFT) implemented as described in Ref. [67].

In the present paper, using the most accurate and reliable results for α-MgH_2 as an example, we will first discuss the chain of calculations and auxiliary experiments necessary to proceed from the raw INS experimental spectrum to the phonon density of states $g(E)$ and further to the $C_V(T)$ and $C_P(T)$ dependences. After that, we will consider the regularity observed in varying the energy position of the optical band along the rows of the periodic table for the hydrides of the 3d- and 4d-raw metals with H atoms occupying octahedral interstitial sites in the close-packed metal lattice. Then for each of the studied hydrides we will demonstrate harmonicity/anharmonicity of hydrogen vibrations in the second and, where possible, in the third optical bands followed from the multiphonon neutron scattering; show the phonon density of states $g(E)$ with the optical part derived from the INS experiment, and show the dependence $C_V(T)$ of the heat capacity at constant volume calculated at temperatures up to 1000 K. The obtained $g(E)$ and $C_V(T)$ dependences will also be presented in a digital form in Supplementary information. The last topic to be discussed will be the strong anisotropy and anharmonicity of the second optical band in PdH and NiH in the < 001 > directions and a possible contribution of the anharmonicity to the inverse isotope effect when considering superconductivity of PdH and $MoH_{1.1}$.

2. The INS spectrum of α-MgH_2 and the resulting $g(E)$ and $C_P(T)$ dependences [5]

A one-gram sample of α-MgH_2 powder (Sigma-Aldrich) was studied at T = 7 K in Ref. [5] with the fine energy resolution direct geometry time-of-flight neutron spectrometer SEQUOIA at the Spallation Neutron Source, Oak Ridge National Laboratory, USA. The collected neutron scattering data were first transformed from the time-of-flight and instrument coordinates to the dynamical structure factor $S(Q,E)$ shown in Fig. 1. According to the *ab initio* calculations of Ref. [83], the phonon density of states of α-MgH_2 is composed of the ranges of lattice modes at E < 40 meV and optical vibrations at 40 < E < 190 meV. Having omitted the elastic peak centered at E = 0 from the experimental $S(Q,E)$ spectrum and approximating the low energy acoustic part of phonon spectrum (E < 5 meV) by the Debye dependence $g(E) \propto E^2$, while assuming that the one-phonon part of the resulting spectrum of inelastic neutron scattering is located in the energy range 0–190 meV [83], the contribution from multiphonon neutron scattering (MPNS) was calculated in an isotropic and harmonic approximation using an iterative model-independent technique [84].

These inelastic $S(Q,E)$ spectrum and calculated MPNS spectrum were transformed to the almost spectrometer-independent, generalized vibrational densities of states according to:

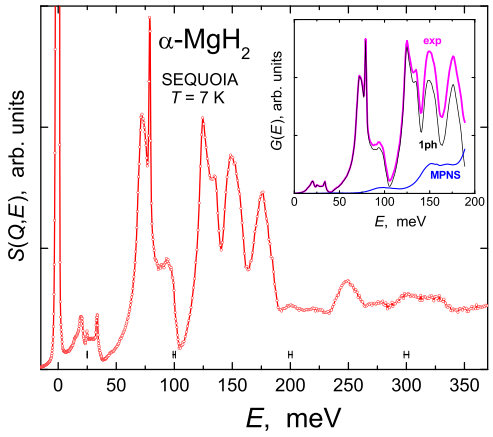

Fig. 1. [5]. The dynamical structure factor $S(Q,E)$ of the α-MgH_2 powder sample (open red circles) as a function of the energy loss ($E > 0$) or gain ($E < 0$) of the inelastically scattered neutrons measured at 7 K with the SEQUOIA spectrometer at ORNL, USA. The horizontal bars at the bottom of the figure indicate the energy resolution. In the inset, the solid magenta line labelled "exp" shows the generalized phonon density of states $G(E)$ derived from $S(Q,E)$ with the subtracted elastic peak at $E = 0$; the blue line "MPNS" represents the multiphonon contribution to $G(E)$ calculated in an isotropic harmonic approximation, and the black line "1 ph" is the one-phonon $G(E)^{1\,ph}$ spectrum of α-MgH_2 obtained from $G(E)$ by subtracting the MPNS contribution.

$$G(E) = \frac{S(Q,E)E\cdot\exp(u_H^2Q^2)}{Q^2[n(E,T)+1]}, \qquad (1)$$

where $n(E,T) = [\exp(E/k_BT) - 1]^{-1}$ was the population Bose factor and $T = 7$ K was the temperature of the sample during the INS measurement. The value of $u_H^2 = 0.019$ Å^2 was obtained as a fitting parameter while calculating the MPNS spectrum. Subtracting the multi-phonon $G(E)$ spectrum from the experimental one gave a one-phonon $G^{1\,ph}(E)$ spectrum. All three $G(E)$ spectra are shown in the inset of Fig. 1.

The $G^{1\,ph}(E)$ spectrum thus obtained was further transformed to the phonon density of states, $g(E)$, by renormalization of the integrated area under the $G(E)^{1\,ph}$ curve to 3 and $3\times2 = 6$ degrees of freedom for the lattice ($E = 0$–40 meV) and optical ($E = 40$–190 meV) modes, respectively. As seen from Fig. 2, the $g(E)$ spectrum of α-MgH_2 constructed in this way agrees with the *ab initio* calculations of Ref. [83].

The heat capacity of α-MgH_2 at constant volume was calculated as:

$$C_V(V_0,T) = R\int\left(\frac{E}{k_BT}\right)^2 g(E)n(E,T)[n(E,T)+1]\,dE, \qquad (2)$$

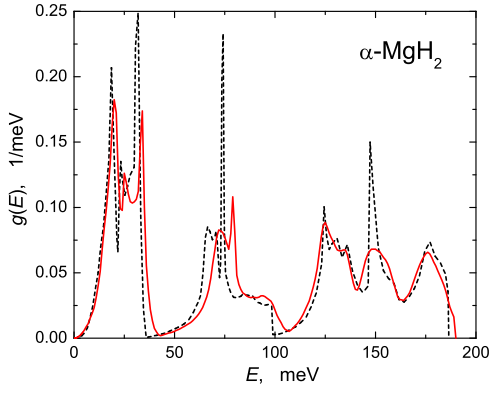

Fig. 2. [5]. The densities $g(E)$ of phonon states of α-MgH_2 obtained from the INS data (solid red curve) and calculated in Ref. [83] (dashed black curve).

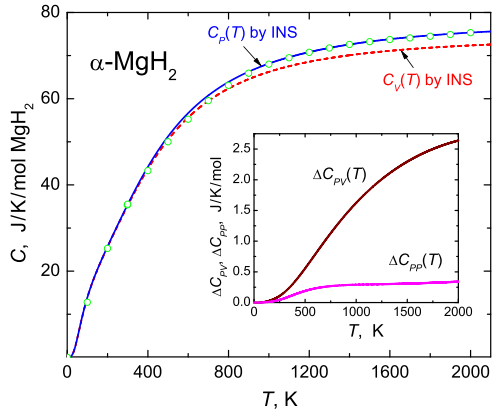

Fig. 3. [5]. The heat capacity of α-MgH_2 as a function of temperature. The open green circles show results of Ref. [80]; the dashed red curve represents the $C_V(V_0,T)$ dependence for α-MgH_2 calculated from the experimental $g(E)$ by using Eq. (2); the solid blue curve shows $C_P(T) = C_V(V_0,T) + \Delta C_{PV}(T) + \Delta C_{PP}(T)$, where $\Delta C_{PV}(T)$ is the adjustment for the difference between $C_P(T)$ and $C_V(T)$, and $\Delta C_{PP}(T)$ takes into account changes in $C_P(T)$ due to the volume expansion (see text).

where $V_0 = V$ (7 K) ≈ V(0 K) is the molar volume of α-MgH_2 at a temperature of 7 K of the INS measurement; $R = 8.314$ J·mol^{-1}K^{-1} is the universal gas constant and $k_B = 1.381\cdot10^{-23}$ J·K^{-1} is the Boltzmann constant. With the $g(E)$ spectrum normalized to 9 states in total, this equation gives $C_V(T)\xrightarrow{T\to\infty}9R = 3R\times3$ per gram-mole of α-MgH_2 in accordance with the Dulong and Petit law. The $C_V(V_0,T)$ dependence thus calculated is shown in Fig. 3 (dashed red curve) together with the available $C_P(T)$ data [80] (open green circles).

The calculated $C_V(V_0,T)$ dependence was further converted to the $C_P(V_0,T)$ dependence at constant pressure using the equation [85]:

$$\Delta C_{PV}(T) = C_P - C_V = \alpha^2TV/\beta, \qquad (3)$$

where $V(T)$ is the molar volume of α-MgH_2; $\alpha = (1/V)(\partial V/\partial T)_P$ is the coefficient of volume expansion and $\beta = -(1/V)(\partial V/\partial P)_T$ is the isothermal compressibility. The $C_P(V_0,T)$ dependence calculated using Eq. (3) was also corrected for the effect of thermal expansion using the equation

$$\Delta C_{PP}(T) \approx \frac{T(1 - V_0/V)}{\beta}\left(\frac{\partial^2V}{\partial T^2}\right)_P \qquad (4)$$

derived in Ref. [78].

The obtained $\Delta C_{PV}(T)$ and $\Delta C_{PP}(T)$ dependences are presented in the inset to Fig. 3. As one can see, $\Delta C_{PP}(T)$ is much smaller than $\Delta C_{PV}(T)$, but taken together these two corrections give the $C_P(V,T)$ dependence (solid blue curve in Fig. 3) that neatly fits the results [80] at high temperatures.

3. Features of experimental studies of high-pressure hydrides

The investigation of α-MgH_2 thus demonstrated that studies on powder samples of metal hydrides using the existing neutron spectrometers can give the phonon densities of states, which are sufficiently accurate for the calculation of the heat capacity at constant pressure (and therefore every standard thermodynamical potential) in a wide temperature interval including temperatures much exceeding the upper limit of thermal stability of the hydride at ambient pressure. Calculating the $C_P(V,T)$ dependences at very high temperatures where they significantly differ from the dependences $C_V(V,T)$, however, requires additional information on the temperature dependences of thermal expansion and compressibility (see Eqs. (3) and (4)), which are not known for most hydrides.

Besides, α-MgH_2 is a dielectric material, and its heat capacity is fully determined by the lattice vibrations, whereas the hydrides of

group VI–VIII transition metals considered in this paper are metals. The contribution $C_{el}(T) \approx \gamma T$ from the conduction electrons to the heat capacity of metals dominates at helium temperatures and remains noticeable at room and higher temperatures. Typical values of γ for transition metals and their hydrides lie in the range of 1–10 mJ/(K^{2}mol Me) [86–88], and the electronic contribution to the total heat capacity reaches 3–10% at room temperature, much exceeding the difference between the C_P and C_V. The $C_V(T)$ dependences of high-pressure hydrides calculated in the present paper do not take C_{el} into account.

Furthermore, some of the high-pressure hydrides considered in this paper are magnetically ordered. Namely, hcp-$MnH_{0.86}$ [22] and fcc-$MnH_{0.41}$ [24] are antiferromagnets, and dhcp-FeH [89] and fcc-CoH [90] are ferromagnets. The values and orientation of magnetic moments in these hydrides are determined experimentally and shown to agree with the predictions of the rigid d-band model first developed for fcc hydrides of 3d-metals and their alloys [91] and later extended to hcp hydrides [21]. However, the temperatures of the magnetic ordering of the hydrides have not yet been determined, because they are much higher than the decomposition temperatures at ambient pressure. Accordingly, it is currently impossible to estimate the magnetic contribution $C_P^{magn}(T)$ to the heat capacity of these hydrides.

One other difficulty with the analysis and use of the INS spectra of most of the high-pressure hydrides stems from the absence of an experimentally determined low-energy acoustic part of these spectra. Fortunately, the calculated MPNS spectra of these hydrides and the heat capacity at room and higher temperatures are not very sensitive to variations of the shape and other uncertainties of the calculated spectra of acoustic vibrations. For example, a replacement of the rather complicated two-peak experimental acoustic part of the INS spectrum with a Debye dependence in NiH hydride only led to very small changes in the MPNS contribution to the first optical band, and these changes became negligibly small in the energy range of the second and third bands. The changes in the heat capacity fell below 1% at 250 K and continued to decrease at higher temperatures (see Section 5.5).

Some hydrides studied by INS were having non-stoichiometric compositions and this complicated the DFT calculations of the density of states of acoustic phonons and calculation of the number of modes of acoustic and optical vibrations. To solve the problem, the DFT calculations were performed for the stoichiometric hydrides while using the experimentally determined lattice parameter(s) of the non-stoichiometric phase. The numbers of phonon modes in the hydride with the non-stoichiometric composition MeH_x were set equal to 3 for the band of acoustic vibrations and equal to 3x for the optical band. The heat capacity $C_V(T)$ of the hydride was calculated using Eq. (2) and the phonon density of states $g(E)$ composed of the acoustic part normalized to 3 states and optical part normalized to 3x states. Fig. 4 compares a value of $C_V(298\ K) = 33.2$ J/K/mol Pd calculated in such a way for PdH_x with $x = 0.63$ (see Section 5.9) with the experimental dependence $C_P(298\ K)$ *vs.* x for palladium hydrides constructed in Ref. [92]. One can observe a good agreement between the calculations and the experimental data. It should be noted, however, that the experimental errors are significantly underestimated in Ref. [92], and these errors rapidly increase when $x > 0.63$.

4. INS spectra of optical vibrations in high-pressure hydrides of 3d- and 4d-metals

Inelastic neutron scattering is one of the most direct and powerful means for studying the lattice dynamics of the metal hydrides, but this method requires the use of rather massive samples and is yet inapplicable to the investigation of microsamples of a broad variety of new high-pressure superhydrides synthesized recently in

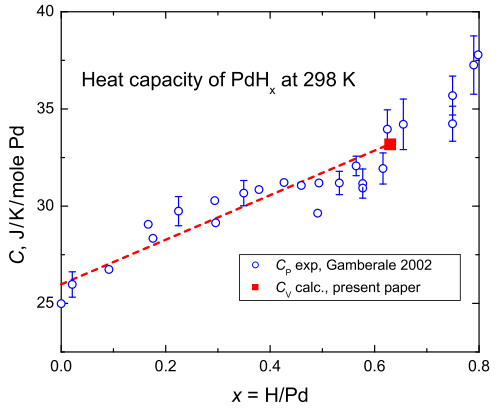

Fig. 4. The experimental values of the heat capacity C_P at constant pressure as a function of the mean hydrogen content x = H/Pd of palladium hydrides measured at 298 K [92] (open blue circles) and the value of the heat capacity C_V at constant volume and T = 298 K calculated for $PdH_{0.63}$ in the present paper (solid red square). The straight dashed line shows the heat capacity for two-phase PdH_x samples specified by the position of the calculated point at $x = 0.63$ for the miscibility region extending from $x \approx 0.01$ to $x \approx 0.63$.

diamond anvil cells at hydrogen pressures of tens of GPa. So far, INS experiments for the high-pressure hydrides have been limited to the *ex-situ* studies of metastable samples synthesized at hydrogen pressures up to 9 GPa in large-volume high-pressure chambers of the Toroid-type at the Institute of Solid State Physics RAS. Even with these chambers, the samples of the required mass of 0.2–5 g were normally collected in a series of syntheses performed at the same pressure-temperature conditions.

The technique for compressing gaseous hydrogen developed at ISSP RAS has proved to be most effective for the hydrogenation of the group VI–VIII transition metals. Except for Pd, none of these metals forms hydrides at low hydrogen pressures. Exposing a metal sample to a hydrogen pressure of up to 9 GPa was sufficient for the synthesis of hydrides of all 3d-metals and all 4d-metals, except for Ru. In particular, hydrides of Fe, Co, Mo, Tc, and Rh have been synthesized at ISSP RAS for the first time.

Neutron diffraction studies showed that hydrides of the group VI–VIII transition metals have close-packed metal sublattices with a face centered cubic (γ), hexagonal close packed (ε), or double hexagonal close packed (ε′) structure, in which hydrogen atoms occupy octahedral interstitial positions (see review [93] and experimental reports published later [21,30]). These metal lattices with octahedral interstices and, for comparison, with alternative tetrahedral interstitial sites are schematically shown in Fig. 5. The hydrides are all metals and most of them have a broad range of H/Me compositions. The full occupancy of octahedral positions in the γ, ε and ε′

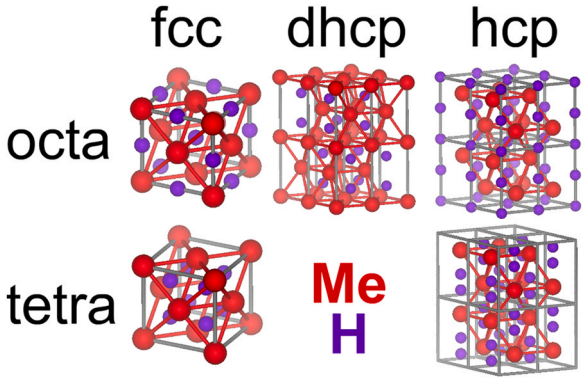

Fig. 5. Close-packed lattices of metal atoms (red circles) and interstices (smaller lilac circles) of octahedral (upper row) and tetrahedral (bottom row) types.

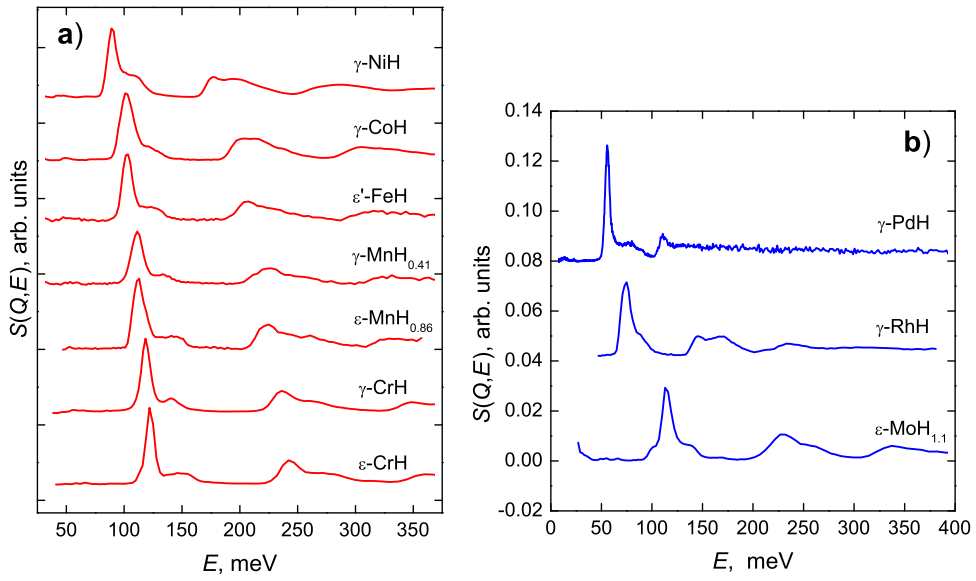

Fig. 6. The dynamical structure factor $S(Q,E)$ as a function of the energy loss E of the inelastically scattered neutrons for monohydrides of 3d-metals (a) and 4d-metals (b): ε-CrH [21], γ-CrH [21], γ-$MnH_{0.41}$ [25], ε-$MnH_{0.86}$ [23], ε′-FeH [94], [29], γ-CoH [30], γ-NiH [95], ε-$MoH_{1.1}$ [96], γ-RhH [47], and γ-PdH [50]. For the convenience of comparison, the curves are shifted along the y-axis.

structures corresponds to an H-to-metal atomic ratio of $x = 1$ and the full occupancy of tetrahedral sites gives $x = 2$.

Fig. 6 shows the INS spectra in the range of optical hydrogen vibrations for the hydrides of group VI–VIII transition metals studied to date. These are "raw" as-measured spectra normalized to the neutron flux at the sample after subtracting the background from the helium cryostat and sample holder. The spectrum of γ-PdH was measured at 25 K with the TFXA neutron spectrometer at ISIS, UK; other spectra were measured at 2–15 K with the IN1-BeF spectrometer at ILL, France.

As one can see from Fig. 6, all spectra appear to be similar. The first, fundamental band of optical hydrogen vibrations consists of a strong peak with a broad shoulder toward higher energies. The peak mostly results from nearly non-dispersive transverse optical modes, while the shoulder mainly arises from longitudinal optical modes, which show a significant dispersion due to the long-range repulsive H–H interaction. The second and, if observed, the third optical H band show a rather smooth intensity distribution and appear at energies approximately two and three times the energy of the fundamental band, respectively.

As one can also see from Fig. 6, the energy E_0 of the main hydrogen peak in the INS spectra of d-metal hydrides monotonically increases with decreasing atomic number of the host metal (from top to bottom in the figure). This systematic behavior of E_0 together with the similarity of the optical vibrational spectra brings a conclusion that in general the position of the main hydrogen peak in the INS spectra of d-metal hydrides with close-packed metal lattices and hydrogen in octahedral interstices does not strongly depend on the particular structure of the hydride – fcc, hcp, or dhcp. It is therefore reasonable to consider the dynamical properties of all these hydrides jointly, as a function of parameters applicable to every close-packed structure.

One such parameter is the nearest hydrogen-metal distance R. In the case of the dihydrides with a close-packed fluorite-type structure (an fcc metal lattice with hydrogen filling the tetrahedral Me_4 interstices) formed by various d-metals, rare earths and even alkali earths, the energy of the main optical hydrogen peak as a function of R well follows the dependence $E_0(R) = A{\cdot}R^{-3/2}$ [20]. As seen from Fig. 7, the available $E_0(R)$ values of the monohydrides show a quite different behavior as compared to the dihydrides. They steeply increase with R and are significantly different for 3d- and 4d-metals.

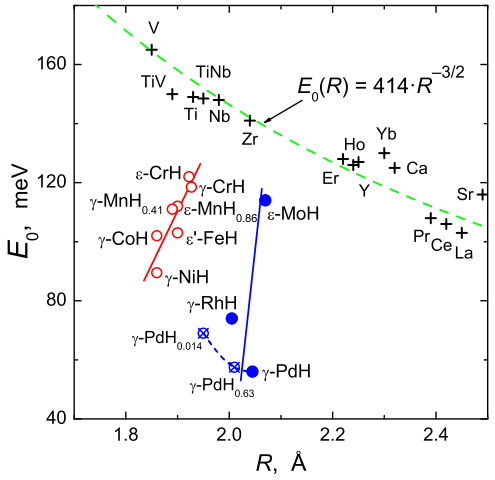

Fig. 7. The energy of the main optical hydrogen peak E_0 *vs.* the distance R between the nearest hydrogen and metal atoms for various dihydrides (crosses; H atoms fill tetrahedra M_4) [20] and for monohydrides of 3d-metals (open red circles; H atoms fill octahedra M_6) and 4d-metals (solid blue circles; H atoms fill octahedra M_6) determined in Ref. [47] from the $S(Q,E)$ dependences shown in Fig. 6. The straight solid lines are a guide for the eyes. The crossed blue circles show the data for the dilute solid solution γ-$PdH_{0.014}$ [97] and low-pressure hydride γ-$PdH_{0.63}$ (this work). The dashed green curve is a least-squares fit to the data for the dihydrides [20]; to save space, the labels indicate only hydrided metals.

The reasons for the $E_0(R) = A{\cdot}R^{-3/2}$ dependence common to all the fluorite-type dihydrides are not well understood yet. What is however clear is that the increase in R should decrease the strength of the interatomic interaction in a given hydride and should therefore decrease E_0. This is in fact observed in the γ-PdH_x solid solutions as x increases (see the dependence at the bottom of Fig. 7). The opposite behavior of $E_0(R)$ for the monohydrides of different d-metals (Fig. 7) thus indicates a significant increase in the hydrogen-metal interaction in the series of the 3d-metals Ni→Co→Fe→Mn→Cr and also of the 4d-metals Pd→Rh→Mo. This effect agrees with predictions provided by the first-principles calculations [98] that the reduction in the number of valence electrons from right to left along the transition metal rows in the periodic table should lead to a

steepening of the potential well for interstitial hydrogen due to a less efficient screening of the ionic core charges.

5. Phonon densities of states and heat capacities of individual hydrides

In this Section, each INS spectrum shown in Fig. 6 is "corrected" by replacing the spurious intensity distribution at energies below the optical band by the acoustic phonon spectrum measured separately with some other neutron spectrometer or calculated using the Born-von-Kármán fit or DFT. In a full analogy with the procedure applied to the INS spectrum of α-MgH_2 and described in Section 2, a contribution from multiphonon neutron scattering is calculated for this "corrected" INS spectrum $S(Q,E)$ and compared with the experimental distribution of scattering intensity above the optical band. Both the "corrected" $S(Q,E)$ spectrum and the calculated MPNS spectrum are then transformed to the generalized phonon density of states; the MPNS contribution is subtracted from the experimental spectrum, and the resulting one-phonon spectrum $G^{1\,ph}(E)$ is further transformed to the phonon density of states $g(E)$ by renormalizing the integrated area under the $G(E)^{1\,ph}$ curve to the number of phonon modes separately for the bands of acoustic and optical vibrations. In the stoichiometric hydrides MeH, the numbers of the acoustic and optical modes were the same and equal to 3. In the hydrides with a non-stoichiometric composition MeH_x, the number of phonon modes was set equal to 3 for the acoustic band and equal to 3x for the optical band. The contributions $C_V^{acoustic}$, C_V^{optic} and $C_V^{total} = C_V^{acoustic} + C_V^{optic}$ of lattice vibrations to the heat capacity of the hydrides are calculated by Eq. (2) using, respectively, the acoustic and optical parts of $g(E)$, and $g(E)$ as a whole. The calculated phonon densities of states and heat capacities are shown on figures and presented in digital form in the Supplementary information files.

5.1. Hcp-CrH and fcc-CrH [21]

According to the reference data, both hcp (ε) CrH [99] and fcc (γ) CrH [100] can be synthesized at high hydrogen pressures. However, later thermodynamic analysis showed [101] that the fcc phase observed in Ref. [100] using *in situ* x-ray diffraction could be not a binary CrH hydride but, most likely, was a product of a chemical reaction of chromium with some other substances present in the high-pressure cell. The spectrum of optical vibrations in a high-pressure ε-CrH sample synthesized at 2 GPa and 325 °C was studied by INS at 15 K using the IN1-BeF spectrometer at ILL [102].

Chromium hydrides with compositions close to CrH can also be produced by cathodic electrodeposition of chromium as described in Refs. [103,104]. In Ref. [21], a sample of γ-CrH and, for comparison, a sample of ε-CrH, about 1.5 g each, were prepared by cathodic electrodeposition, powdered in liquid nitrogen, and studied by neutron diffraction at 8 K using the time-of-flight DN-2 diffractometer at the Joint Institute for Nuclear Research in Dubna and by INS at 10 K using the inverted-geometry time-of-flight KDSOG-M neutron spectrometer at JINR. The optical part of the INS spectrum of γ-CrH was additionally studied at 5 K with a better statistical accuracy using the IN1-BeF spectrometer at ILL.

Neutron diffraction showed that hydrogen occupies octahedral interstitial sites in the fcc metal lattice of γ-CrH with a = 3.854(3) Å and in the hcp metal lattice of ε-CrH with a = 2.719(3) Å, c = 4.433(4) Å, and c/a = 1.630(2). No magnetic ordering was detected in either hydride at 8 K in agreement with earlier studies on nuclear magnetic resonance and magnetic susceptibility, which revealed no signs of magnetic ordering in these hydrides at temperatures down to 3 K [104]. Results of the INS investigation of the high-pressure sample of ε-CrH and of the γ-CrH sample produced electrolytically are shown in Fig. 8.

As seen from Fig. 8a, the INS spectra of ε-CrH and γ-CrH are pretty much the same and look similar to the spectra of monohydrides of all other 3d- and 4d-metals of groups VI–VIII studied so far and shown in Fig. 6. Like all those, the spectra of chromium hydrides are composed of the range of acoustic modes (E < 40 meV) and optical H vibrations (E > 90 meV). The first, fundamental band of optical H vibrations consists of a strong peak centered at E_0 ~120 meV with a shoulder towards the higher energies extending up to about 170 meV. The second and third optical H bands resulting from multiphonon neutron scattering have a smoother intensity distribution and appear at energies approximately two and three times the energy of the fundamental band, respectively.

The acoustic parts of the INS spectra of ε-CrH and γ-CrH hydrides are approximately the same because of the nearly cubic and almost coinciding arrangements of neighboring chromium atoms in the hcp modification of CrH with a c/a ratio close to the ideal value of $\sqrt{8/3}$ ≈ 1.633, and in the fcc modification. The double-peak shape of $S(Q,E)$ and $g(E)$ in the range of lattice modes clearly seen in Fig. 8a is typical of the monohydrides with close-packed metal lattices, for example, γ-PdH [50] and γ-NiH [84]. By analogy with the spectrum of γ-PdH [50], the peaks at energies of 25 and 33 meV in the spectra of chromium hydrides can be attributed to the transverse and longitudinal acoustic zone-boundary modes, respectively. A high-energy cut-off of the lattice modes is observed at approximately 38 meV.

As one can see from Fig. 8a, the contributions from multiphonon neutron scattering calculated in an isotropic and harmonic approximation add a little intensity to the shoulder of the main optical peak and fairly well describe the main features of the experimental $S(Q,E)$ spectra at energies above 180 meV. This suggests that the potential wells for hydrogen atoms in ε-CrH and γ-CrH hydrides are, on average, harmonic and isotropic at energies of up to those of the third excited states of optical H vibrations, at least.

In the phonon density of states $g(E)$ shown in Fig. 8b, the main optical peak is centered at E_0 = 122 meV for ε-CrH and at E_0 = 118 meV for γ-CrH. Both peaks have a full width at half maximum of about 9 meV, which virtually coincides with the resolution Δ ≈ 8 meV of the IN1-BeF spectrometer in this energy range (see the horizontal bars in Fig. 8a). The slightly lower E_0 value for γ-CrH can be attributed, at least partly, to the longer interatomic distances R in this hydride resulting in a weaker interatomic interaction. Specifically, $R = a/2$ = 1.927 Å for γ-CrH and $R = \sqrt{a^2/3 + c^2/16}$ = 1.922 Å for ε-CrH.

The calculated $C_V(T)$ dependences shown in Fig. 8c should fairly accurately represent the heat capacities of the ε-CrH and γ-CrH hydrides at medium and high temperatures because of the small contribution from the electronic heat capacity and as both hydrides are not magnetically ordered at temperatures down to 3 K [104].

Recently, two new chromium hydrides have been synthesized in diamond anvils and studied *in situ* by x-ray diffraction using synchrotron radiation [105]. These were Cr_2H_3 stable at hydrogen pressures from 17 to 24 GPa, and CrH_2 stable at pressures from ~28 GPa to a maximum applied pressure of 120 GPa. Following the theoretical predictions [106], Cr_2H_3 and CrH_2 were considered as ordered solid solutions of hydrogen in ε-CrH, formed by the hydrogen filling of tetrahedral interstices in the hcp chromium lattice, which underwent slight monoclinic and orthorhombic distortions, respectively.

5.2. Hcp-$MnH_{0.86}$ [23,107] and fcc-$MnH_{0.41}$ [25]

When heated at atmospheric pressure, manganese forms 4 allotropic modifications: α-Mn and β-Mn with complex cubic lattices; fcc γ-Mn and body centered cubic (bcc) δ-Mn. Phase transformations in the Mn-H system were studied at pressures up to 4.4 GPa and temperatures up to 1300 K using a quenching technique [108] and up

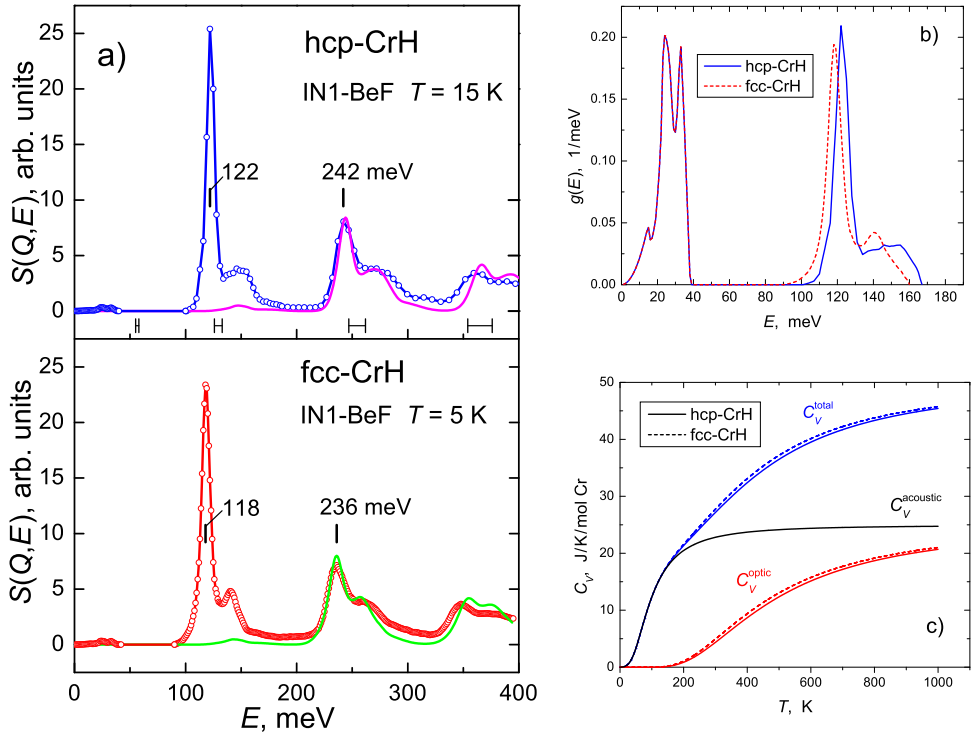

Fig. 8. (a) The "corrected" dynamical structure factor $S(Q,E)$ as a function of the energy loss E of the inelastically scattered neutrons for hcp (ε) CrH (upper panel, open blue circles) and fcc (γ) CrH (lower panel, open red circles) composed of the acoustic part (E < 40 meV) measured at T = 10 K with the KDSOG-M neutron spectrometer at JINR and the optical part (E > 90 meV) measured at T = 5 K and 15 K with the IN1-BeF neutron spectrometer at ILL [21]. The vertical bars show the centers of the experimental optical peaks. The solid magenta and green curves show the calculated multiphonon contributions for hcp-CrH and fcc-CrH, respectively. (b) The phonon densities of states $g(E)$ for hcp-CrH (solid curve) and fcc-CrH (dashed curve). (c) Heat capacities $C_V(T)$ due to the lattice vibrations in hcp-CrH (solid curve) and fcc-CrH (dashed curve).

to 8 GPa and 1300 K using *in situ* x-ray diffraction [109]. To the best of our knowledge, studies at higher pressures have not been carried out. At hydrogen pressures up to 4.4 GPa, manganese hydrides were shown to include 4 different phases: primary solid solutions α-MnH_x and β-MnH_x with x < 0.1; concentrated fcc solid solutions (hydrides) γ-MnH_x and hcp hydrides ε-MnH_x. Each of these phases is thermally stable under ambient conditions and can be handled in air. The hydrogen content was earlier shown to vary in the range 0 < x < 0.5 for the γ phase [110] and from x = 0.65–0.96 for the ε phase [111]. The temperature of transformation of the low-temperature ε hydrides to the high-temperature γ hydrides increases from ≈ 620 K at the triple point α + γ + ε at 0.7 GPa to ≈ 1120 K at 4.4 GPa [108]. Fukai et al. [109] discovered another triple point γ + ε + ε′ at approximately these T and P and found the stability field of ε′ hydride with a double hcp manganese lattice at higher pressures. Regretfully, our attempts to quench this new ε′ hydride and study it at atmospheric pressure were unsuccessful.

Neutron diffraction investigation of α-$MnH_{0.073}$ showed that the dissolved hydrogen randomly occupies interstitial positions of the 12e type (space group $I4\bar{3}m$), which form dumbbells 0.68 Å long located at the centeres of the edges and faces of the cubic unit cell of α-Mn [26]. Due to the small distance between the sites in the dumbbell, these positions cannot be occupied by hydrogen atoms at the same time due to the H···H 'blocking effect' [112], which requires that the distance between hydrogen atoms in a metal should not be less than 2 Å. The small distance of 0.68 Å between the sites in the dumbbell also results in a giant effect of hydrogen tunnelling, which is clearly visible in the inelastic neutron scattering spectra of α-$MnH_{0.073}$ even at temperatures as high as 100 K [26,113]. A description of the available experimental results and theoretical considerations describing the tunnelling effect can be found in Ref. [27].

According to the neutron diffraction data [22], hydrogen atoms in the ε-MnH_x hydrides with $x \geq 0.83$ are randomly distributed over octahedral interstices in the hcp metal lattice at T = 120 K. The hydrides are antiferromagnets with the Néel temperature of $T_N \approx 360$ K and have a layered collinear spin structure formed of ferromagnetic (110) planes coupled antiferromagnetically.

Fig. 9 shows results of an INS investigation of a powder sample of hcp-$MnH_{0.86(4)}$ with a mass of about 3 g and the lattice parameters a = 2.694(8), c = 4.357(11), and c/a = 1.617(6) at room temperature. The sample was synthesized at a hydrogen pressure of 2.6 GPa and temperature 620 K and measured at 290 K with the KDSOG-M spectrometer at JINR, Dubna [107] and at 5 K with the IN1-BeF spectrometer at ILL, Grenoble [23]. The "corrected" $S(Q,E)$ spectrum presented in Fig. 9a combines the acoustic part at neutron energy transfers E < 40 meV obtained with KDSOG-M and the optical part at E > 90 meV measured with IN1-BeF with better statistical accuracy.

As seen from Fig. 9a, the experimental intensity distribution inside the second optical band located in the energy range from 200 to 300 meV is fairly well reproduced by the spectrum of multiphonon neutron scattering (solid green curve) calculated in a harmonic and isotropic approximation. This indicates that the potential wells for H atoms in ε-$MnH_{0.86}$ are harmonic and isotropic (at least, on average) at energies equal to and somewhat higher than the energies of the second excited states of the optical H vibrations. In the phonon density of states of ε-$MnH_{0.86}$ presented in Fig. 9b, the acoustic and optical parts are normalized to 3 and 3 × 0.86 states, respectively, in accordance with the non-stoichiometric composition of the hydride. The magnetic contribution (not determined) to the temperature dependence of the heat capacity of ε-$MnH_{0.86}$ shown in Fig. 9c should increase at temperatures up to $T_N \approx 360$ K and vanish at higher temperatures.

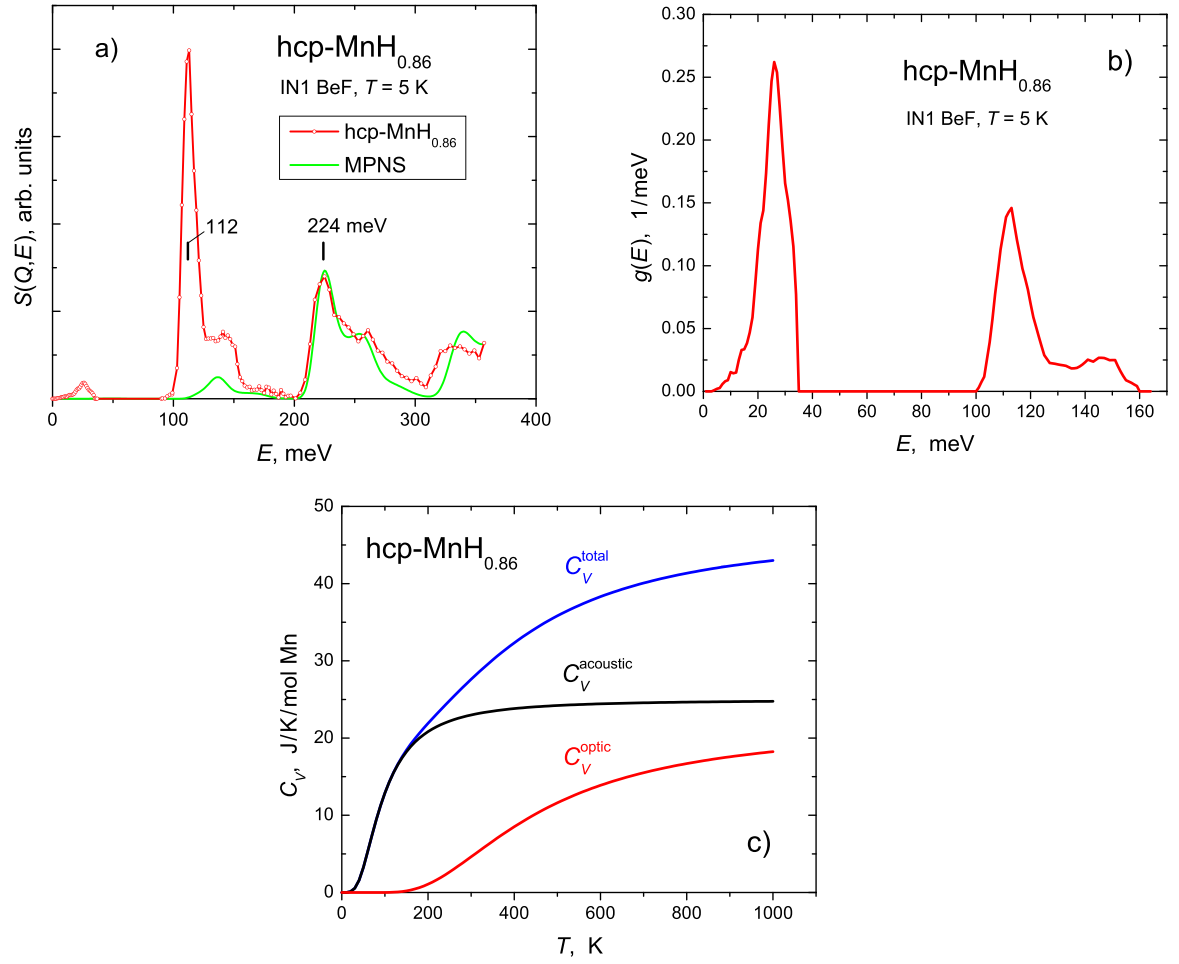

Fig. 9. (a) The "corrected" experimental INS spectrum of a powder sample of hcp-$MnH_{0.86}$ hydride (open red circles) and a contribution from MPNS (solid green curve) calculated in an isotropic and harmonic approximation [23]. The experimental spectrum is composed of the acoustic part measured at 290 K with the KDSOG-M spectrometer at JINR [107] and of the optical part at E > 90 meV measured at 5 K with the IN1-BeF spectrometer at ILL [23]. The vertical bars show the centeres of the experimental optical peaks. (b) The phonon density of states $g(E)$ for hcp-$MnH_{0.86}$ derived from the experimental INS spectra. (c) Heat capacities $C_V(T)$ due to the lattice vibrations in hcp-$MnH_{0.86}$.

According to the neutron diffraction study of a powder sample of γ-$MnH_{0.41}$ hydride performed at 300 K [24], hydrogen atoms randomly occupy octahedral interstices in its fcc metal lattice with the unit cell parameter a = 3.776 Å. The hydride is an antiferromagnet with T_N > > 300 K and a layered collinear structure formed of ferromagnetic (001) planes coupled antiferromagnetically.

Fig. 10 presents the results of an INS investigation at 2 K [25] of the same powder sample of fcc-$MnH_{0.41}$ hydride weighing 0.29 g, which was studied by neutron diffraction in Ref. [24].

Similar to the INS spectrum of hcp-$MnH_{0.86}$ (Fig. 9a), the calculated MPNS contribution fairly well describes the energy range and the distribution of scattering intensity in the second optical band of fcc-$MnH_{0.41}$ (Fig. 10a), which points to its harmonic and isotropic character. The small difference between the almost coinciding positions of the main optical peak at E_0 = 113 and 112 meV in the $S(Q,E)$ spectra of fcc-$MnH_{0.41}$ and hcp-$MnH_{0.86}$, respectively (see Fig. 7), correlates with a slightly shorter H-Mn distance R = 1.888 Å in fcc-$MnH_{0.41}$ compared with R = 1.899 Å in hcp-$MnH_{0.86}$. The acoustic and optical parts of $g(E)$ for fcc-$MnH_{0.41}$ (Fig. 10b) are normalized to 3 and 3 × 0.41 states, respectively, in accordance with the composition of the hydride. Presumably, the magnetic contribution $C_P^{magn} = T(\partial S^{magn}/\partial T)_P$ to the heat capacity $C_V^{total}(T)$ of fcc-$MnH_{0.41}$ at temperatures up to 300 K and even higher should be small because of the weak temperature dependence of $S^{magn}(T)$ due to the high Néel point T_N > > 300 K [24].

5.3. Dhcp-FeH [29,94,114]

On the T-P phase diagram of iron, the fields of the low-temperature low-pressure bcc α-Fe, low-temperature high-pressure hcp ε-Fe, and high-temperature fcc γ-Fe meet at a triple point at 9.7 GPa and 720 K [115]. At high hydrogen pressures, the hydrogen solubility in α-Fe is small and does not exceed several atomic percent [116,117]; the γ-Fe phase and hydrogen form continuous solid solutions with 0 < x < 1 [117–119], and an approximately stoichiometric hydride ε′-FeH with a double hcp metal lattice is formed instead of ε-Fe [28,120]. The stability fields of these phases join at a triple point at 5 GPa and 550 K. The temperature of the ε′↔γ transformation increases from this point to about 660 K at 6.7 GPa; the temperature hysteresis of this transformation does not exceed 15 K [116].

The formation and decomposition of the dhcp ε′ hydride are sluggish processes. For example, the α→ε′ transition at increasing pressure begins at 3.5–5 GPa, but noticeable amounts of non-reacted α-Fe were still observed in the Fe-H samples exposed to the hydrogen pressures beyond 9 GPa at temperatures up to 620 K [120,121]. The *in-situ* x-ray measurements [122] showed also that the α→ε′ transition is a complex process involving the formation of an intermediate metastable phase with an hcp (ε) metal lattice. As a rule, the transition of the ε phase to the ε′ phase is incomplete, and most ε′ samples contain a certain amount of the hcp impurity, which can be considered as a solid hydrogen solution in the high-pressure

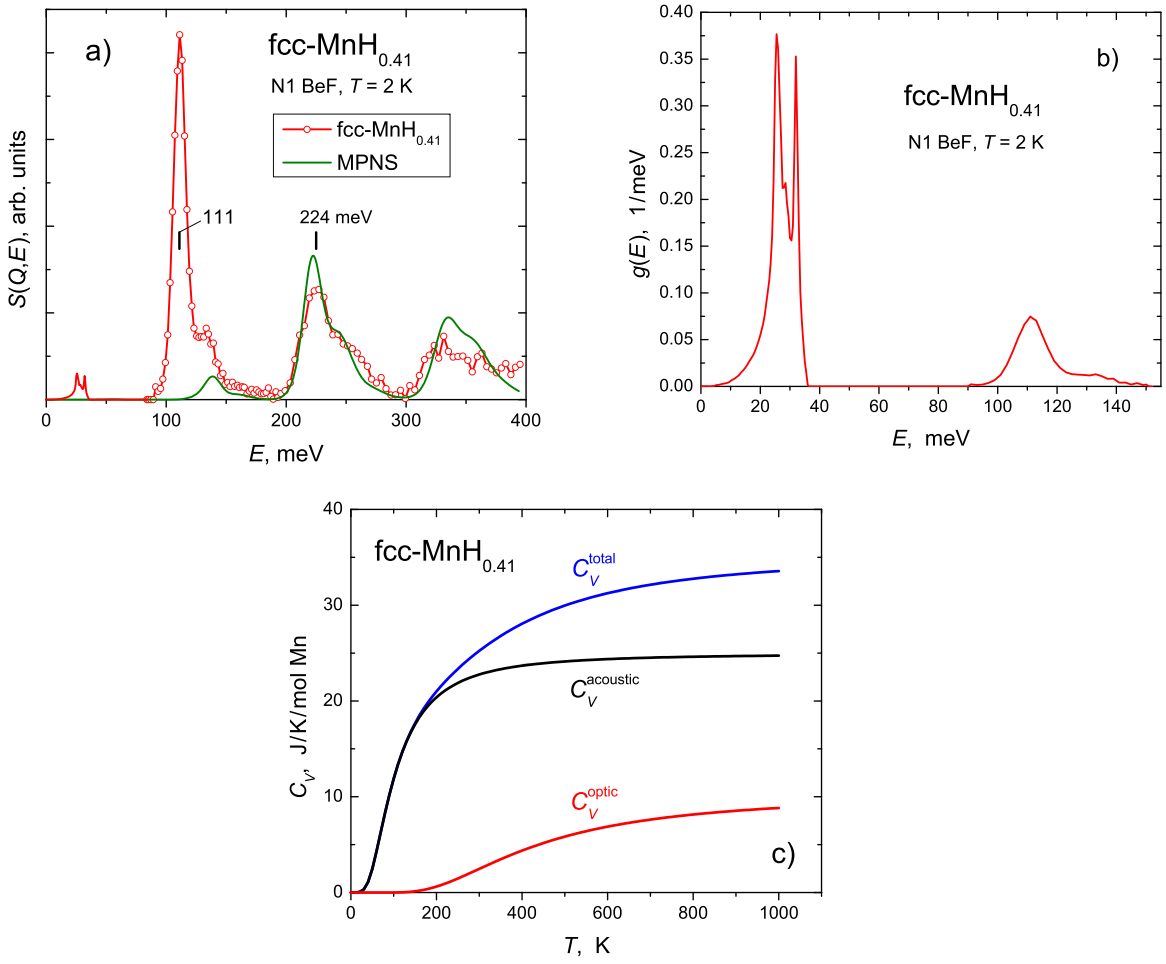

Fig. 10. (a) The "corrected" experimental spectrum $S(Q,E)$ of a powder sample of fcc-$MnH_{0.41}$ hydride (open red circles) and the MPNS contribution (solid olive curve) calculated in an isotropic and harmonic approximation [25]. The $S(Q,E)$ spectrum is composed of the acoustic part in the range of the neutron energy transfers $E < 40$ meV calculated using DFT and of the optical part at $E > 90$ meV measured at 2 K with the IN1-BeF spectrometer at ILL. The vertical bars show the centers of the experimental optical peaks. (b) The phonon density of states $g(E)$ for fcc-$MnH_{0.41}$. The acoustic part of $g(E)$ is calculated using DFT and the optical part is derived from the experimental INS spectrum. (c) Heat capacities $C_V(T)$ due to the lattice vibrations in fcc-$MnH_{0.41}$.

hcp phase of iron. One of our Fe-D samples loaded with deuterium at 9.2 GPa and 620 K proved to mostly contain the ε phase, and a neutron diffraction investigation showed [28] that the composition of this phase was $FeD_{0.42(4)}$ and deuterium randomly occupied octahedral interstitial positions in its hcp metal lattice. The dhcp crystal structure of ε′-FeH was imperfect and contained about 20% of stacking faults, as was shown by ^{57}Fe Mössbauer spectroscopy [123] and confirmed by neutron diffraction [28].

We were unable to recover any γ-FeH_x sample synthesized at high pressures and study it at atmospheric pressure, since these samples inevitably disintegrated into a mixture of the ε′-FeH and α-Fe phases upon cooling under H_2 pressure [116,119]. As a consequence, the INS investigation was only carried out for a sample of the ε′ phase [94]. The sample weighing 0.17 g was synthesized under a hydrogen pressure of 7.1 GPa and a temperature of 400 K and consisted of 0.12 mm thick hydrogenated plates of polycrystalline iron preliminarily purified by zone melting, cold rolled and finally refined in hydrogen gas at 1140 K for 100 h. To diminish the texture effects, the plates of the hydrogenated sample were broken under liquid nitrogen into pieces of around 0.5 mm across. We refrained from further comminution of the pieces because an x-ray examination showed that grinding Fe-H samples in a mortar leads to severe smearing of their diffraction lines, presumably due to the partial disordering of the stacking of close-packed layers in the dhcp ε′ hydride. The sample was examined by neutron diffraction at 90 K [28], which showed that it consisted of the dhcp hydride with $a = 2.679$ Å, $c = 8.77$ Å, and an almost ideal ratio $c/a = 2\cdot1.637 \approx 2\sqrt{8/3}$; the sample also contained several percent of unreacted α-Fe and did not contain ε hydride. Since the α-Fe phase was practically free of hydrogen, its contribution to the INS spectrum of the sample was negligibly small.

The "corrected" $S(Q,E)$ spectrum of this sample shown in Fig. 11a is composed of the optical part at $E > 80$ meV measured at 5 K by inelastic neutron scattering on the IN1-BeF spectrometer at ILL [94] and the acoustic part at $E < 40$ meV measured in a diamond anvil cell at room temperature and a hydrogen pressure of 4 GPa by nuclear resonant x-ray scattering using a sample enriched with ^{57}Fe [114]. The optical spectrum of ε′-FeH published in Ref. [94] was additionally corrected in Ref. [29] by subtracting the background from an empty helium cryostat. The acoustic and optical parts of the phonon density of states represented in Fig. 11b are normalized to 3 states each. The ε′ hydride of iron is a ferromagnet with a magnetic moment of 2.2 Bohr magneton per Fe atom and a Curie temperature of $T_C > > 80$ K [89]. At elevated temperatures, one can expect a large magnetic contribution to the vibrational heat capacity $C_V^{total}(T)$ of ε′-FeH shown in Fig. 11c.

Recent *in situ* synchrotron x-ray diffraction studies of the Fe-H system in laser-heated diamond anvil cells showed that the dhcp-FeH phase is stable at pressures up to ~67 GPa [124]. A further increase in the hydrogen pressure resulted in the formation of a

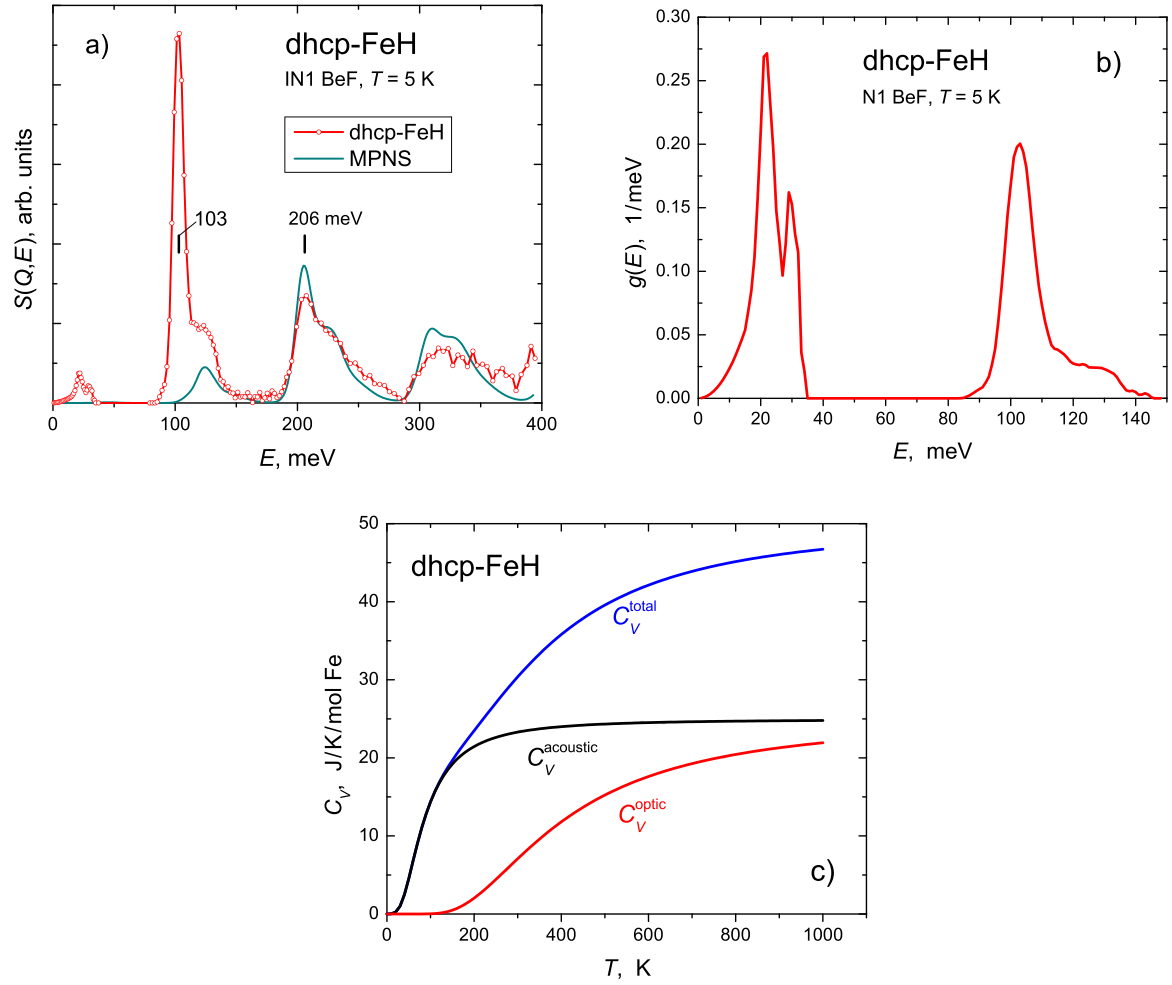

Fig. 11. (a) The "corrected" experimental spectrum $S(Q,E)$ for dhcp (ε′) hydride FeH (open red circles) and the MPNS contribution (solid dark cyan curve) calculated in an isotropic and harmonic approximation. The $S(Q,E)$ spectrum is composed of the acoustic part at E < 40 meV measured at room temperature and a hydrogen pressure of 4 GPa by nuclear resonant x-ray scattering [114] and of the optical part at E > 80 meV measured at 5 K with the IN1-BeF spectrometer [29,94]. The vertical bars show the centers of the experimental optical peaks. (b) The phonon density of states $g(E)$ for dhcp-FeH derived from the experimental vibrational spectra. (c) Heat capacities $C_V(T)$ due to the lattice vibrations in dhcp-FeH.

tetragonal FeH_2 phase at 67 GPa [124], cubic FeH_3 phase at 86 GPa [124], and a tetragonal FeH_5 phase with the same space group $I4/mmm$ as for FeH_2 at a pressure of 130 GPa [125].

5.4. Fcc-CoH [30]

When heated at atmospheric pressure, the low-temperature hcp (ε) modification of cobalt transforms to the high-temperature fcc (γ) modification at $T_\gamma \approx 720$ K, and the temperature T_γ of this transition approximately linearly increases with pressure in inert medium at a rate $dT_\gamma/dP \approx 30$–33 K/GPa [126,127]. In a hydrogen atmosphere, T_γ slightly increases at pressures up to 2.5 GPa compared to its dependence in the inert medium [127], reaches a maximum value of $T_\gamma \approx 1080$ K at a pressure of 6 GPa [128] and then drops below 520 K at 7 GPa [129]. At temperatures 500–600 K, the hydrogen solubility in the low-temperature hcp phase of cobalt monotonically increases with pressure and reaches an atomic ratio H/Co of $x \approx 0.5$ at $P = 6.5$ GPa [127]. At $P \geq 7$ GPa, the hydrogen solubility in cobalt abruptly rises to $x \approx 1$ due to the formation of a stoichiometric fcc-CoH hydride [129]. As shown in Ref. [130], the unusual shape of the T-P diagram of the Co-H system results from an isomorphic phase transformation in the metastable solid fcc solutions Co-H, which terminates at a critical point at $P \approx 5$ GPa and T < 500 K.

The hcp and fcc hydrides of cobalt are thermally stable at atmospheric pressure at temperatures below 250 K. Both cobalt and its hydrides are ferromagnets. At temperatures 80–200 K, the magnetic moments in the hcp hydrides decrease from 1.71 μ_B/atom Co at $x = 0$ to about 1.55 μ_B/atom Co at $x = 0.5$, and decreases to about 1.3 μ_B/atom Co for the fcc hydride with $x \approx 1$ [90]; μ_B is the Bohr magneton. A neutron diffraction investigation at ambient pressure and 120 K showed [131] that hydrogen atoms are randomly distributed over octahedral interstices in the hcp cobalt hydrides with $x \leq 0.26$ and form layered superstructures in the solutions with $x \geq 0.34$, occupying every third octahedral basal layer at $x = 0.34$ and every second layer at $x \geq 0.38$. No hcp cobalt hydrides have been studied by INS so far.

A powder sample of fcc-$CoH_{1.00(3)}$ weighing 0.4 g was prepared at a hydrogen pressure of 9 GPa and a temperature of 620 K and studied by neutron diffraction at ambient pressure and 95 K with the D20 and D1B neutron diffractometers at ILL and by inelastic neutron scattering at 5 K using the neutron spectrometer IN1-BeF also at ILL [30]. Neutron diffraction showed that hydrogen occupied octahedral interstitial sites in the fcc metal lattice of γ-CoH with $a = 3.7124(5)$ Å. The results of the INS investigation of the same sample of fcc-CoH are shown in Fig. 12. As seen from Fig. 12a, the calculated MPNS contribution fairly well describes the energy range and the distribution of scattering intensity in the second and third optical bands

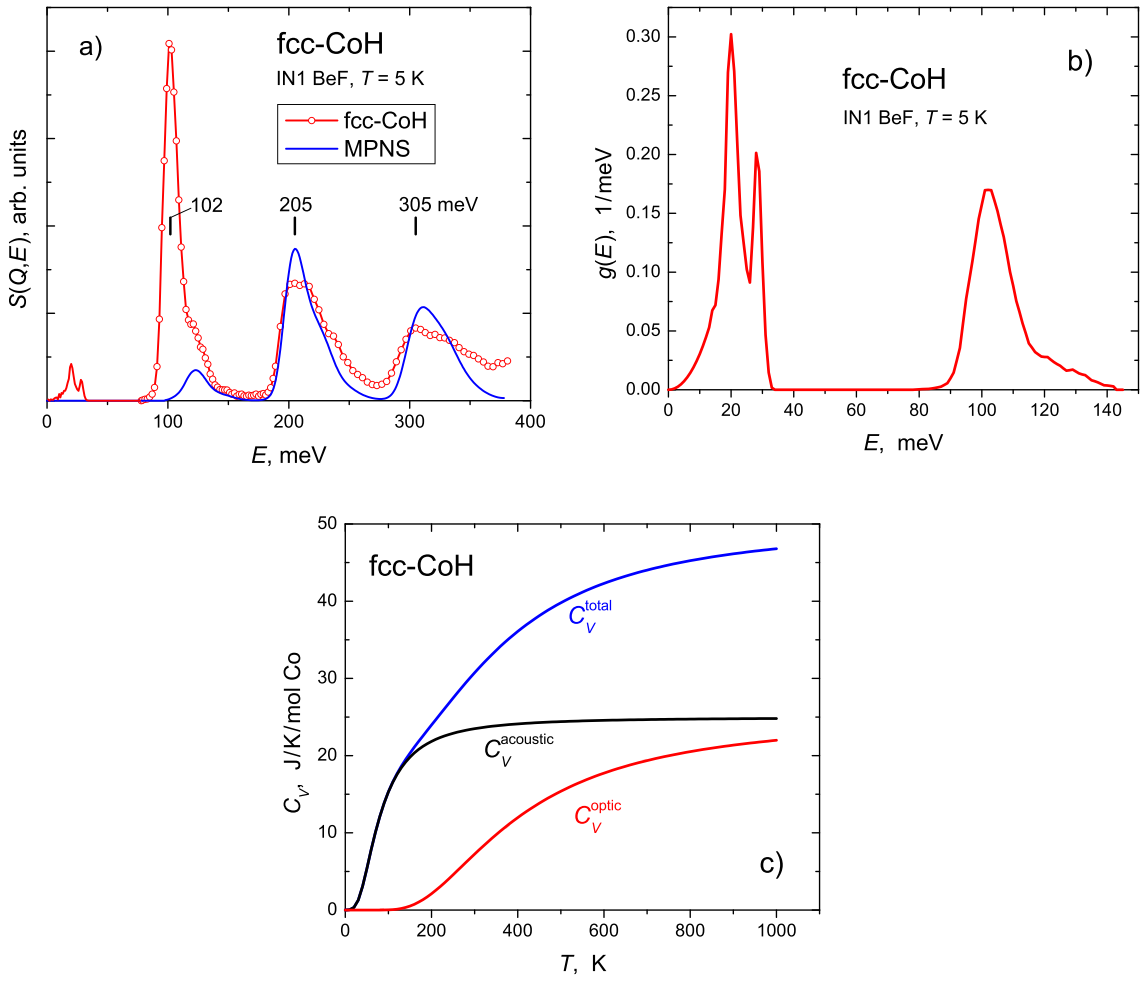

Fig. 12. (a) The "corrected" experimental spectrum $S(Q,E)$ of a powder sample of fcc-CoH hydride (open red circles) and the MPNS contribution (solid blue curve) calculated in an isotropic and harmonic approximation [30]. The $S(Q,E)$ spectrum is composed of the acoustic part in the range of neutron energy transfers E < 40 meV calculated using DFT and of the optical part at E > 80 meV measured at 5 K with the IN1-BeF spectrometer [30]. The vertical bars show the centers of the experimental optical peaks. (b) The phonon density of states $g(E)$ for fcc-CoH. The acoustic part of $g(E)$ is calculated using DFT and the optical part is derived from the experimental INS spectrum. (c) Heat capacities $C_V(T)$ due to the lattice vibrations in fcc-CoH.

of the experimental spectrum, which points to its mostly harmonic and isotropic character. The acoustic and optical parts of the phonon density of states of fcc-CoH shown in Fig. 12b are normalized to 3 states each. Since fcc-CoH is a ferromagnet with a yet undetermined, but high Curie temperature of T_C > >200 K [90], its vibrational heat capacity $C_V^{total}(T)$ shown in Fig. 12c should considerably increase at temperatures up to T_C due to the magnetic contribution.

Recent synchrotron x-ray diffraction studies of the Co-H system in diamond anvil cells showed that the fcc-CoH phase is stable at hydrogen pressures of up to about 33 GPa [132–134]. At a pressure of 33–40 GPa, fcc-CoH transforms to fcc-CoH_2 with the H atoms presumably occupying tetrahedral interstices [133,134], and a CoH_3 phase with a primitive cubic metal lattice is finally formed after heating the sample above 1070 K at 75 GPa [134].

5.5. Fcc-NiH [84,95]

Nickel hydride is formed *via* an isomorphic $\gamma_1 \rightarrow \gamma_2$ transition and can be produced electrolytically and under high hydrogen pressure [135]. At room temperature, the $\gamma_1 \rightarrow \gamma_2$ transition is accompanied by an abrupt increase in the hydrogen solubility from $x \approx 0.01$ to $x \approx 1$ [135,136]. The available experimental data on the pressures of formation and decomposition of nickel hydride and deuteride at temperatures up to about 650 K are presented and critically analysed in Ref. [32]. The compositions of the coexisting γ_1 and γ_2 phases get closer to each other with increasing temperature, and the line of the $\gamma_1 \leftrightarrow \gamma_2$ equilibrium terminates in a critical point at 633 K, 1.4 GPa, and $x \approx 0.5$ in accordance with Ref. [137]. The Curie temperature of ferromagnetic γ_1 solutions decreases with hydrogen pressure from T_C = 627 K at atmospheric pressure to $T_C \approx 551$ K near the line of the $\gamma_1 \rightarrow \gamma_2$ transition due to the increase in the equilibrium hydrogen solubility in nickel [136] (in an inert medium, the Curie point of Ni slowly and approximately linearly increases with pressure [138]). The γ_2 phase is neither ferromagnetic, nor superconducting at temperatures down to 0.3 K [139].

A $NiH_{1.05(5)}$ sample prepared at a hydrogen pressure of 2 GPa and a temperature of 523 K was studied by neutron diffraction at 120 K and shown to have a NaCl-type crystal structure, in which H atoms occupied all octahedral interstices in the fcc metal lattice with a = 3.740 Å [31]. A sample of fcc nickel hydride with the same composition $NiH_{1.05(5)}$ assigned for the INS investigation was made from polycrystalline plates with strong (001)[100] texture and a total weight of 2.5 g [95]. The sample was loaded with hydrogen at 3 GPa and 573 K and had an fcc metal lattice with a = 3.732(6) Å at 100 K according to x-ray diffraction. The INS spectra were measured at 5 K with the IN1-BeF spectrometer at ILL using two different orientations of the sample, with the [100] axis of the texture at an angle of ψ = 0 and 45° to the direction of neutron momentum transfer **Q** [95]. The second and third bands of optical H vibrations in the spectrum

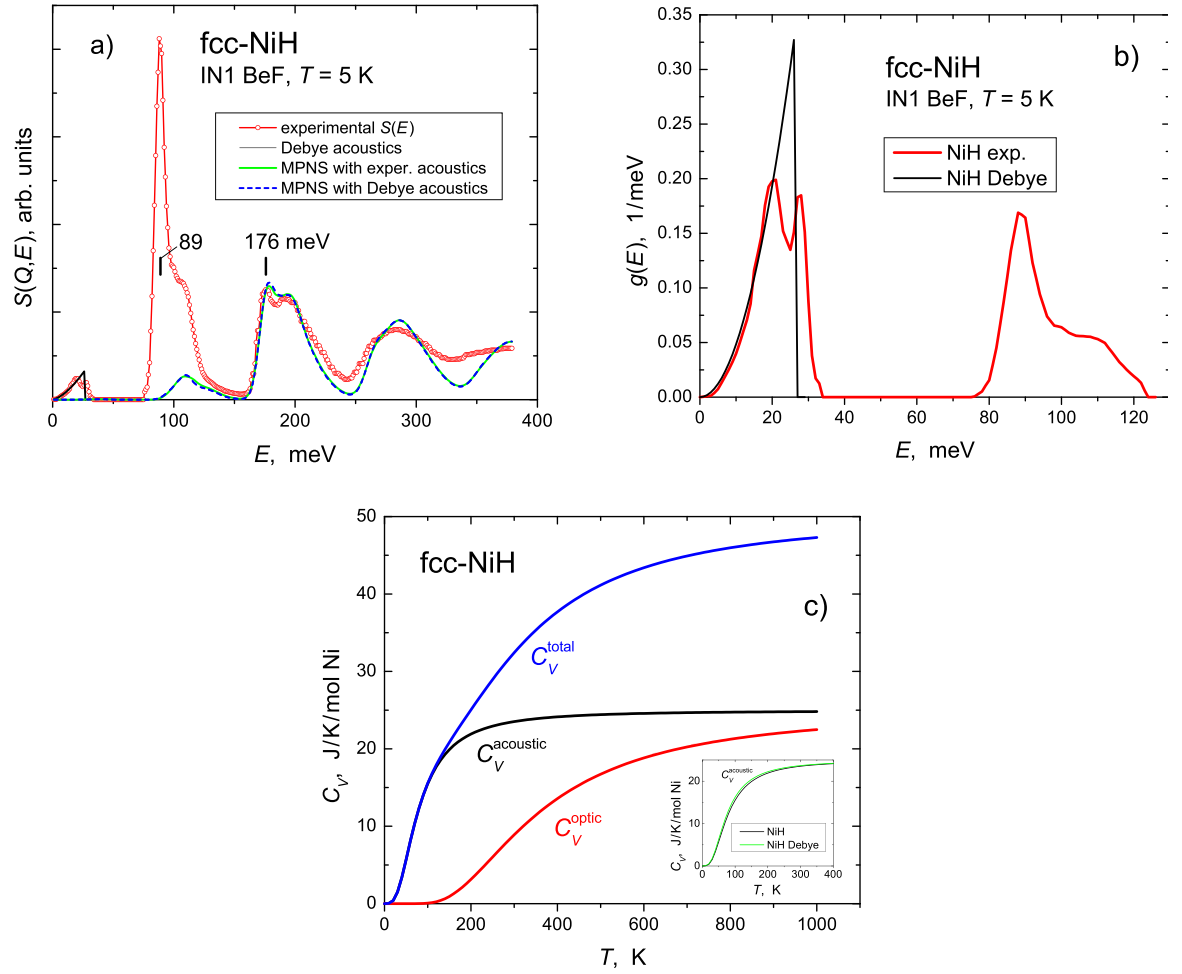

Fig. 13. (a) Open red circles show a "corrected" experimental spectrum $S(Q,E)$ of fcc-NiH hydride composed of the acoustic part in the range of neutron energy transfers E < 35 meV measured at 230 K with the KDSOG-M spectrometer [84] and of the optical part at E > 75 meV measured on the IN1-BeF spectrometer at 5 K and an angle of $\psi = 45°$ between the [100] axis of the sample texture and the direction of neutron momentum transfer [95]. The vertical bars show the centers of the experimental optical peaks. The solid black curve shows the Debye approximation of the acoustic spectrum; the Debye energy is 26(2) meV [84]. The solid green and dashed blue curves represent the contributions from multiphonon neutron scattering calculated, respectively, using the acoustic part of the spectrum measured experimentally and calculated in the Debye approximation. (b) The red curve depicts the phonon density of states $g(E)$ for fcc-NiH derived from experiment (open red circles in Fig. 13a). The black curve shows the Debye dependence $g(E) \sim E^2$ fitted to the acoustic part of the experimental spectrum. (c) Heat capacities $C_V(T)$ due to the lattice vibrations in fcc-NiH calculated from the experimental $g(E)$ (red curve in Fig. 13b). The inset compares the $C_V^{acoustic}(T)$ dependences calculated from the experimental $g(E)$ (black curve) and its Debye approximation (green curve).

measured at $\psi = 0°$ (with **Q** in the < 100 > directions from the H atom toward the nearest Ni atoms in the NiH crystal) turned out to be substantially anharmonic. The $\psi = 45°$ spectrum (with **Q** along the < 110 > directions and close to the < 111 > directions) was almost harmonic and similar to the INS spectra of previously studied NiH samples with a random orientation of crystal grains [84]. The unusual anisotropy and anharmonicity of hydrogen optical vibrations in NiH will be considered in more detail in Section 6.1. A "corrected" 45° spectrum of fcc-NiH is shown in Fig. 13a.

The acoustic part of the INS spectrum of fcc-NiH used in the present paper was measured in Ref. [84] with low statistical accuracy. To estimate the inaccuracies in the calculated MPNS spectrum and in the $C_V(T)$ dependences resulting from the inaccuracy in the acoustic part of the $S(Q,E)$ spectrum, we performed calculations using the experimental acoustic spectrum and its Debye approximation shown in Fig. 13a by the open red circles and by the solid black curve, respectively. As seen from Fig. 13a, a replacement of the experimental acoustic spectrum by the Debye dependence noticeably changes the MPNS contribution only in the energy range of the first optical band. Using Debye's $g(E)$ instead of the experimental density of states of acoustic phonons (the black and red curves, respectively, in Fig. 13b) leads to an increase in $C_V^{acoustic}(T)$ by 10% at 50 K, by 5% at 100 K, by less than 1% at 250 K, and this inaccuracy continues to decrease at higher temperatures (see the inset in Fig. 13c). That is, at T > 50 K, the error induced in the heat capacity by the radical change in the acoustic $g(E)$ does not exceed the inaccuracy of most calorimetric measurements.

According to the recent *in situ* synchrotron x-ray diffraction studies performed in diamond anvil cells, fcc-NiH remains stable at hydrogen pressures up to 61 GPa at room temperature and transforms to monoclinic Ni_2H_3 upon laser heating to above 1000 K at 52–61 GPa [140,141].

5.6. *Hcp-$MoH_{1.1}$ [96]*

The hcp (ε) non-stoichiometric molybdenum hydride MoH_x with x > 1 is formed from a dilute solid solution of hydrogen in bcc (α) molybdenum at hydrogen pressures above 3.5– 4 GPa [142]. An *in situ* x-ray diffraction investigation in a diamond anvil cell at room temperature and pressures up to 30 GPa showed [143] that the hydrogen content of the hcp hydride monotonically increases from $x \approx 1.1$ at 4 GPa to $x = 1.35(10)$ at 15 GPa and then stops changing. High-temperature phase transformations in the Mo-H system were studied by *in situ* x-ray diffraction at hydrogen pressures up to

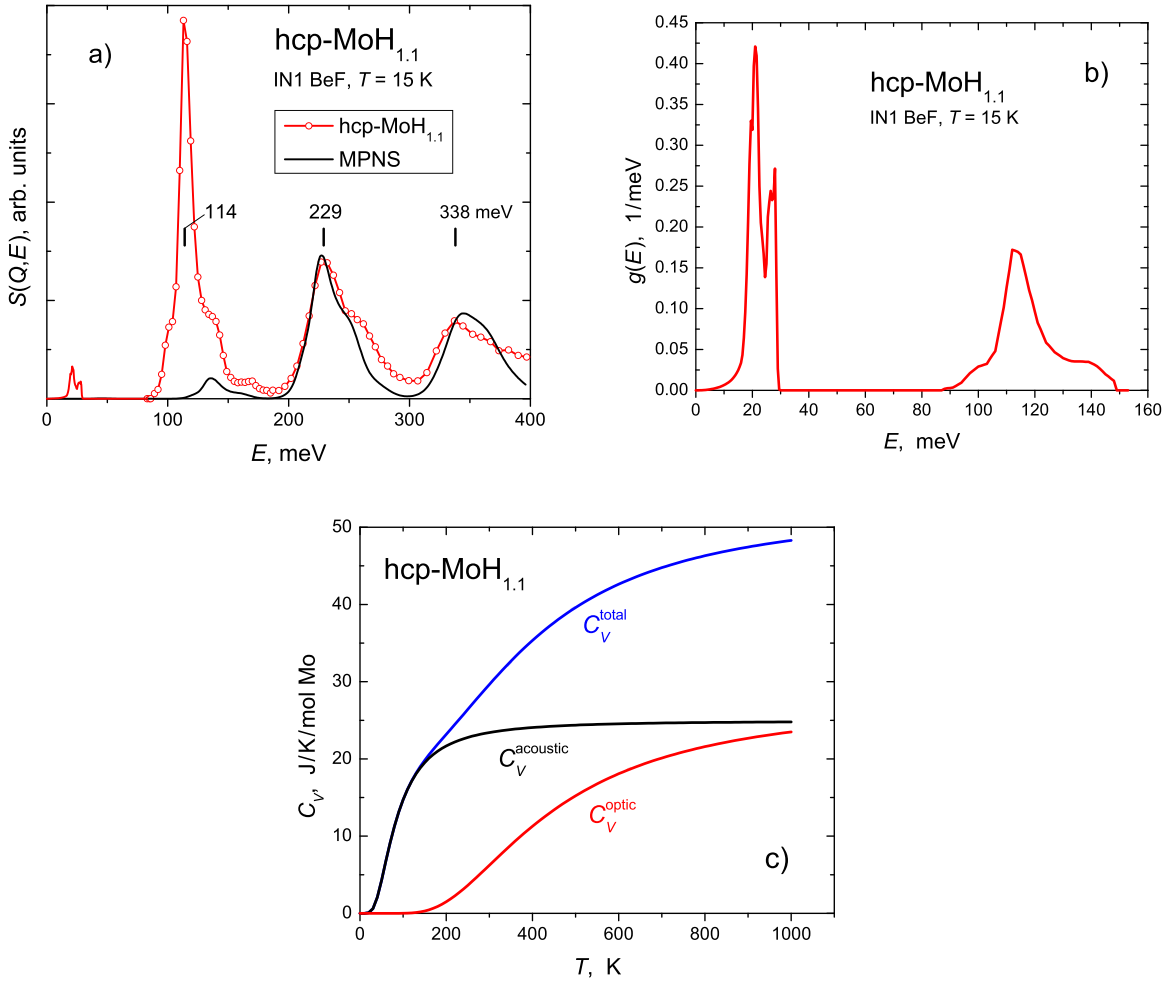

Fig. 14. (a) The "corrected" experimental spectrum $S(Q,E)$ of a polycrystalline sample of hcp-$MoH_{1.1(1)}$ hydride (open red circles) [96] and the MPNS contribution (solid black curve) calculated in an isotropic and harmonic approximation. The $S(Q,E)$ spectrum is composed of the acoustic part in the range of the neutron energy transfers $E < 35$ meV calculated using DFT and of the optical part at $E > 80$ meV measured at 15 K with the IN1-BeF spectrometer [96]. The vertical bars show the centers of the experimental optical peaks. (b) The phonon density of states $g(E)$ for hcp-$MoH_{1.1}$. The acoustic part of $g(E)$ is calculated using DFT and normalized to 3 states; the optical part is derived from the experimental INS spectrum and normalized to 3.3 states. (c) Heat capacities $C_V(T)$ due to the lattice vibrations in hcp-$MoH_{1.1}$.

5.3 GPa and temperatures up to 1470 K using a multi-anvil apparatus [144]. The formation of a high-temperature fcc-MoH hydride at $T > 750$–840 K reported in Ref. [144] was not, however, confirmed in a later work [145] using a Toroid-type apparatus and quenching technique. Instead, the stability region of the low-temperature hcp-$MoH_{1.1}$ hydride was found to grow with pressure, and the temperature of its boundary with the region of dilute α solutions rose with pressure from about 750 K at 3.5 GPa to 1070 K at 5.5 GPa. Thus, the hcp molybdenum hydride MoH_x with $x \approx 1.1$–1.35 is the only hydride currently available for investigation in the Mo-H system.

Samples of "overstoichiometric" hydrides MoH_x with $x > 1$ are thermally stable at atmospheric pressures at temperatures below 220 K [142]. Presumably [143], hydrogen atoms in these samples should completely occupy octahedral interstitial sites in the hcp metal lattice, which gives $x_{octa} = 1$, and partially fill tetrahedral interstices, so that the total $x = x_{octa} + x_{tetra}$. However, a neutron diffraction pattern of a powder sample $MoH_{1.19}$, measured in a metastable state at atmospheric pressure and $T = 120$ K, could only be interpreted as if the hydride composition was $MoH_{0.95(5)}$ and hydrogen atoms occupied the O-sites only [31]. A recent neutron diffraction study of a $MoD_{1.07}$ sample at 100 K showed [46] that the complete filling of the O-sites and partial filling of the T-sites is most likely. The puzzling conclusion of Ref. [31] was probably the result of an unfortunate combination of some negative factors such as the anomalously large amplitude of incoherent neutron scattering by H atoms. Nevertheless, an unambiguous solution to the problem of site occupancy in hcp molybdenum hydrides still needs further experimental investigations of samples with higher hydrogen content.

Fig. 14 shows results of an INS study of an hcp-$MoH_{1.1(1)}$ sample weighing 2.2 g and consisting of a stack of plates cut from high-purity single-crystal molybdenum foil 0.2 mm thick with the electrical resistance ratio $R_{300\,K}/R_{4.2\,K} \approx 1000$, which were loaded with hydrogen at 5 GPa and 620 K [96]. According to the x-ray diffraction study of several plates at 120 K, the lattice parameters of the hcp metal lattice of the sample were $a = 2.93$ Å, $c = 4.74$ Å, and $c/a = 1.62$. The INS experiment was carried out at 15 K using the IN1-BeF neutron spectrometer.

The INS study provided no reliable evidence of the occupancy of T-sites in the $MoH_{1.1}$ sample. Possible contributions to the $S(Q,E)$ spectrum of molybdenum hydride from neutron scattering by H atoms occupying the T-sites were considered in Ref. [46]. In particular, an extrapolation of the fundamental frequency of hydrogen optical vibrations at the T-sites in hypothetical hcp-MoH_2, predicted by *ab initio* calculations [146], to the lattice parameters of $MoH_{1.1}$ gave a broad peak at ~200 meV. As seen from Fig. 14a, near this energy there is neither a peak, nor a hump, nor any other feature, which could be attributed to the H vibrations at the T-sites. In the calculation of the MPNS spectrum (solid black curve in Fig. 14a) we

assumed that the scattering intensity in the range 0–180 meV is entirely due to neutron scattering by H atoms occupying the O-sites.

As seen from Fig. 14a, the multiphonon calculation in the harmonic isotropic approximation correctly reproduces the position of the experimental two-phonon peak at 231 meV. This indicates the absence of a noticeable anharmonicity in the INS spectrum of the $MoH_{1.1}$ sample in the energy range of the first and second bands of optical vibrations of H atoms at the O-sites. The excess intensity in the 250–300 meV range, which is not reproduced by the calculation, may result from the neglected vibrations of the H atoms at the T-sites.

Under the assumption that the number of acoustical modes in $MoH_{1.1}$ is determined by the number of Mo atoms, and the number of optical modes by the number of H atoms, the acoustic part of the phonon density of states $g(E)$ was normalized to 3 states and the optical part to $1.1 \times 3 = 3.3$ states (see Fig. 14b). The heat capacities $C_V(T)$ shown in Fig. 14c were calculated by Eq. (2) using the $g(E)$ dependence thus obtained. Molybdenum hydride is a superconductor with the same $T_c = 0.92$ K as molybdenum metal and no magnetic order is observed in it at temperatures down to 0.3 K [147]. Therefore, there should be no magnetic contribution to its heat capacity at elevated temperatures.

5.7. Fcc-RhH [47]

Rhodium metal has an fcc (γ) structure and forms hydride with an fcc metal lattice, too, [148] *via* an isomorphic $\gamma_1 \rightarrow \gamma_2$ transition at hydrogen pressures of 4.5–5 GPa in the temperature range from 300 K [149] to 870 K [82,150]. Near the line of this transition, the hydrogen content of the dilute γ_1 solid hydrogen solution increases with temperature from $x \leq 0.01$ at 520 K [148] to $x \approx 0.05$ at 870 K [82], while the composition of the γ_2 hydride remains virtually unchanged and close to RhH [82,150]. The hydride can be retained in a metastable state at ambient pressure and $T < 170$ K, if the sample is previously cooled under high hydrogen pressure. A neutron diffraction investigation at 120 K demonstrated [31] that a γ-$RhH_{1.00(3)}$ sample synthesized at 623 K and 7 GPa had a NaCl-type crystal structure with H atoms occupying every octahedral site in the fcc Rh lattice with the parameter $a = 4.010(5)$ Å, which was expanded by 5.6% compared to $a = 3.799(3)$ Å of fcc Rh metal without hydrogen.

According to the results of a room-temperature *in situ* synchrotron x-ray diffraction investigation in a diamond anvil cell [149,151], an increase in the hydrogen pressure to 8 GPa leads to the transformation of fcc-RhH with octahedrally co-ordinated H atoms into fcc-RhH_2 with H atoms occupying tetrahedral interstices. Our efforts to prepare a bulk sample of RhH_2 at a hydrogen pressure of 9 GPa and temperatures from 300 to 870 K, however, were unsuccessful [82]. Most likely, the formation pressure of RhH_2 is higher than 9 GPa in the case of bulk samples because of the larger baric hysteresis caused by the elastic stresses accompanying the growth of the dihydride phase.

A sample of fcc-$RhH_{0.98(3)}$ weighting 0.9 g and made of textured 0.1 mm foil of rhodium metal was hydrogenated at 7 GPa and 600 K and studied by inelastic neutron scattering at atmospheric pressure and 5 K in the range of neutron energy transfers 35–380 meV using the IN1-BeF neutron spectrometer at ILL [47]. The hydrogenated plates of Rh were brittle and easily cracked to about a hundred small pieces, which were placed in a flat aluminum container and arranged in one layer, side by side, randomly with respect to their rolling direction. The sample was measured in two different orientations, with an angle $\psi = 0°$ and 45° between the vector of the neutron momentum transfer, $\mathbf{Q}$, and the normal to the sample plane. Fig. 15a shows the obtained $S(Q,E)$ spectra, in which the spurious scattering intensity at $E < 45$ meV is replaced by an acoustic spectrum calculated using DFT.

As seen from Fig. 15a, the experimental spectra measured at $\psi = 0°$ and 45° strongly differ from the calculated harmonic multiphonon spectrum in the ranges of the second and third optical bands. Meanwhile, these bands in the INS spectra of similar fcc monohydrides of palladium [50] and nickel [95] show significant anharmonicity only for the $\mathbf{Q}$'s directed close to the < 100 > axes, which are directions from the H atom to the nearest metal atom. For other directions of the neutron momentum transfer, the spectra of PdH and NiH were isotropic and harmonic and almost coincide with the directionally averaged spectra of powder samples. In Ref. [47], the pieces of the RhH foil were only averaged with respect to the rolling direction, and the contributions to the $\psi = 0°$ and $\psi = 45°$ spectra from optical vibrations polarized along the < 100 > axes were significantly different. In particular, the contribution from the < 100 > vibrations to the $\psi = 0°$ spectrum should be small, because the probability density $P_{110}(0°)$ of the < 110 > orientations alone already exceeded $P_{100}(0°)$ of the < 100 > orientations by a factor of 5. At the same time, the second and third bands in both $\psi = 0°$ and $\psi = 45°$ spectra were nearly identical, strongly anharmonic, and shifted towards higher energies compared to the calculated harmonic spectrum. This suggests that at the energies of the second and third optical bands, the potential well for H atoms in fcc-RhH is steeper than parabolic in most directions.

Nevertheless, in order to have something to compare with, we calculated the vibrational heat capacities $C_V(T)$ (see Fig. 15c) in a harmonic approximation using Eq. (2) and the phonon density of states $g(E)$ of fcc-RhH shown in Fig. 15b. Regarding other properties of fcc-RhH we can add that it is neither ferromagnetic, nor superconducting at temperatures down to 0.3 K [139] and that the absence of superconductivity agrees with the theoretical predictions [152].

5.8. Fcc-PdH [50] and fcc-PdD [51]

Palladium hydrides are formed *via* an isomorphic $\gamma_1 \rightarrow \gamma_2$ transition (often called the $\alpha \rightarrow \beta$ transition), which terminates in a critical point at $P_{cr} \approx 2$ MPa; $T_{cr} \approx 565$ K, and $x_{cr} \approx 0.25$ (see review paper [153]). At room temperature, the $\gamma_1 \rightarrow \gamma_2$ transition is accompanied by an abrupt increase in the hydrogen solubility in fcc Pd metal from $x \approx 0.01$ to $x \approx 0.62$ and occurs at a low hydrogen pressure of about 70 Pa [153]. A further increase in pressure leads to a gradual increase in the hydrogen content of the γ_2 phase up to $x \approx 1$ at $P \approx 1.5$ GPa [154]. Phase relations in the Pd-D system are similar; the line of the isomorphic $\gamma_1 \rightarrow \gamma_2$ transition ends in a critical point at $P_{cr} \approx 3.6$ MPa; $T_{cr} \approx 549$ K, and $x_{cr} \approx 0.25$ [153]. The thermal stability of palladium hydrides and deuterides synthesized at high pressures decreases with increasing concentration, and the samples with $x \approx 1$ rapidly decompose when heated in vacuum to temperatures above ~220 K. Neutron diffraction has shown (see [155] and references therein) that H and D atoms fill only octahedral interstitial sites in, respectively, palladium hydrides and deuterides at room and lower temperatures. According to *in situ* neutron diffraction studies at temperatures of 582–583 K, a significant fraction of the D atoms (up to 1/3 at $x = 0.6$) in the deuterides additionally occupy tetrahedral interstices [155,156].

A single-phase powder sample of fcc-$PdH_{0.99(3)}$ prepared at 4 GPa and 573 K and weighing 5 g was studied by INS at 25 K in the range of energy transfers 30–800 meV on the time-focused crystal analyzer (TFXA) neutron spectrometer on the ISIS spallation neutron source, at the Rutherford Appleton Laboratory, UK. The parameter of the fcc lattice of the sample (a = 4.095 Å at 100 K, x-ray diffraction)

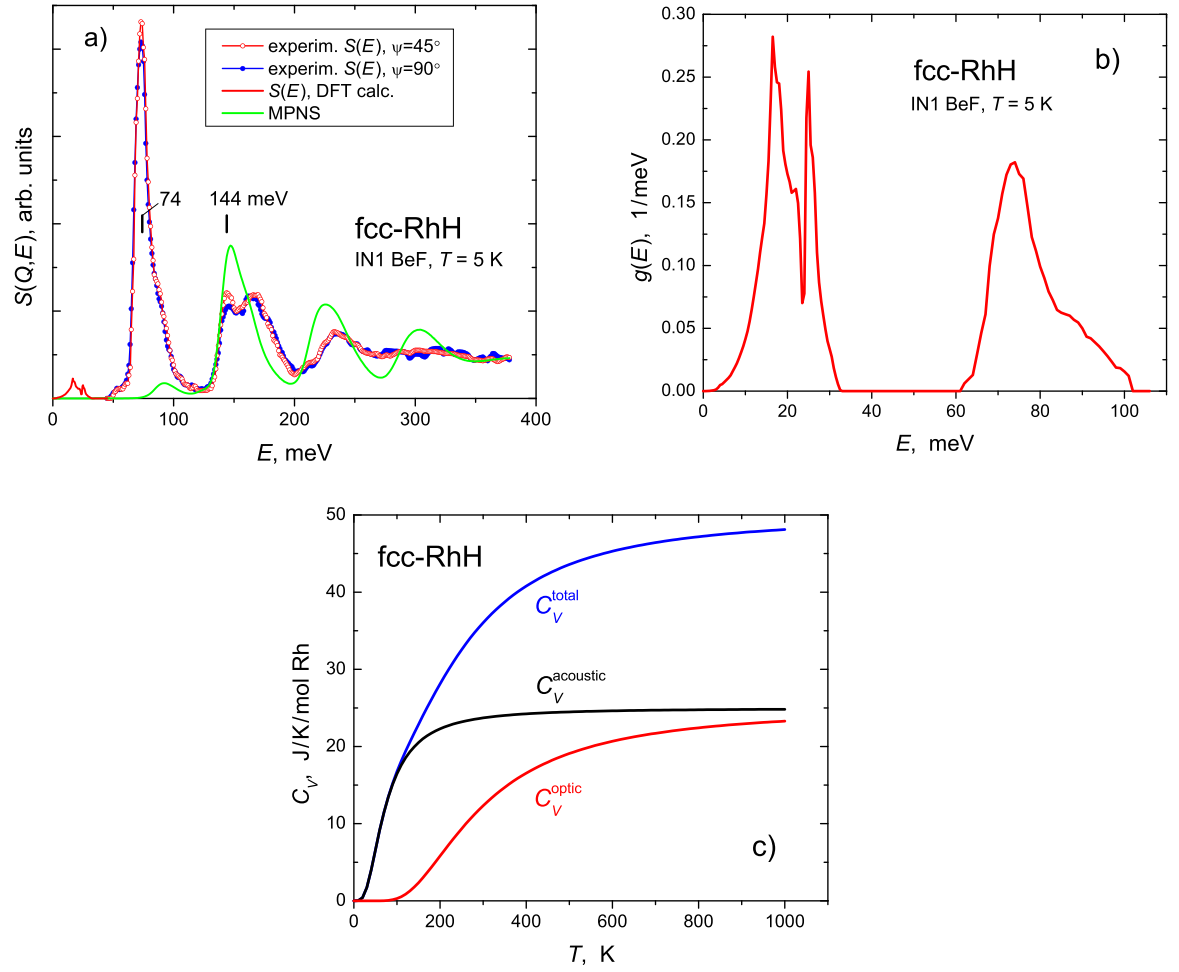

Fig. 15. (a) The "corrected" experimental spectrum $S(Q,E)$ of a polycrystalline sample of fcc-RhH hydride (open red circles) and the MPNS contribution (solid green curve) calculated in an isotropic and harmonic approximation [47]. The $S(Q,E)$ spectrum is composed of the acoustic part in the range of the neutron energy transfers E < 35 meV calculated using DFT and of the optical part at E > 55 meV measured at 5 K with the IN1-BeF spectrometer [47]. The vertical bars show the centers of the experimental optical peaks in the $\psi = 45°$ spectrum. (b) The phonon density of states $g(E)$ for fcc-RhH. The acoustic part of $g(E)$ is calculated using DFT and the optical part is derived from the experimental INS spectrum. (c) Heat capacities $C_V(T)$ due to the lattice vibrations in fcc-RhH.

and its superconducting transition temperature (9.33 K, midpoint of the signal of disbalance of an ac bridge) well agreed with its stoichiometric composition [153]. The obtained spectrum $S(Q,E)$ of optical vibrations in this sample is shown in Fig. 16a.

The $S(Q,E)$ spectrum of optical vibrations in the fcc-PdD sample shown in Fig. 16b was constructed in a less straightforward manner. We could not produce a sample of isotopically pure PdD because the aluminum trideuteride used in the high-pressure synthesis was contaminated with protium and had a ratio H/(D+H) of $y = 0.029$. The problem was solved by studying three different $PdD_{1-y}H_y$ samples with $y = 0.050$, 0.072, and 0.091 [51]. The samples weighing 2 g each were synthesized at 5 GPa and 600 K in an atmosphere of gaseous deuterium/hydrogen mixtures produced inside the high-pressure cell by thermal decomposition of AlD_3 and AlH_3 powders mixed in the necessary proportions. The samples had virtually the same atomic ratio (D+H)/Pd = 1.00(3) and the same lattice parameter a = 4.087(4) Å at 100 K determined by x-ray diffraction. These samples were studied by INS under identical conditions at $T = 5$ K using the IN1-BeF spectrometer, and each obtained spectrum was written in the form $S = yS_H + (1-y)S_{PdD}$, where S_{PdD} is the spectrum of the undisturbed PdD matrix and S_H is the spectrum resulting from neutron scattering on the H atoms and also from changes in the scattering from the D atoms caused by their interactions with differently vibrating H atoms. Assuming that S_{PdD} and S_H are the same for all samples, each pair of equations gives a pair of the S_{PdD} and S_H spectra. Fig. 16b shows the S_{PdD} spectrum derived from the optical $S(Q,E)$ spectra of $PdD_{1-y}H_y$ samples with the most different values of $y = 0.050$ and 0.091 because of their better statistical accuracy [51].

The low-energy acoustic parts of the $S(Q,E)$ spectra of PdH and PdD shown in Figs. 16a and 16b are obtained from the experimental spectrum of an fcc-PdH sample, which was made of highly textured foil (see Section 6.1), hydrogenated at the same H_2 pressure of 4 GPa and a temperature of 573 K as the fcc-PdH powder sample, and had the same lattice parameter and superconducting temperature. As seen from Figs. 16a and 16b, the calculated multiphonon contributions (thick solid curves) are small in the range of the first optical bands and satisfactorily describe the intensity distribution in the second and higher bands. The discrepancy between the calculated and experimental spectra suggests a certain anharmonicity of hydrogen vibrations in the second and higher bands. To characterize this anharmonicity numerically, note that the peak in the second optical band of fcc-PdH is positioned at 110 meV, which is lower by 2 meV than the doubled energy of 56 meV of the peak in the first band (Fig. 16a). The peak in the second band of fcc-PdD is observed

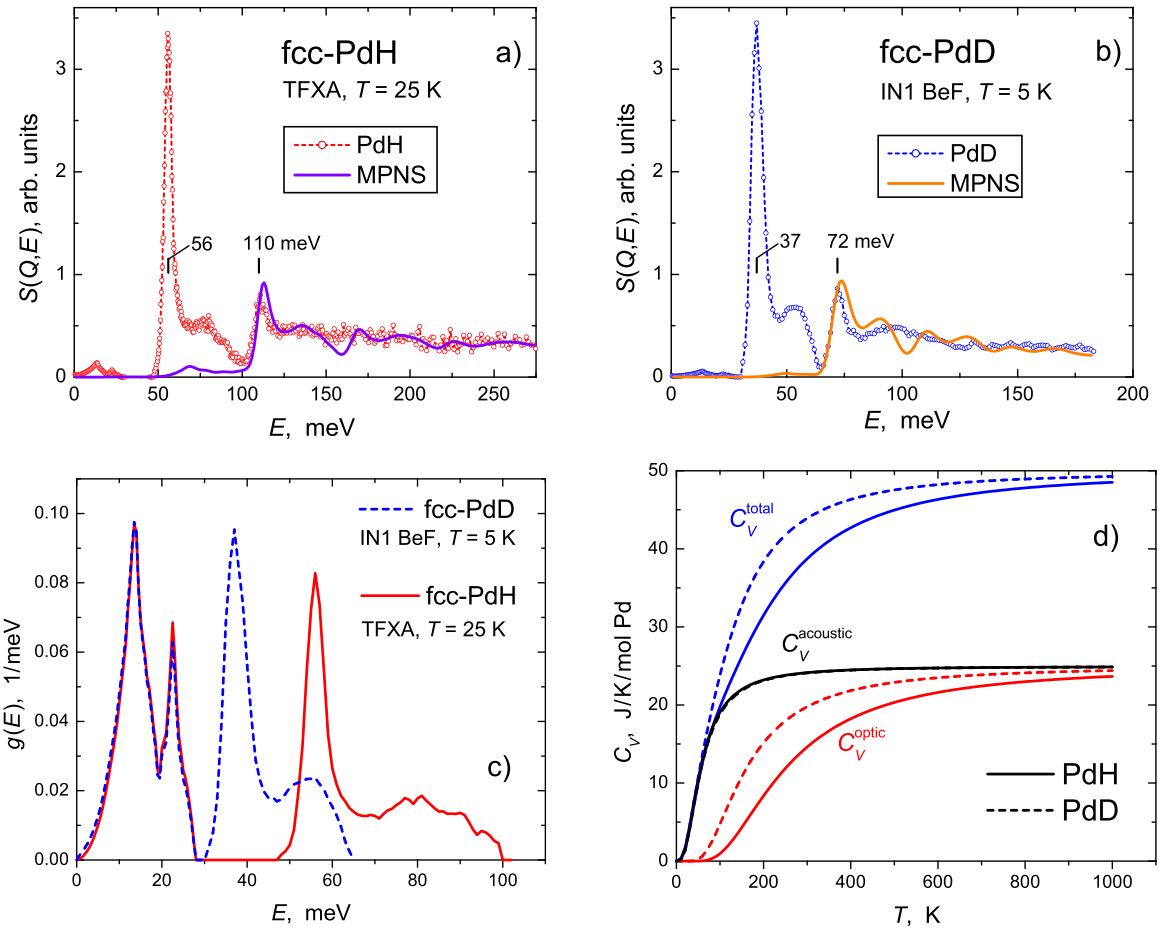

Fig. 16. The open circles connected with a dashed line represent the "corrected" dynamical structure factors $S(Q,E)$ of powder samples (a) of fcc-PdH measured at 25 K with the TFXA neutron spectrometer [50] and (b) of fcc-PdD measured at 5 K with the IN1-BeF spectrometer [51]. The acoustical parts of these spectra at E < 30 meV are taken from a separate experiment using a textured PdH sample [50]. The solid curves show multiphonon contributions calculated in a harmonic isotropic approximation. The vertical bars indicate the experimental peak positions in the first and second optical bands. (c) The phonon density of states $g(E)$ for fcc-PdH (solid red curve) and fcc-PdD (dashed blue curve) derived from the experimental INS spectra. (d) Heat capacities $C_V(T)$ due to the lattice vibrations in fcc-PdH (sold curves) and fcc-PdD (dashed curves).

at 72 meV, which is 2 meV lower than twice the energy of 37 meV of the peak in the first band (Fig. 16b).

The phonon densities of states $g(E)$ for fcc-PdH and fcc-PdD shown in Fig. 16c are derived from experiment and their acoustic parts at E < 30 meV and optical parts at higher energies are normalized to 3 states each. The heat capacities $C_V(T)$ presented in Fig. 16d clearly demonstrate a dependence on the hydrogen isotope.

The study of the low-concentrated solid protium solutions in stoichiometric palladium deuteride also disclosed a new feature of the effect of a light impurity on the vibrational spectrum of the host phase [51]. Along with the local defect mode detached from the optical band of the host atoms and shifted to higher energies, which was earlier observed in a few deuterides including $PdD_{0.6}$ [157], this INS investigation revealed profound changes inside the optical D band due to covibrations of heavy D atoms and light H atoms. These covibrations form a band located above the main peak in the optical band of PdD. The vibrational states of D atoms in this new band are mostly borrowed from the main peak and considerably decrease its intensity.

The observed changes inside the optical D band are caused by interactions of H atoms with the neighboring D atoms, so the strength of this interaction is nearly independent of the H concentration, when the concentration is low. Therefore, even in infinitely diluted H solutions in PdD, the magnitude of changes induced by the H impurity inside the optical D band should remain comparable with the intensity of the defect, local modes of H vibrations.

As noted in Ref. [51], strong changes inside the vibrational band of the host phase due to a light impurity should be intrinsic to many systems. The most likely reason why these changes were not discovered in the H-doped $PdD_{0.6}$ [157] was the broadening of the INS spectra due to the nonstoichiometric composition of the deuteride, which contained 40% vacancies in the D sublattice. Homogeneous samples of stoichiometric PdD and PdH can only be prepared at high hydrogen pressures. According to recent *in situ* x-ray diffraction studies in diamond anvil cells, the hydrogen content of fcc palladium hydride remained unchanged and close to $x = 1$ at pressures from ~1–23 GPa at room temperature [151] and further at pressures up to 100 GPa [158], even when laser heating was used [159].

5.9. *Fcc-$PdH_{0.63}$*

The upper boundary of the miscibility gap in the fcc solid solutions PdH_x is located at $x \approx 0.61$–0.63 at room and lower temperatures [153,160]. Due to the low formation pressure, single-phase samples of fcc-$PdH_{0.63}$ are easy to prepare and also easy to handle

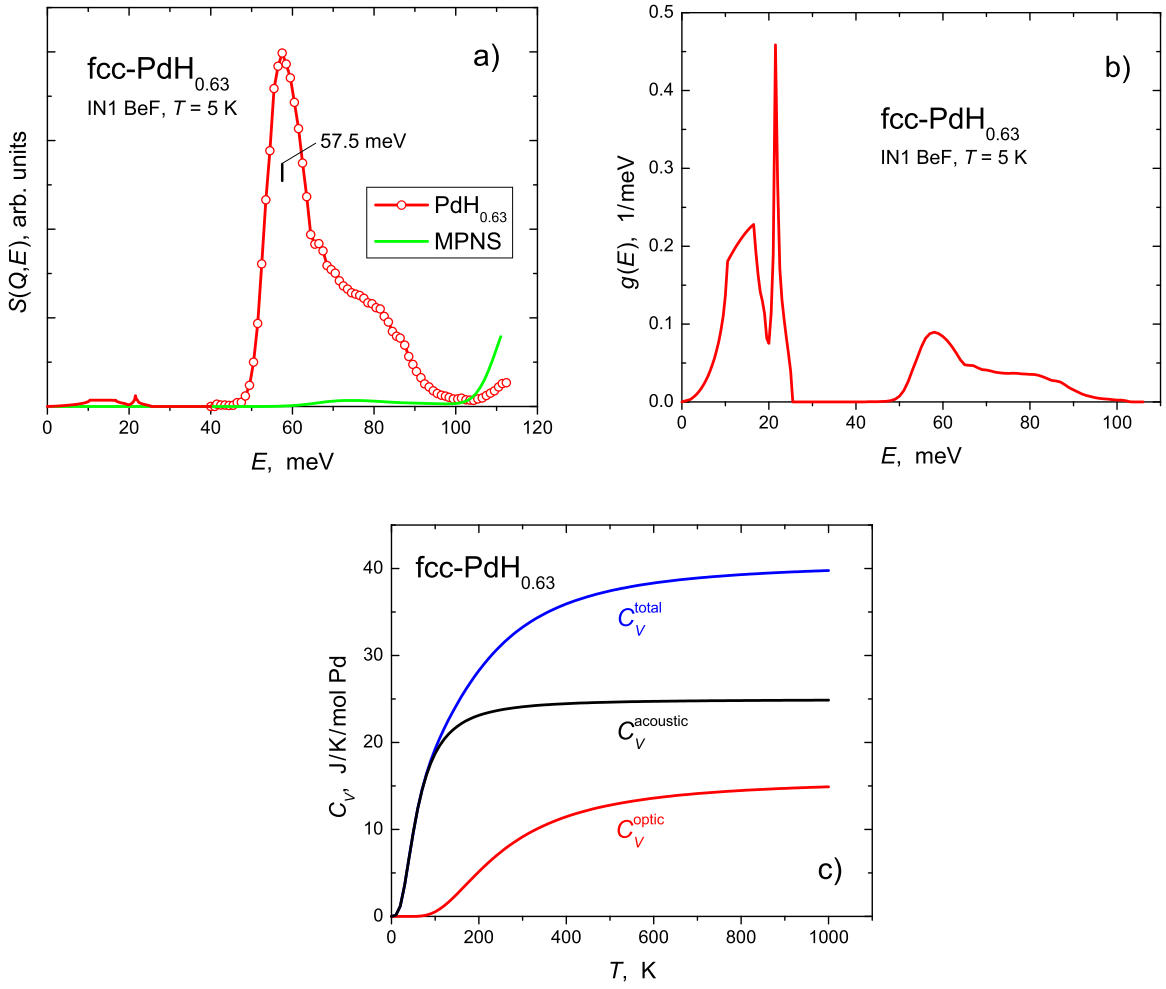

Fig. 17. (results of this paper). (a) The "corrected" experimental spectrum $S(Q,E)$ of a polycrystalline sample of fcc-$PdH_{0.63}$ (open red circles) and the MPNS contribution (solid green curve) calculated in an isotropic and harmonic approximation. The $S(Q,E)$ spectrum is composed of the acoustic part in the range of the neutron energy transfers $E < 30$ meV calculated in the Born-von Kármán model using the force constants for $PdD_{0.63}$ [161,162] and of the optical part at $E > 40$ meV measured at 5 K with the IN1-BeF spectrometer. (b) The phonon density of states $g(E)$ for fcc-$PdH_{0.63}$. The acoustic part of $g(E)$ is normalized to 3 states and the optical part to $3 \times 0.63 = 1.89$ states. (c) Heat capacities $C_V(T)$ resulting from $g(E)$ presented in figure (b).

because of the low decomposition rate under ambient conditions. Besides, the $PdH_{0.63}$ phase enters two-phase mixtures $\gamma_1 + \gamma_2$ with the mean hydrogen content $x < 0.63$ inside the concentration range of the miscibility gap. As a consequence, this phase often appears in experiments, and we decided that it would be useful to determine its phonon density of states and heat capacity based on INS measurements.

A sample of $PdH_{0.63(3)}$ weighing 1.2 g was made of 0.3 mm thick palladium plates hydrogenated in a Sieverts-type apparatus using high-purity hydrogen gas produced by thermal decomposition of TiH_2. The composition of the sample was determined from the H_2 uptake. X-ray diffraction showed that the sample was single-phase and had an fcc metal lattice with $a = 4.022(3)$ Å at 85 K in agreement with previous results [48]. The first band of optical H vibrations in this sample was studied at 5 K on the IN1-BeF neutron spectrometer. The measured $S(Q,E)$ spectrum is shown in Fig. 17a by open red circles and combined with the low-energy spectrum of acoustic vibrations (solid red curve) calculated based on the force constants obtained from the Born-von Kármán model for $PdD_{0.63}$ [161,162]. The resulting "corrected" INS spectrum was further used to calculate the multiphonon contribution to $S(Q,E)$ (solid green curve in Fig. 17a), phonon density of states (Fig. 17b) and heat capacity (Fig. 17c). As noted in Section 3, the calculated value of the heat capacity $C_V^{total}(298K)$ of $PdH_{0.63(3)}$ at room temperature agrees with the experimental data available in the literature (see Fig. 4).

6. Anisotropy and anharmonicity in the INS spectra of high-pressure hydrides of d-metals

6.1. Anisotropy and anharmonicity of the second and higher optical bands in fcc-PdH [50] and fcc-NiH [95]

INS studies have revealed an unusual "45°" anisotropy and anharmonicity of the second and third optical bands of stoichiometric hydrides of palladium [50] and nickel [95] by using polycrystalline samples with a strong texture (001)[100].

The initial foils of Pd and Ni were cold-rolled, annealed in vacuum at 1073–1273 K, and quenched in water. Studying their pole figures by the Schultz method showed [95] that in both the Ni and the Pd foil, the grain orientations (001) [100] were dominant, with the (001) plane parallel to the rolling plane and the [100] axis parallel to the rolling direction. The pole figures of the Pd foil were closer to the ideal ones, with the < 100 > pole at a tilt angle of $\vartheta = 0°$ and four < 110 > poles at $\vartheta = 45°$, in the directions parallel and perpendicular to the rolling direction. The figures for the Ni foil

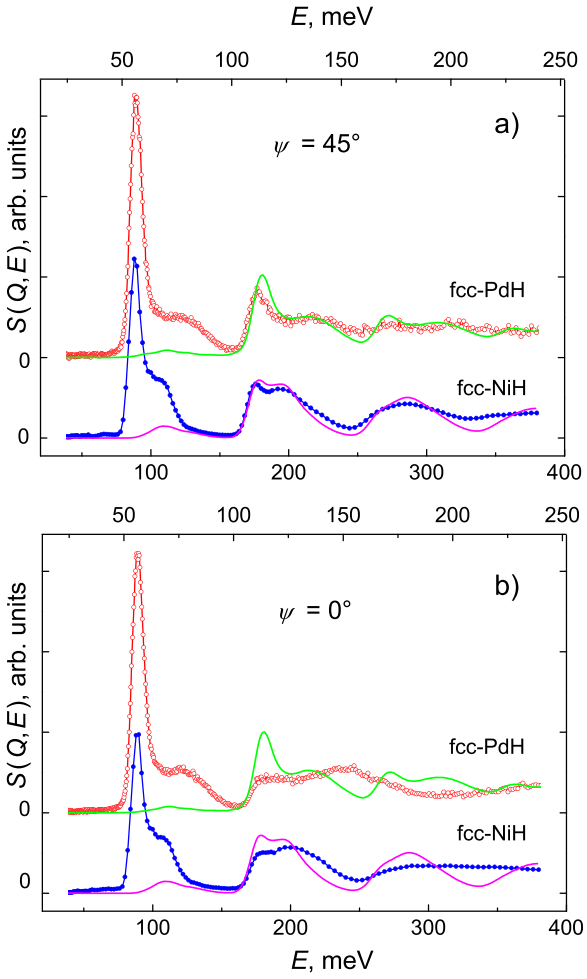

Fig. 18. The INS spectra of fcc-PdH [50] (open red circles, upper scale, TFXA spectrometer, 25 K) and fcc-NiH [95] (solid blue circles, bottom scale, IN1-BeF spectrometer, 5 K) and the MPNS contributions to these spectra calculated in an isotropic harmonic approximation (solid curves). ψ is the angle between the vector **Q** of neutron momentum transfer and the [100] axis of the sample texture.

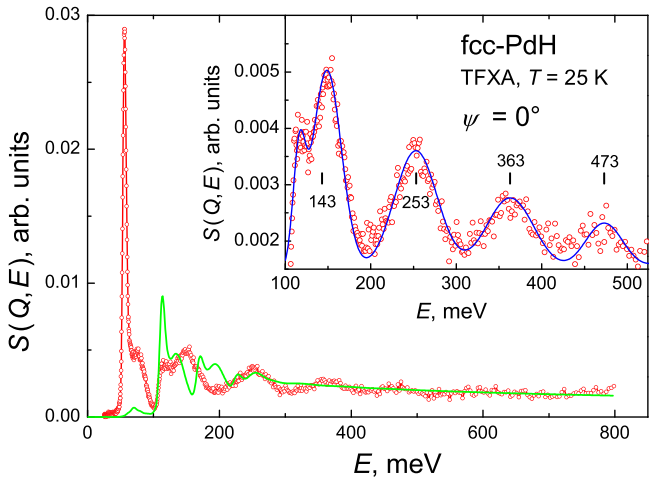

Fig. 19. The experimental INS spectrum of the textured sample of fcc-PdH measured at ψ = 0° with the TFXA spectrometer at 25 K (open red circles) [50] and the MPNS contribution to this spectrum calculated in an isotropic harmonic approximation (solid green curve). The inset shows the high-energy part of the spectrum on a large scale. The solid blue curve in the inset approximates the experimental spectrum as a sum of Gaussians with centers indicated by the vertical bars.

demonstrated a spread of about 15–25° in the grain orientations in the plane perpendicular to the rolling direction.

The hydrogenation conditions of the Pd and Ni samples cut out of these foils and the results of the examination of the crystal structures and superconducting properties of the obtained fcc-$PdH_{0.99(3)}$ and $NiH_{1.05(5)}$ hydrides have been described, respectively, in Sections 5.8 and 5.5. X-ray diffraction at 100 K showed that the hydrogenated plates of these samples had approximately the same texture as the starting metal foils [95]. The PdH sample was studied by INS at 25 K and neutron energy transfers from 2 to 800 meV using the TFXA spectrometer at ISIS, UK [50], and the NiH sample was measured at 5 K and 26 < E < 380 meV with the IN1-BeF spectrometer at ILL, France [95]. Before the INS measurements, the plates of each sample were placed in a flat aluminum container and arranged in one layer, side by side, randomly with respect to their rolling direction. The samples were measured in two different orientations, at an angle of ψ = 0 and 45° between the direction of neutron momentum transfer **Q** and the normal to the sample plane, which coincided with the axis [100] of the sample texture. The obtained spectra $S(Q,E)$ are shown in Fig. 18.

Taking into account the random orientation of the rolling directions of the sample plates in the aluminum container, the spectrum measured at ψ = 0° corresponded to **Q** in the < 100 > directions (from the H atom towards the nearest metal atoms in the PdH and NiH crystals), while ψ = 45° selected **Q** oriented along the < 110 > directions and close to the < 111 > directions. A comparison with the spectra of multiphonon neutron scattering calculated in a harmonic approximation (solid curves in Fig. 18) shows that the ψ = 45° spectra of the textured PdH and NiH samples are almost harmonic and similar to the INS spectra of, respectively, the powder PdH sample (Fig. 16a) and the NiH samples with a random orientation of crystal grains studied previously [84]. The first optical bands of the ψ = 0° spectra nearly coincide with the first optical bands in the corresponding ψ = 45° spectra, whereas the second bands are significantly deformed and shifted to higher energies. The effects in the spectra of PdH and NiH are similar, but more clearly seen in the case of the PdH sample because of its sharper texture: the relative probability densities for the orientations [100] and [110] at the experimental angles ψ = 0° and 45° are $P_{100}(0°)/P_{100}(45°) = 110$ and $P_{110}(45°)/P_{110}(0°) = 12$ for PdH, while $P_{100}(0°)/P_{100}(45°) = 26$ and $P_{110}(45°)/P_{110}(0°) = 2$ for NiH [95].

At energy transfers E > 250 meV, the ψ = 45° spectrum of PdH looks flat and featureless. In contrast, the ψ = 0° spectrum shows clear modulation and can roughly be approximated with equidistant Gaussians, as one can see from Fig. 19. The Gaussians representing the third, fourth, and fifth optical bands of PdH are located at about 110 meV from each other, and the position of the center of gravity at 143 meV for the second band also retains this periodicity.

As demonstrated in Ref. [50], all the main features of the INS spectrum of PdH can be qualitatively explained based on the results of *ab initio* calculations performed in Ref. [163]. To illustrate these results, Fig. 20a shows several profiles of the potential energy U of the H atom plotted as a function of its displacement δ/a from the center of the octahedral interstitial site. The potentials in the < 111 > and < 110 > directions initially lie close to each other and have a parabolic shape, while the potential in the < 001 > directions is initially close to those in the other directions, but then rises with a much steeper parabolic shape. Consequently, the low-energy levels in the < 001 > directions should have the same separation as in the other directions, but at higher energies, the separation should become large and uniform because of the steeper parabolic potential. Fitting a parabola to the outer parts of the potential in the < 001 > directions (blue curve in Fig. 20a) confirm a uniform experimental spacing of the order of 110 meV (see the inset in Fig. 19), which is approximately twice as large as the spacing 56 meV at low energies indicated by the first optical peak.

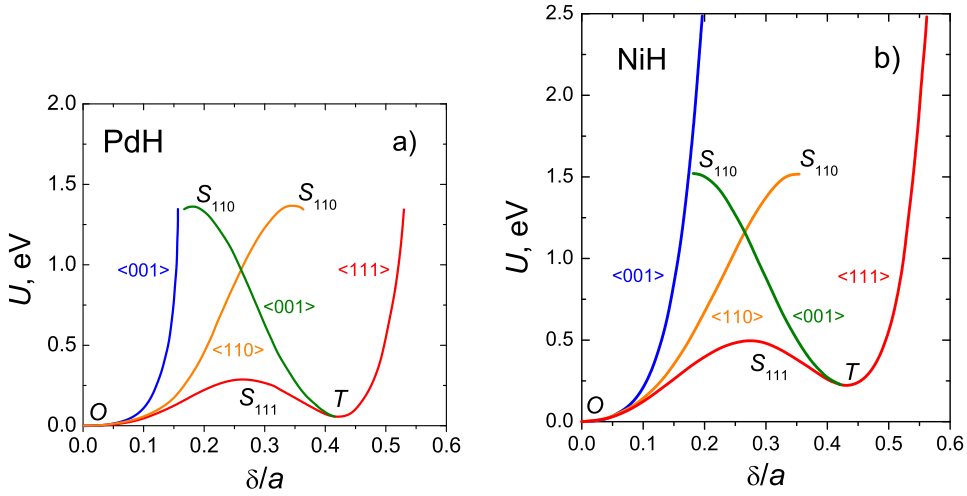

Fig. 20. The calculated profiles $U(\delta/a)$ of the potential energy in the < 001 > , < 110 > , and < 111 > directions for an H atom (a) in fcc-PdH with a = 4.07 Å [163] and (b) in fcc-NiH with a = 3.65 Å [98]. The displacements δ/a are measured from the octahedral minimum labeled as O. T is the tetrahedral minimum; S_{111} and S_{110} are saddle points.

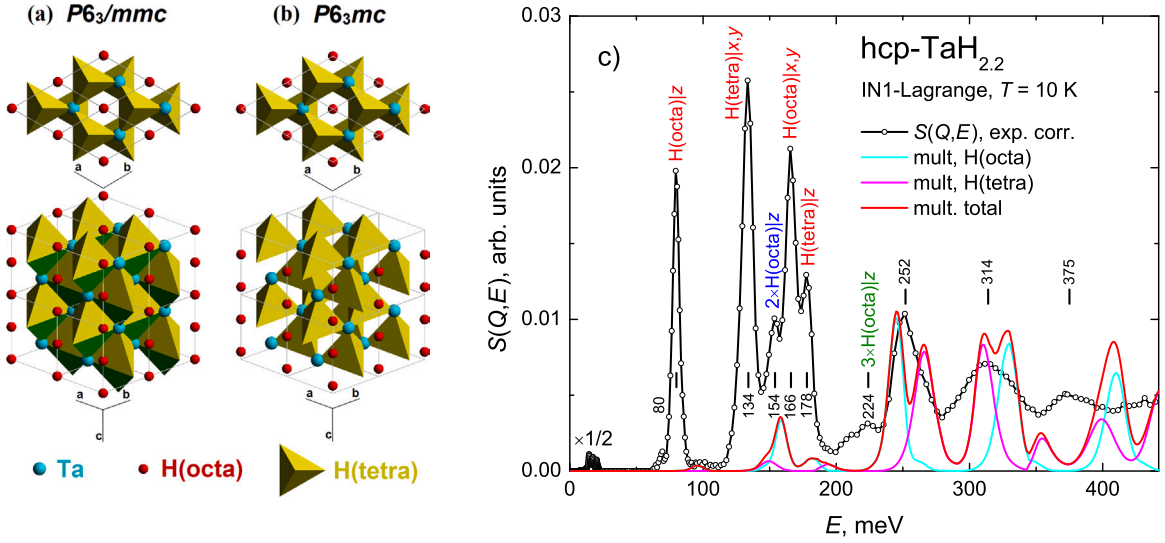

Fig. 21. [67]. An ordered (a) and, for comparison, a disordered (b) models of the arrangement of hydrogen atoms in the octahedral (O) and tetrahedral (T) interstitial sites of the hcp metal lattice of TaH_2. The Ta and H(octa) atoms are shown with large cyan and small red spheres, respectively; the tetrahedra show the T sites occupied by the H(tetra) atoms. In each model, shown in two projections, H atoms fill all the O-sites and one half of the T-sites. In the ordered $P6_3mc$ model (a) which represents the experimentally determined crystal structure of $TaH_{2.2}$, H(tetra) atoms fill only the T-sites with the lower z coordinate. The H(octa) and H(tetra) atoms are displaced from the centers of the corresponding interstices by − 0.12c and + 0.006c, respectively, along the z axis. In the disordered $P6_3/mmc$ model (b), H(tetra) atoms are randomly distributed among all available T sites. (c) The "corrected" dynamical structure factor $S(Q,E)$ of a powder hcp-$TaH_{2.2}$ sample (open black circles connected with a black curve), and the estimated contributions from multiphonon neutron scattering on the H(octa) atoms (cyan curve), H(tetra) atoms (magenta curve) and the sum of these contributions (red curve). The $S(Q,E)$ spectrum is composed of the acoustic part in the range of the neutron energy transfers E < 25 meV calculated using DFT and of the optical part at E > 60 meV measured at 10 K with the IN1-Lagrange spectrometer [67]. The vertical bars show the centers of the experimental peaks.

As noted in Ref. [50], the calculations [163] also predicted a threshold energy of about 250 meV between adjacent octa- and tetrahedral sites in the < 111 > directions (see the red curve with a saddle point S_{111} in Fig. 20a). This suggests that the higher vibrational states of H atoms in PdH should have somewhat delocalized wave functions in these directions, explaining the absence of higher energy levels in the $\psi = 45°$ spectrum (Fig. 18a).

Similar *ab initio* calculations for fcc-NiH [98] gave analogous results (see Fig. 20b), but the steepness of the potential wells increased compared to fcc-PdH [163]. According to [98], this change was mainly due to the smaller unit-cell volume of NiH (the authors used the theoretical equilibrium lattice constants a = 4.07 Å for PdH [163] and a = 3.65 Å for NiH [98] instead of experimental values of a = 4.09 Å and a = 3.74 Å, respectively [93]). Due to the higher value of about 500 meV of the potential in the saddle point S_{111} separating the minima at the octa- and tetrahedral sites (see the red curve in Fig. 20b), the wave functions of the second and third vibrational states in NiH are less delocalized in the < 111 > directions than in PdH, so that both the second and third optical bands of the INS spectrum of NiH are clearly seen (Fig. 18a).

Note once again that the first (fundamental) optical hydrogen band in PdH and NiH is practically isotropic, and strong anharmonicity is only observed in the second and higher bands for neutron momentum transfers **Q** directed close to one of the < 100 > axes. For other directions of **Q**, the INS spectrum remains nearly harmonic. Presumably, the anharmonicity of optical vibrations exclusively in the directions from the H atom to the nearest metal atoms is characteristic of monohydrides of all d-metals of groups VI–VIII (except for Rh), in which H atoms sit at the centers of octahedral interstices in the close-packed metal lattice of any type (fcc, hcp, or dhcp). In the powder INS spectra of these hydrides averaged over all orientations of **Q**, the contribution from the anharmonic vibrations

was small; therefore the spectra showed only small deviations from the isotropic harmonic behavior, at least in the energy range of the first, second and third optical bands.

6.2. Anisotropy and anharmonicity of optical vibrations in hcp-$TaH_{2.2}$ [67]

The relative weakness of the effects of anisotropy and anharmonicity in the optical spectra of powdered monohydrides of d-metals of groups VI–VIII can be illustrated by comparison with the INS results for the dihydride of a group V metal – tantalum. This dihydride has recently been obtained under high hydrogen pressure [164] and demonstrates how strong the anisotropy and anharmonicity of the optical H vibrations can be [67].

A single-phase powder sample of $TaH_{2.2(1)}$ weighing 325 mg was synthesized at 9 GPa and 373 K and studied at ILL by neutron diffraction at 100 K using the D20 diffractometer and by inelastic neutron scattering at 10 K using a new high-luminosity IN1-Lagrange spectrometer [165], which replaced the IN1-BeF spectrometer. According to the neutron diffraction data, the sample had an hcp metal lattice (space group $P6_3/mmc$) with a = 3.223 Å, c = 5.143 Å, and c/a = 1.596, in which H atoms occupied all octahedral (O) interstices and one half of tetrahedral (T) interstices that corresponds to the stoichiometric composition TaH_2 (the statistical accuracy of the diffraction pattern was insufficient to determine the crystallographic positions of the "overstoichiometric" hydrogen δ(H/Ta) = 0.2). In agreement with the theoretical predictions [166], the arrangement of the H atoms over the T-sites was proven to be ordered, which lowered the symmetry of the full crystal structure of the dihydride to $P6_3mc$. Due to the resulting asymmetry in the local environment of the O-sites, the H(octa) atoms are significantly displaced by $0.12c \approx 0.6$ Å from the centers of the O-sites along the z axis in the direction opposite to the nearest neighboring H(tetra) atoms. The H(tetra) atoms are also displaced from the centers of the T-sites along the z axis away from the nearest H(octa) atoms, but the displacement is much smaller and only amounts to $0.006c \approx 0.03$ Å. The ordered structure $P6_3mc$ of tantalum dihydride is schematically shown in Fig. 21a in comparison with the disordered structure $P6_3/mmc$ presented in Fig. 21b (hcp-$MoH_{1.1}$ hydride is expected to have this $P6_3/mmc$ structure with a 5% filling of the T-sites [46]).

As seen from Fig. 21c, the optical vibrations of H atoms at both the T- and O-sites are highly anisotropic and anharmonic. As for the anisotropy, the potential wells at the O-sites are softer along the z axis than in the x, y plane, while the T-sites show opposite anisotropy. Namely, the fundamental optical band of the H(octa) vibrations is split into two peaks located at H(octa)$|z$ = 80 meV and H(octa)$|x,y$ = 166 meV, and the band of the H(tetra) vibrations consists of two peaks at H(tetra)$|z$ = 178 meV and H(tetra)$|x,y$ = 134 meV. The splitting of the band of the H(octa) vibrations along the z axis is so large that the peak of the second band (denoted as 2 ×H(octa)$|z$ in Fig. 21c) appears at 154 meV, below the fundamental peak of the H (octa) vibrations in the x, y plane, which is located at H(octa)$|x,y$ = 166 meV. As for the anharmonicity, the peak of the second band of the H(octa) vibrations polarized along the z axis is observed at 154 meV instead of 2 × 80 = 160 meV expected for the harmonic excitations, and the peak of the third band is at 3 ×H(octa)$|z$ = 224 meV instead of 3 × 80 = 240 meV. The calculated "harmonic" energies of other multiphonon processes of neutron scattering on the H(octa) and H(tetra) atoms are also overestimated. This suggests a trumpet-like shape of the potential well for both H(octa) and H(tetra) atoms. The effect is also called soft anharmonicity: the higher the energy of the excited state, the smaller the energy difference between the consecutive states.

As noted in Ref. [67], the potential well for the H(octa) atom is mostly formed by the six nearest Ta atoms, and this environment has nearly cubic symmetry because the ratio of c/a = 1.596 of the hcp Ta lattice of tantalum dihydride is close to the "ideal" value of $(c/a)_{id} = \sqrt{8/3} \approx 1.633$. Therefore, it is the interaction with the nearest H (tetra) atoms, which breaks the cubic symmetry of the potential well at the O-sites, pushes H(octa) atoms away from the geometrical center of the octahedral interstices and leads to the strong anisotropy of the H(octa) vibrations.

Mention also that in contrast to the "45°" anisotropy of the optical spectra of fcc-PdH [50] and fcc-NiH [95] (the difference is maximal for the vibrations polarized along the < 001 > and < 110 > axes oriented at an angle of 45° to each other), the spectrum of hcp-$TaH_{2.2}$ [67] shows a usual "90°" anisotropy (the spectra with $\boldsymbol{Q}$ parallel and perpendicular to the c-axis differ the most).

Recent synchrotron x-ray diffraction studies of the Ta-H system in diamond anvil cells have revealed a formation of tantalum trihydride TaH_3 with a cI16-type structure of the metal lattice at room temperature and hydrogen pressures above 60 GPa [167].

7. Isotopic dependence of the frequency of optical vibrations in hydrides of palladium [51], nickel [32], and molybdenum [46]

Interest in the anharmonicity and isotopic dependence of optical vibrations in palladium hydrides PdH_x is mainly due to the unusual inverse isotope effect in the superconductivity of these hydrides. Namely, the temperature $T_c \approx 11.7$ K of the superconducting transition in PdD proved to be higher than $T_c \approx 9.5$ K in PdH [153,168,169]. The effect is called inverse because it contradicts the Bardeen-Cooper-Schrieffer (BCS) theory of phonon-mediated superconductivity in a harmonic approximation [170], which predicts that the superconducting critical temperature should be proportional to the phonon frequencies. Therefore, since the isotopic substitution of H by heavier D lowers the frequencies of all phonons, it should normally decrease the T_c of the hydride.

In fact, most superconducting hydrides demonstrate the normal isotope effect in accordance with the theoretical predictions: bcc-$SH(D)_3$ [171], fcc-$LaH(D)_{10}$ [172], bcc-$YH(D)_6$ [173,174], hcp-$YH(D)_9$ [174], hcp-$CeH(D)_9$ [175], and many others. One hydride, $cI16$-$Th_4H(D)_{15}$ [176], shows a zero isotope effect. Three hydrides, fcc-PdH(D) [168], face centered orthorhombic $TiH(D)_{0.71}$ [177], and hcp-MoH(D) [147]), exhibit the inverse isotope effect.

Among the hydrides of the last group, fcc-PdH(D) has been studied most extensively both theoretically and experimentally, but the origin of the inverse isotope effect has not been established with certainty. Theoretical considerations suggest (see, *e.g.*, [178] and references therein) that the superconductivity in palladium hydrides arises mainly due to the interaction of electrons with optical vibrations of hydrogen atoms; the inverse isotope effect originates from the strong anharmonicity of these vibrations; the anharmonicity manifests itself in a large deviation of the ratio $E_H/E_D \approx 1.5$ of the fundamental frequencies of optical vibrations in PdH and PdD from the harmonic value $\sqrt{m_D/m_H} \approx \sqrt{2} \approx 1.41$, where m_D and m_H are the atomic masses of D and H.

As for the experiment, the conclusion about the strong anharmonicity of optical vibrations in palladium hydrides was mostly based on the presence of a broad shoulder of the second optical peak in the INS spectrum of a dilute solid solution fcc-$PdH_{0.014}$ [97]. In our opinion, the origin of this shoulder is rather mysterious and deserves further careful study. Similar shoulders were later observed for the second optical peaks in the INS spectra of powder samples of stoichiometric fcc-PdH [50] and fcc-PdD [51] and were fairly well explained by the two-phonon neutron scattering, *i.e.*, in the isotropic harmonic approximation (see Section 5.8, Figs. 16a and 16b). In agreement with theoretical predictions [163], an INS study of a highly textured sample of fcc-PdH revealed no anisotropy and almost no anharmonicity in the first band of its optical vibrations, which are supposed to couple to the electron system and enhance

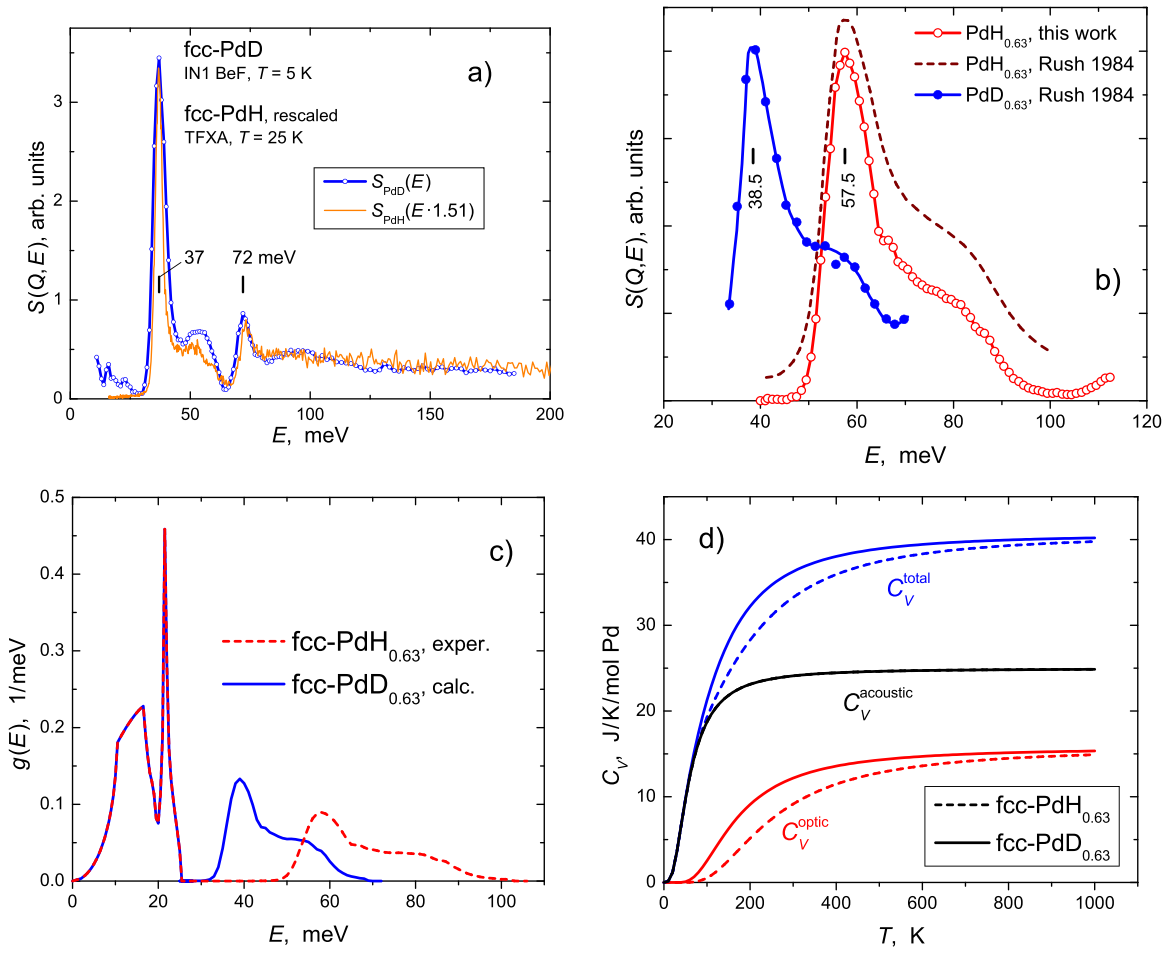

Fig. 22. (a) The INS spectrum of fcc-PdD derived from the experimental spectra of powder samples $PdD_{1-y}H_y$ measured at 5 K with the IN1-BeF spectrometer [51] (open blue circles connected with a solid blue line) and the experimental INS spectrum of a powder sample of fcc-PdH measured at 25 K with the TFXA neutron spectrometer [50] and compressed by a factor of $r = 1.51$ along the energy scale (solid orange line without circles). The vertical bars show the centers of the experimental peaks in the spectrum of PdD. The scaling factor $r = 1.51$ was chosen to reproduce the position at 37 meV of the maximum of the main optical peak in the spectrum of PdD. (b) The experimental INS spectrum of fcc-$PdH_{0.63}$ copied from Fig. 17a (open red circles, results of this paper) and the spectra of fcc-$PdH_{0.63}$ (dashed brown curve) and fcc-$PdD_{0.63}$ (solid blue curve drawn through blue circles) recalculated from the experimental data of Ref. [97]. (c) The phonon density of states $g(E)$ for fcc-$PdD_{0.63}$ (solid blue curve) calculated from $g(E)$ for fcc-$PdH_{0.63}$ (Fig. 17b), whose optical part was rescaled using $E_H/E_D = 1.49$ in accordance with Ref. [97]. (d) Heat capacities $C_V(T)$ for fcc-$PdD_{0.63}$ (solid curves) and fcc-$PdH_{0.63}$ (dashed curves) resulting from the $g(E)$'s presented in figure (c).

the superconductivity of palladium hydrides [178,179] (see Section 6.1). Since calculations of the effect of hydrogen on the superconductivity of metal hydrides include the summation over all polarizations of hydrogen optical vibrations, this practically excludes a significant contribution from the anharmonicity of vibrations in the first and second optical bands.

Another unusual experimental finding of Ref. [97] was an anomalously large "anharmonic" ratio $E_H/E_D = 1.49(1)$ of the energies of the first (fundamental) peaks of optical vibrations in dilute solid solutions $PdH_{0.014}$ and $PdD_{0.014}$ and in non-stoichiometric hydride $PdH_{0.63}$ and deuteride $PdD_{0.63}$. As shown in Fig. 22a, virtually the same ratio $E_H/E_D = 1.51$ was later obtained from a comparison of the INS spectra of powder samples of stoichiometric PdH [50] and PdD [51]. As seen from Fig. 22b, the shape and position of the fundamental peak in the spectrum of $PdH_{0.63}$ measured in Ref. [97] are also in good agreement with the results of the present paper. Therefore, we considered the scaling factor $E_H/E_D \approx 1.5$ to be reliably determined for the PdH_x phases of any composition and calculated the phonon density of states (Fig. 22c) and heat capacity (Fig. 22d) of fcc-$PdD_{0.63}$ using the experimental value of $E_H/E_D = 1.49$ from Ref. [97].

The scaling factor E_H/E_D was earlier experimentally determined for rather many binary metal hydrides with different crystal structures and different types of chemical bonds, and most hydrides were shown to have $E_H/E_D < \sqrt{2}$. For example, this factor equals to 1.34 for TaH(D) with H(D) atoms at the tetrahedral (T) interstices of the bcc metal lattice [66]; 1.35–1.37 for $AlH(D)_3$ with H(D) atoms between two Al atoms in a distorted primitive simple cubic metal lattice [7]; 1.37 for $YH(D)_2$ (T-sites in the fcc lattice) [36]; 1.37 for γ-ZrH(D) (T-sites in the face centered orthorhombic lattice) [39,180]; 1.37–1.41 for $NbH(D)_{0.85}$ (T-sites in the bcc lattice) [43]; 1.40 for $LaH(D)_3$ (octahedral (O) and T-sites in the fcc lattice) [181]; 1.40 for $UH(D)_3$ (T-sites in the A15-type metal lattice) [182]; 1.41 for LiH(D) (O-sites in the fcc lattice) [183]. The values of $E_H/E_D < \sqrt{2}$ are characteristic of the hydrides with "soft" (trumpet-like) anharmonicity of the potential wells for H(D) atoms. Large $E_H/E_D = 1.49 > \sqrt{2}$ was observed for the second optical peak in the strongly anisotropic and anharmonic INS spectra of bcc-$V_2H(D)$ [184], in which H(D) atoms vibrate inside the O-sites with a double-well potential [18].

Among the studied hydrides, only palladium hydride combines the isotropy of the fundamental optical vibrations with the ratio $E_H/E_D \approx 1.5$ considerably exceeding $\sqrt{2}$. Assuming that the atoms of H and D see the same potential, such a ratio suggests a well-like type of the potential well (the steepness of the potential increases with the distance δ/a from the center of the O-site). On the other hand, the ratios of the energies of the main peaks in the second and first

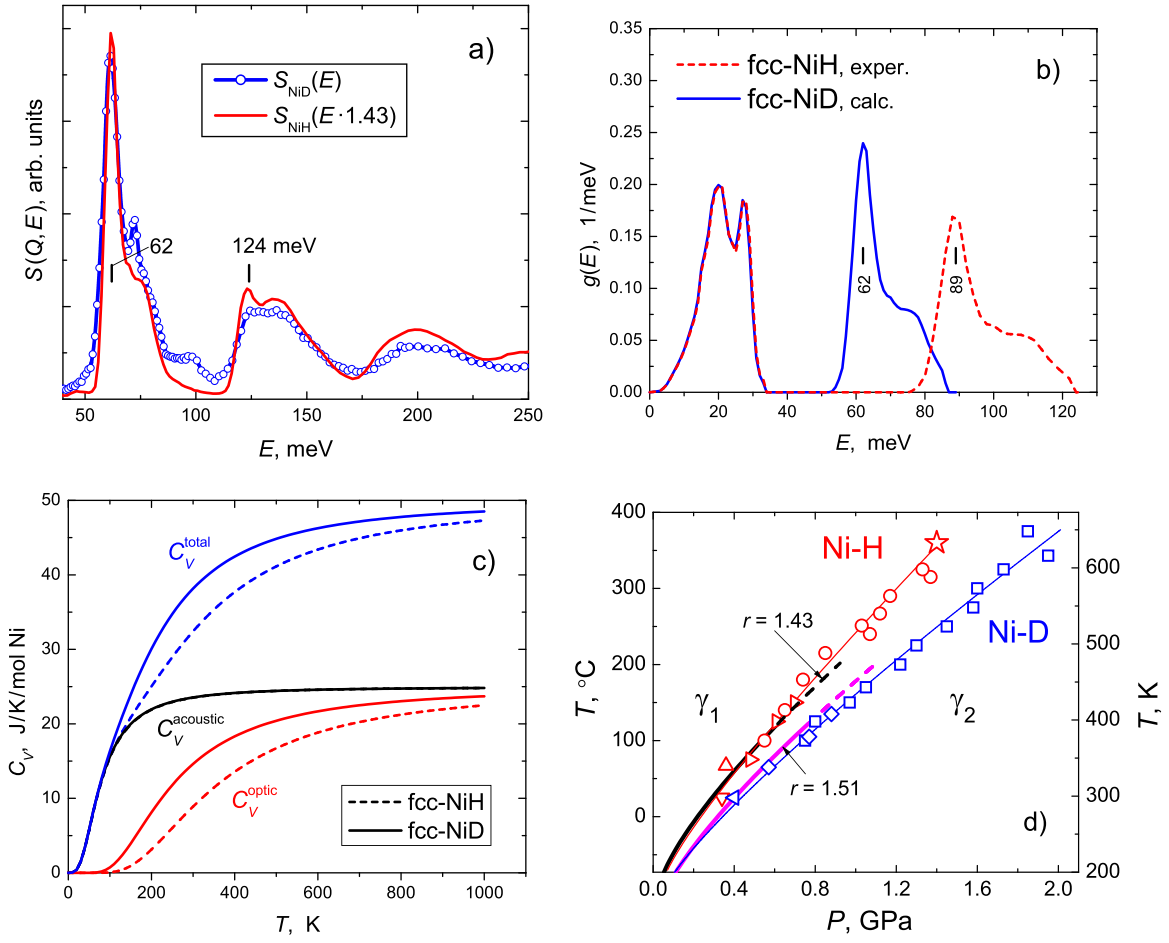

Fig. 23. (a) The INS spectrum of a powder sample of fcc-NiD (open blue circles) [32] and the "45°" spectrum of the textured polycrystalline sample of fcc-NiH [95] compressed by a factor of 1.43 along the energy scale (solid red curve). The spectra were measured with the IN1-BeF spectrometer at $T = 5$ K and 10 K, respectively. The scaling factor 1.43 was chosen to reproduce the position at 62 meV of the maximum of the main optical peak in the spectrum of NiD. The vertical bars show the centers of the experimental optical peaks in the spectrum of NiD. (b) The phonon density of states $g(E)$ for fcc-NiD (solid blue curve) calculated from $g(E)$ for fcc-NiH (dashed red curve; copied from Fig. 13b). (c) Heat capacities $C_V(T)$ for fcc-NiD (solid curves) and fcc-NiH (dashed curves) resulting from the $g(E)$'s presented in figure (b). (d) Temperature dependences of the decomposition pressures of γ_2 phases in the Ni–H and Ni–D systems [32]. The experimental dependences are shown by symbols fitted with thin solid curves, which are red for γ_2-NiH_x and blue for γ_2-NiD_x. The thick magenta and black curves show the dependences for the γ_2-NiH phase calculated from the experimental dependence for the γ_2-NiD phase using the scaling factors $r = 1.51$ and 1.43, respectively.

optical bands in the INS spectra of PdH (110/56 = 1.964, see Fig. 16a) and PdD (72/37 = 1.946, see Fig. 16b) are both lower than a harmonic value of 2. This suggests a trumpet-like type of the potential well (with the steepness decreasing with increasing δ/a). This discrepancy can only be eliminated under the assumption that H atoms in PdH and D atoms in PdD vibrate in slightly anharmonic, trumpet-like potential wells, but the Pd-H force constants in Pd-H are stronger than Pd-D constants in PdD. As was first conjectured in Ref. [185], the strengthening of the H-Pd interaction compared to the D-Pd interaction can be due to the larger amplitude of zero-point vibrations of the H atoms. Note that this mechanism of the increase in the E_H/E_D ratio should not necessarily lead to anharmonicity of the H optical vibrations.

To find out what values of E_H/E_D are characteristic of monohydrides of d-metals of VI–VIII groups, we measured an INS spectrum of fcc-NiD, a close chemical and structural analogue of fcc-PdD [32]. A 3 g sample of NiD was prepared at the Institute of Physical Chemistry PAS, Warsaw, by a reaction of powdered nickel metal of 99.5 wt% purity and grain size of 3–7 μm with a D_2 gas of 99.995 wt% purity compressed to 0.9 GPa at room temperature using the high-pressure apparatus described in Ref. [186]. The obtained fcc-NiD phase had a lattice parameter of $a = 3.724(4)$ Å determined at 85 K by x-ray diffraction.

The INS spectrum $S(Q,E)$ of the NiD sample was measured at 10 K with the IN1-BeF spectrometer and shown in Fig. 23a together with the spectrum of NiH, which was previously measured at 10 K with the same neutron spectrometer [95] and compressed along the energy scale by a factor of $r = 1.43$. As one can see, the two spectra are very similar. Small differences in these spectra are due to impurity of less than 0.1 at% H in the NiD sample [32]. Namely, the hump at energies of 86–106 meV originates from the H local modes and a parasitic peak at approx. 72 meV (superimposed onto the high-energy shoulder of the main optical peak of NiD) is likely to result from the band of covibrations of the H and D atoms (such a band located at energies right above the main optical peak was observed in hydrogen-doped PdD samples [51]).

In view of the contamination of the $S(Q,E)$ spectrum of NiD with scattering intensity from the H impurity, the optical part $g_{NiD}^{optic}(E)$ of the total density $g_{NiD}(E)$ of phonon states for NiD was calculated from $g_{NiH}^{optic}(E)$ assuming that $g_{NiD}^{optic}(E) = r \cdot g_{NiH}^{optic}(E \cdot r)$ and using $r = 1.43$. The acoustic part $g_{NiD}^{acoustic}(E)$ was calculated similarly using $r = \sqrt{m_{NiD}/m_{NiH}} \approx 1.008$. The obtained $g_{NiD}(E)$ shown in Fig. 23b was further used to calculate the heat capacities for NiD shown in Fig. 23c.

The experimental $g_{NiH}(E)$ and "rescaled" $g_{NiD}(E)$ were also used to calculate the difference between the decomposition pressures of NiH

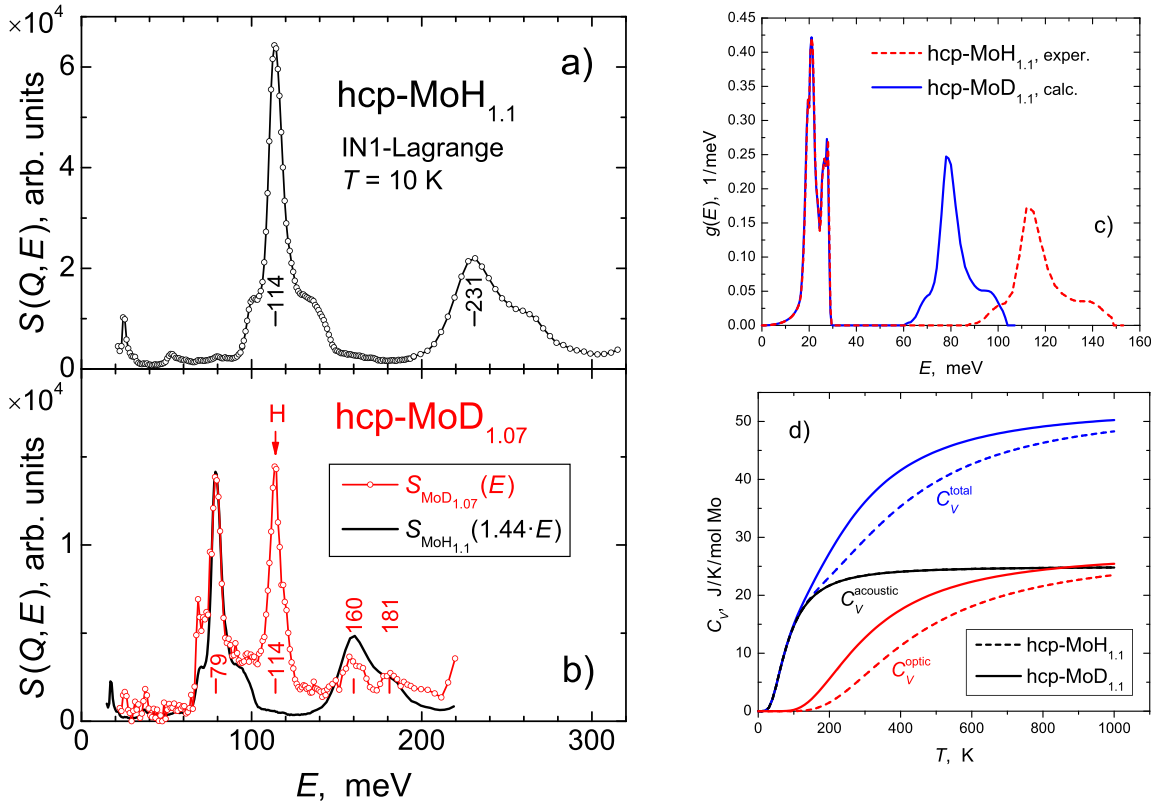

Fig. 24. The INS spectra of powder samples of (a) hcp-$MoH_{1.1}$ (black circles) and (b) hcp-$MoD_{1.07}$ (red circles) [46]. Both spectra are measured at 10 K with the IN1-Lagrange neutron spectrometer. The solid black curve in figure (b) shows the spectrum of hcp-$MoH_{1.1}$ compressed along the energy scale by a factor of 1.44 in order to reproduce the position at 79 meV of the maximum of the main optical peak in the spectrum of $MoD_{1.07}$. The vertical bars show the centers of the experimental optical peaks. (c) The phonon density of states $g(E)$ for hcp-$MoD_{1.1}$ (solid blue curve) calculated from $g(E)$ for hcp-$MoH_{1.1}$ (dashed red curve; copied from Fig. 14b). (d) Heat capacities $C_V(T)$ for hcp-$MoD_{1.1}$ (solid curves) and hcp-$MoH_{1.1}$ (dashed curves) resulting from the $g(E)$'s presented in figure (c).

and NiD (the decomposition pressure of a hydride is usually much closer to the equilibrium value than the formation pressure [187]). As seen from Fig. 23d, the calculation using $r = 1.43$ well reproduced the experimental dependence of this difference in a rather wide temperature interval of ± 100 K around room temperature, where the compositions of nickel hydride and deuteride are close to NiH and NiD. Using $r = 1.51$ characteristic of the Pd-H/D system resulted in the dependence inconsistent with experiment.

We can therefore conclude that the anomalously high value of $E_H/E_D \approx 1.5$ for the PdH_x and PdD_x phases distinguishes the Pd-H/D system from most other Me-H/D systems including its closest analogue, the Ni-H/D system. It was reasonable to expect that the unusual E_H/E_D ratio and the unusual inverse isotope effect in the superconductivity of the Pd-H/D system are interrelated. To learn whether a large E_H/E_D ratio is a prerequisite for the inverse isotope effect in metal hydrides, we studied INS spectra of molybdenum hydride and deuteride [46]. These hydride and deuteride are superconductors with $T_c = 0.92$ K and 1.11 K, respectively [147]. Assuming the ratio of the superconducting temperatures of deuteride and hydride as a measure of the magnitude of the isotope effect, this gives similar values of 1.11/0.92 ≈ 1.21 for $MoD_{1.26}$ and $MoH_{1.27}$ [147] and 11.7/9.5 ≈ 1.23 for PdD and PdH [153,168,169].

Single-phase powder samples $MoH_{1.1(1)}$ weighing 1114 mg and $MoD_{1.07(3)}$ weighing 99 mg were made of high-purity single-crystal molybdenum foil 0.2 mm thick with the electrical resistance ratio $R_{300\,K}/R_{4.2\,K} \approx 1000$, which was loaded, respectively, with hydrogen at 5 GPa, 350 °C and with deuterium at 7.4 GPa, 300 °C. Figs. 24a and 24b show the INS spectra of these samples measured at 10 K with the IN1-Lagrange neutron spectrometer at ILL [46].

The INS spectrum of the powder $MoH_{1.1}$ sample (Fig. 24a) well agrees with the spectrum of polycrystalline $MoH_{1.1}$ studied earlier [96] with the IN1-BeF spectrometer (Fig. 14a). This coincidence excludes the presence of significant distortions in the spectrum of the polycrystalline sample (Fig. 14a) due to its texture. The new powder $MoH_{1.1}$ sample was measured with the same experimental setup as the $MoD_{1.07}$ sample that allows a direct comparison of their INS spectra.

The $MoD_{1.07}$ sample was noticeably contaminated with protium released from the isotopically impure AlD_3 compound used as an internal deuterium source in the high-pressure cell. The protium concentration in the studied sample of molybdenum deuteride could roughly be estimated as H/(D+H) = 0.07, based on the intensity of the peak at 114 meV of the local (defect) mode of hydrogen vibrations in the INS spectrum (Fig. 24b, open red circles). Other features of the INS spectrum of this sample can be fairly well reproduced by the spectrum of $MoH_{1.1}$ compressed along the energy scale by a factor of $r = 1.44$ (solid black curve in Fig. 24b). These include the main peak at 79 meV in the first optical band and also the peak at 160 meV with the shoulder at 181 meV in the second optical band.

As in the case of NiD with the INS spectrum contaminated with scattering intensity from the H impurity (Fig. 23a), the optical part $g^{optic}_{MoD_{1.1}}(E)$of the total density $g_{MoD_{1.1}}(E)$ of phonon states for $MoD_{1.1}$ was calculated from $g^{optic}_{MoH_{1.1}}(E)$ assuming that $g^{optic}_{MoD_{1.1}}(E) = r \cdot g^{optic}_{MoH_{1.1}}(E \cdot r)$ and using $r = 1.44$. The acoustic part $g^{acoustic}_{MoD_{1.1}}(E)$ of $g_{MoD_{1.1}}(E)$ was calculated in the same way using $r = \sqrt{m_{MoD_{1.1}}/m_{MoH_{1.1}}} \approx 1.006$. The resulting spectrum $g_{MoD_{1.1}}(E)$ is shown in Fig. 24c. The spectra $g^{optic}_{MoD_{1.1}}(E)$, $g^{acoustic}_{MoD_{1.1}}(E)$, and$g_{MoD_{1.1}}(E) = g^{optic}_{MoD_{1.1}}(E) + g^{acoustic}_{MoD_{1.1}}(E)$ were further used to calculate the heat capacities $C_V^{optic}(T)$, $C_V^{acoustic}(T)$, and $C_V^{total}(T)$ for $MoD_{1.1}$ depicted in Fig. 24d.

The energy interval and the distribution of the scattering intensity in the second and third optical bands in $MoH_{1.1}$ are well reproduced by the spectrum of multiphonon neutron scattering (see Fig. 14a), *i.e.*, in a harmonic approximation. The energy ratio of the peaks in the second and first optical bands of $MoD_{1.07}$ is also close to a harmonic value of 2 (see Fig. 24b). Finally, the INS spectrum of optical vibrations in $MoD_{1.07}$ is well fitted by the spectrum of $MoH_{1.1}$ compressed by the energy scale by a factor of $r = 1.44$ close to a harmonic value of $\sqrt{2}$ (Fig. 24b). Taken together, these findings suggest that the H atoms in $MoH_{1.1}$ and the D atoms in $MoD_{1.07}$ vibrate in very similar and almost parabolic potential wells. Such a result is rather unexpected because it precludes from any simple explanation of the inverse isotope effect in the superconductivity of molybdenum hydride. The currently available *ab-initio* calculations [188] also failed to determine the correct sign of the isotope effect for hcp-MoH(D).

In any case, the INS studies of molybdenum hydride and deuteride have unambiguously shown that neither strong anharmonicity of optical vibrations, nor the anomalously large ratio of $E_H/E_D \approx 1.5$ is necessary for the presence of the inverse isotope effect in superconductivity of metal hydrides. The reasons for the inverse isotope effect in both molybdenum and palladium hydride remain a mystery to be solved.

8. Concluding remarks

This review paper mainly considers the results of INS studies of high-pressure monohydrides of d-metals of VI–VIII groups, which proved to be the most informative and amenable to unambiguous interpretation due to the simple crystal structures and almost harmonic behavior of optical hydrogen vibrations. Meanwhile, applying inelastic neutron scattering to the investigation of much more complicated vibrational spectra of higher hydrides and hydrides of the alloys and multi-component intermetallic compounds can be very valuable. First, this concerns hydrides that are promising in applications as hydrogen storage materials. A comprehensive overview of INS studies carried out on the various hydrides of such type can be found in Ref. [189]. The available INS data obtained for a variety of ternary metal hydrides and related to their hydrogen storage properties are reviewed in Ref. [190]. The review paper [191] considers representative studies in the light-weight hydrogen storage materials characterized by neutron scattering techniques including INS. Several experimental studies have been devoted to the INS studies of hydrogen storage materials with high H storage capacities formed by light metals, such as Mg_2NiH_4 [192] and metal alanates $LiAlH_4$ and $Ca(AlH_4)_2$ [193].

Around 20 years ago [194], neutron diffraction studies revealed the presence of Ni–D···D–Ni–D···D–Ni chains containing anomalously close D···D contacts of ≈ 1.56–1.63 Å which were found in the deuterated *R*NiIn compounds (*R* = Ce, La, Nd). A recent INS investigation of quaternary hydrides $LaNiInH_{1.6}$ and $CeNiInH_{1.4}$ showed that these close H···H contacts are indeed present and manifest themselves with a specific double-peak feature clearly visible in the INS spectra and originating from the H-Ni-H bending and H-Ni-H rocking vibrations when Ni-H bond distances are very short, around 1.5 Å [195]. This demonstrates that neutron spectroscopy can become one of the effective means of characterization of the hydrides that violate the so-called "blocking rule" postulating a minimum distance of about 2 Å between individual H atoms in the metal lattice [112], which causes the limitations of the maximum volumetric hydrogen capacity of a particular material.

Many interesting materials providing valuable INS studies data are among the hydrides of metal alloys, too. As an example, under a hydrogen pressure of a few GPa and elevated temperature, disordered fcc alloys PdCu and PdAg undergo atomic ordering and form nearly stoichiometric hydrides $PdCuH_{0.9}$ and $PdAgH_{0.9}$ with primitive tetragonal unit cells composed of alternate layers of, respectively, Pd and Cu atoms [196] and Pd and Ag atoms [197] with hydrogen atoms occupying the Pd layers only. An INS study of these hydrides showed [196] that their fundamental optical bands are split into two peaks corresponding to the H vibrations polarized parallel and perpendicular to the Pd planes. This made it possible to isolate the contributions from the Pd-H, Cu-H, and Ag-H interactions and to roughly estimate the energies of 93 and 116 meV of local H vibrations, respectively, in dilute the Cu-H and Ag-H solid solutions.

Inelastic neutron scattering has also been proven to be an effective tool for studying high-pressure hydrocarbons. In particular, applying high hydrogen pressure increases the hydrogen content of hydrofullerites $C_{60}H_x$ from $x \approx 24$ at $P = 0.6$ GPa to $x \approx 60$ at $P = 5$ GPa when saturated by hydrogen bucky balls containing only singular C-C bonds are formed [198]. An INS investigation of a single-phase sample of bcc $C_{60}H_{27}$ loaded with hydrogen at 0.6 GPa and 623 K and quenched to the liquid N_2 temperature showed that it consists of $C_{60}H_x$ molecules with $x \approx 24$ and interstitially accommodated molecular hydrogen [199]. The interstitial hydrogen amounted to about 1.4 H_2 molecules per one C_{60} unit ($H_2/C \approx 0.023$) and evolved from the sample when heated to room temperature, while the $C_{60}H_{24}$ molecules appeared to be stable at such conditions. An INS investigation of a sample of the hydrogenated single-wall carbon nanotubes, which was synthesized at 3 GPa and 620 K and had the composition $CH_{0.66}$, also showed the presence of a similar amount of molecular hydrogen ($H_2/C \approx 0.03$) along with the H atoms covalently bound to the carbon atoms [200]. Heating the sample to 623 K in vacuum removes all molecular hydrogen, while the release of the covalently bound hydrogen starts at approx. 740 K and continues up to 900 K.

One novel hydrocarbon synthesized at high pressures is a multilayer graphane (hydrographite) which shows a high saturation with hydrogen and a composition close to CH [201]. It is formed from graphite and gaseous hydrogen at pressures above 2 GPa and temperatures from 720 to 970 K; its crystal structure belongs to the space group $P6_3mc$ and consists of one-layer sheets of graphane in the chair conformation stacked along the hexagonal *c* axis in the –ABAB– sequence. Hydrographite is thermally stable under ambient conditions and decomposes into graphite and molecular H_2 when heated in vacuum above 770 K. An attempt to study the lattice dynamics of hydrographite by infrared spectroscopy failed [201] because the penetration depth of the light is small and the light scattering by various defect states at the sample surface was observed instead of the light absorption by the regular crystal structure of the bulk sample. Hydrographite has never been studied by neutron scattering methods and it could be in focus of the future studies by neutron spectroscopy.

Low-concentration solid solutions of hydrogen in metals with fcc and hcp crystal structures are also promising materials for the future INS studies. An INS investigation of a powder and a single-crystalline samples of $ReH_{0.09}$ hydrogenated at 6 GPa and 598 K showed that their fundamental optical band was split into two sharp peaks centered at 100 and 130 meV, which corresponded to the vibrations polarized along the *c* axis and in the basal plane of the crystal lattice, respectively [68]. While the occurrence of the splitting agrees with the crystal symmetry of the Re–H solid solutions, the large magnitude of the effect is difficult to explain. In fact, according to the neutron diffraction study, hydrogen atoms randomly occupy octahedral interstices in the hcp metal lattice of $ReH_{0.09}$, and are not shifted from the centers of these interstices, which show nearly cubic symmetry [68]. In addition to the unknown reason for the band splitting, there seemed to be no chances that this band would

transform into a single narrow peak of independent local vibrations of H atoms when the hydrogen concentration of the solid solution tends to zero.

In the case of the palladium-hydrogen system, the suggested small width and the absence of a shoulder of the main peak in the optical spectra of dilute solid solutions $PdH_{0.014}$ and $PdD_{0.014}$ studied by INS in Ref. [97] also raise questions because of the insufficient energy resolution of the experimental spectra and the presence of a broad and intense shoulder of the peak in the second optical band of the $PdH_{0.014}$ sample. The INS spectra of low-concentration Pd-H solutions cannot be interpreted with certainty due to a rapid decrease in the hydrogen solubility for the primary solid solutions with decreasing temperature causing a possible clustering of hydrogen. Solid solutions of hydrogen in Re, Ru, and Co, which are formed at high hydrogen pressures (see [93] and references therein), are apparently devoid of this drawback and a careful study of the evolution of their INS spectra with decreasing hydrogen concentration can show whether the optical band shrinks to a narrow peak as the concentration tends to zero.

With the discovery of high-temperature superconductivity in hydrides with unusually high hydrogen content, such as H_3S [171] and LaH_{10} [172], considerable efforts were undertaken to synthesize new hydrogen-rich materials and study their properties. Fortunately, some of the recently discovered hydrogen-rich materials, such as RhH_2 [149], Zr_4H_{15} [202], and U_4H_{15} [202,203] can be recovered to ambient pressure, paving the way to produce massive samples for the neutron scattering studies. Particularly promising are the caesium-hydrogen and rubidium-hydrogen systems, in which hydrides with composition up to CsH_9 [204] and RbH_9 [205] are predicted to be formed at pressures below 10 GPa.

To conclude, Inelastic Neutron Scattering investigations of hydrogen storage materials, particularly those hydrogenated at high pressures and studied by combining INS and neutron diffraction characterisation, provide a vast resource of the valuable data on structure and dynamics of the metal-hydrogen interactions and demonstrates a great potential of reaching new and interesting results of the fundamental studies of the structure-properties relationship in the metal-hydrogen systems assisting in a search for the materials with good prospects of their applications as efficient hydrogen storage materials and in hydrogen energy systems.

CRediT authorship contribution statement

Vladimir E. Antonov: Writing – original draft, Supervision, Writing – review & editing. **Vladimir K. Fedotov:** Writing – original draft. **Alexandre S. Ivanov:** Writing – original draft. **Alexander I. Kolesnikov:** Writing – original draft, Formal analysis. **Mikhail A. Kuzovnikov:** Writing – original draft, Formal analysis, Writing – review & editing. **Marek Tkacz:** Writing – original draft. **Volodymyr A. Yartys:** Writing – original draft, Supervision, Writing – review & editing.

Declaration of Competing Interest

The authors declare that they have no known competing financial interests or personal relationships that could have appeared to influence the work reported in this paper.

Acknowledgements

The work was partly supported by the Russian Foundation for Basic Research [Grant no. 20-02-00638]. It is also part of a project that has received funding from the European Research Council (ERC) under the European Union's Horizon 2020 research and innovation programme [Grant no. 948895, MetElOne]. AIK acknowledges the support by the Scientific User Facilities Division, Office of Basic Energy Sciences, US Department of Energy. VAY acknowledges a support from the EU Horizon 2020 program in the frame of the H2020-MSCA RISE-2017 action, HYDRIDE4MOBILITY project, with Grant agreement 778307.

Appendix A. Supporting information

Supplementary data associated with this article can be found in the online version at doi:10.1016/j.jallcom.2022.164208.

References

[1] J.M. Besson, G. Weill, G. Hamel, R.J. Nelmes, J.S. Loveday, S. Hull, Equation of state of lithium deuteride from neutron diffraction under high pressure, Phys. Rev. B 45 (1992) 2613–2619, https://doi.org/10.1103/PhysRevB.45.2613
[2] D. Colognesi, A.J. Ramirez-Cuesta, M. Zoppi, R. Senesi, T. Abdul-Redah, Extraction of the density of phonon states in LiH and NaH, Phys. B 350 (2004) E983–E986, https://doi.org/10.1016/j.physb.2004.03.271
[3] C.G. Shull, E.O. Wollan, G.A. Morton, W.L. Davidson, Neutron diffraction studies of NaH and NaD, Phys. Rev. 73 (1948) 842–847, https://doi.org/10.1103/PhysRev.73.842
[4] M. Bortz, B. Bertheville, G. Bottger, K. Yvon, Structure of the high pressure phase γ-MgH_2 by neutron powder diffraction, J. Alloy. Compd. 287 (1999) L4–L6, https://doi.org/10.1016/S0925-8388(99)00028-6
[5] A.I. Kolesnikov, V.E. Antonov, V.S. Efimchenko, G. Granroth, S.N. Klyamkin, A.V. Levchenko, M.K. Sakharov, Y. Ren, Neutron spectroscopy of magnesium dihydride, J. Alloy. Compd. 509S (2011) S599–S603, https://doi.org/10.1016/j.jallcom.2010.10.156
[6] J. Graetz, J.J. Reilly, V.A. Yartys, J.P. Maehlen, B.M. Bulychev, V.E. Antonov, B.P. Tarasov, I.E. Gabis, Aluminum hydride as a hydrogen and energy storage material: past, present and future, J. Alloy. Compd. 509S (2011) S517–S528, https://doi.org/10.1016/j.jallcom.2010.11.115
[7] A.I. Kolesnikov, V.E. Antonov, Yu.E. Markushkin, I. Natkaniec, M.K. Sakharov, Lattice dynamics of AlH_3 and AlD_3 by inelastic neutron scattering: high-energy band of optical bond-stretching vibrations, Phys. Rev. B 76 (2007) 064302, https://doi.org/10.1103/PhysRevB.76.064302
[8] E. Zintl, A. Harder, Über Alkalihydride, Z. Phys. Chem. 14B (1931) 265–284, https://doi.org/10.1515/zpch-1931-1422
[9] G. Auffermann, G.D. Barrera, D. Colognesi, G. Corradi, A.J. Ramirez-Cuesta, M. Zoppi, Hydrogen dynamics in heavy alkali metal hydrides obtained through inelastic neutron scattering, J. Phys. Condens. Matter 16 (2004) 5731–5743, https://doi.org/10.1088/0953-8984/16/32/010
[10] H. Wu, W. Zhou, T.J. Udovic, J.J. Rush, T. Yildirim, Structure and vibrational spectra of calcium hydride and deuteride, J. Alloy. Compd. 436 (2007) 51–55, https://doi.org/10.1016/j.jallcom.2006.07.042
[11] V.E. Antonov, I.O. Bashkin, V.K. Fedotov, S.S. Khasanov, T. Hansen, A.S. Ivanov, A.I. Kolesnikov, I. Natkaniec, Crystal structure and lattice dynamics of high-pressure scandium trihydride, Phys. Rev. B 73 (2006) 054107, https://doi.org/10.1103/PhysRevB.73.054107
[12] A.I. Kolesnikov, A.M. Balagurov, I.O. Bashkin, V.K. Fedotov, G.M. V.Yu. Malyshev, E.G. Mironova, Ponyatovsky, A real-time neutron diffraction study of phase transitions in the Ti-D system after high-pressure treatment, J. Phys. Condens. Matter 5 (1993) 5045–5058, https://doi.org/10.1088/0953-8984/5/29/003
[13] A.I. Kolesnikov, V.K. Fedotov, I. Natkanets, S. Khabrylo, I.O. Bashkin, E.G. Ponyatovskii, Transfer of hydrogen to octahedral lattice positions in the superconducting titanium hydride phase, JETP Lett. 44 (1986) 509–512 WOS:A1986G482900015 [Pis'ma Zh. Eksp. Teor. Fiz. 44 (1986) 396–398 (in Russian).
[14] I.O. Bashkin, A.I. Kolesnikov, M.A. Adams, Pressure effect on the hydrogen vibrations in γ-TiH and γ-ZrH, J. Phys. Condens. Matter 12 (2000) 4757–4765, https://doi.org/10.1088/0953-8984/12/22/308
[15] F.D. Manchester, A. San-Martin, H-Ti (Hydrogen-Titanium), in: F.D. Manchester (Ed.), Phase Diagrams of Binary Hydrogen Alloys, ASM International, Materials Park, 2000, pp. 238–258.
[16] S. Ikeda, N. Watanabe, K. Kai, Crystal analyser TOF spectrometer (CAT), Phys. B +C 120 (1983) 131–135, https://doi.org/10.1016/0378-4363(83)90355-8
[17] R.E. Marsh, On the structure and twinning of monoclinic β-V_2H, Acta Cryst. B43 (1987) 415–416, https://doi.org/10.1107/S010876818709757X
[18] R. Hempelmann, D. Richter, D.L. Price, High-energy-neutron vibrational spectroscopy on β-V_2H, Phys. Rev. Lett. 58 (1987) 1016–1019, https://doi.org/10.1103/PhysRevLett.58.1016
[19] J.F. Smith, D.T. Peterson, The H-V (Hydrogen-Vanadium) system, J. Phase Equilib. 3 (1982) 55–60, https://doi.org/10.1007/BF02873412
[20] D.K. Ross, P.F. Martin, W.A. Oates, R.K. Bakhsh, Inelastic neutron scattering measurements of optical vibration frequency distributions in hydrogen-metal systems, Z. Phys. Chem. 114 (1979) 221–230, https://doi.org/10.1524/zpch.1979.114.114.221
[21] V.E. Antonov, A.I. Beskrovnyy, V.K. Fedotov, A.S. Ivanov, S.S. Khasanov, A.I. Kolesnikov, M.K. Sakharov, I.L. Sashin, M. Tkacz, Crystal structure and lattice dynamics of chromium hydrides, J. Alloy. Compd. 430 (2007) 22–28, https://doi.org/10.1016/j.jallcom.2006.05.021

[22] A.V. Irodova, V.P. Glazkov, V.A. Somenkov, S.S. Shilshtein, V.E. Antonov, E.G. Ponyatovskii, Neutron-diffraction study of antiferromagnetic ordering in manganese hydrides, Fizika Tverdogo Tela 29 (1987) 2714–2720, WOS:A1987K722200024 (in Russian) [Engl. transl.: Sov. Phys. Solid State 29 (1987) 1562–1565].

[23] A.I. Kolesnikov, V.E. Antonov, V.K. Fedotov, G. Grosse, A.S. Ivanov, F.E. Wagner, Lattice dynamics of high-pressure hydrides of the group VI–VIII transition metals, Phys. B 316–317 (2002) 158–161, https://doi.org/10.1016/S0921-4526(02)00447-7

[24] V.K. Fedotov, V.E. Antonov, A.I. Kolesnikov, A.I. Beskrovnyi, G. Grosse, F.E. Wagner, Neutron diffraction investigation of γ manganese hydride, Solid State Commun. 107 (1998) 787–790, https://doi.org/10.1016/S0038-1098(98)00229-4

[25] V.E. Antonov, K. Cornell, B. Dorner, V.K. Fedotov, G. Grosse, A.I. Kolesnikov, F.E. Wagner, H. Wipf, Neutron spectroscopy of γ manganese hydride, Solid State Commun. 113 (2000) 569–572, https://doi.org/10.1016/S0038-1098(99)00535-9

[26] V.K. Fedotov, V.E. Antonov, K. Cornell, G. Grosse, A.I. Kolesnikov, V.V. Sikolenko, V.V. Sumin, F.E. Wagner, H. Wipf, Neutron scattering studies of the structure and lattice dynamics of a solid solution of hydrogen in α manganese, J. Phys. Condens. Matter 10 (1998) 5255–5266, https://doi.org/10.1088/0953-8984/10/24/004

[27] A.I. Kolesnikov, A. Podlesnyak, R.A. Sadykov, V.E. Antonov, M.A. Kuzovnikov, G. Ehlers, G.E. Granroth, Pressure effect on hydrogen tunneling and vibrational spectrum in α-Mn, Phys. Rev. B 94 (2016) 134301, https://doi.org/10.1103/PhysRevB.94.134301

[28] V.E. Antonov, K. Cornell, V.K. Fedotov, A.I. Kolesnikov, E.G. Ponyatovsky, V.I. Shiryaev, H. Wipf, Neutron diffraction investigation of the dhcp and hcp iron hydrides and deuterides, J. Alloy. Compd. 264 (1998) 214–222, https://doi.org/10.1016/S0925-8388(97)00298-3

[29] V.E. Antonov, M. Baier, B. Dorner, V.K. Fedotov, G. Grosse, A.I. Kolesnikov, E.G. Ponyatovsky, G. Schneider, F.E. Wagner, High-pressure hydrides of iron and its alloys, J. Phys. Condens. Matter 14 (2002) 6427–6445, https://doi.org/10.1088/0953-8984/14/25/311

[30] V.E. Antonov, T.E. Antonova, V.K. Fedotov, T. Hansen, A.S. Ivanov, A.I. Kolesnikov, Neutron scattering studies of γ-CoH, J. Alloy. Compd. 404–406 (2005) 73–76, https://doi.org/10.1016/j.jallcom.2004.11.107

[31] A.V. Irodova, V.P. Glazkov, V.A. Somenkov, S.S. Shilshtein, V.E. Antonov, E.G. Ponyatovskii, Neutron-diffraction investigation of molybdenum, rhodium and nickel hydrides structure, Kristallografiya 33 (1988) 769–771, WOS:A1988N644600045 (in Russian) [Engl. transl.: Sov. Phys. Crystallography 33 (1988) 453–455].

[32] V.E. Antonov, A.S. Ivanov, M.A. Kuzovnikov, M. Tkacz, Neutron spectroscopy of nickel deuteride, J. Alloy. Compd. 580 (2013) S109–S113, https://doi.org/10.1016/j.jallcom.2013.03.021

[33] N.E. Brese, M. O'Keeffe, R.B. Von Dreele, Synthesis and crystal structure of SrD_2 and SrND and bond valence parameters for hydrides, J. Solid State Chem. 88 (1990) 571–576, https://doi.org/10.1016/0022-4596(90)90255-V

[34] D. Colognesi, G. Barrera, A.J. Ramirez-Cuesta, M. Zoppi, Hydrogen self-dynamics in orthorhombic alkaline earth hydrides through incoherent inelastic neutron scattering, J. Alloy. Compd. 427 (2007) 18–24, https://doi.org/10.1016/j.jallcom.2006.03.031

[35] D. Khatamian, W.A. Kamitakahara, R.G. Barnes, D.T. Peterson, Crystal structure of $YD_{1.96}$ and $YH_{1.98}$ by neutron diffraction, Phys. Rev. B 21 (1980) 2622–2624, https://doi.org/10.1103/PhysRevB.21.2622

[36] T.J. Udovic, J.J. Rush, I.S. Anderson, Local-mode dynamics in YH_2 and YD_2 by isotope-dilution neutron spectroscopy, Phys. Rev. B 50 (1994) 15739–15743, https://doi.org/10.1103/PhysRevB.50.15739

[37] V.K. Fedotov, V.E. Antonov, I.O. Bashkin, T. Hansen, I. Natkaniec, Displacive ordering in the hydrogen sublattice of yttrium trihydride, J. Phys. Condens. Matter 18 (2006) 1593–1599, https://doi.org/10.1088/0953-8984/18/5/012

[38] S.S. Sidhu, N.S. Satya Murthy, F.P. Campos, D.D. Zauberis, Neutron and x-ray diffraction studies of nonstoichiometric metal hydrides, in: R. Ward (Ed.), Nonstoichiometric Compounds, Advances in Chemistry, American Chemical Society, Washington, 1963, pp. 87–98, https://doi.org/10.1021/ba-1964-0039.ch008

[39] A.I. Kolesnikov, I.O. Bashkin, A.V. Belushkin, E.G. Ponyatovsky, M. Prager, Inelastic neutron scattering study of ordered gamma-ZrH, J. Phys. Condens. Matter 6 (1994) 8989–9000, https://doi.org/10.1088/0953-8984/6/43/005

[40] R.E. Rundle, C.G. Shull, E.O. Wollan, The crystal structure of thorium and zirconium dihydrides by X-ray and neutron diffraction, Acta Cryst. 5 (1952) 22–26, https://doi.org/10.1107/S0365110X52000071

[41] J.G. Couch, O.K. Harling, L.C. Clune, Structure in the neutron scattering spectra of zirconium hydride, Phys. Rev. B 4 (1971) 2675–2681, https://doi.org/10.1103/PhysRevB.4.2675

[42] V.A. Somenkov, A.V. Gurskaya, M.G. Zemlyanov, M.E. Kost, N.A. Chernoplekov, A.A. Chertkov, Neutron scattering study of structure and phase transitions in niobium hydrides and deuterides, Fizika Tverdogo Tela 10 (1968) 1355–1363 (in Russian) [Engl. transl.: Sov. Phys. Solid State 10 (1968) 1076–1082].

[43] D. Richter, S.M. Shapiro, Study of the temperature dependence of the localized vibrations of H and D in niobium, Phys. Rev. B 22 (1980) 599–605, https://doi.org/10.1103/PhysRevB.22.599

[44] N.A. Chernoplekov, M.G. Zemlyanov, V.A. Somenkov, A.A. Chertkov, Study of the dynamics of group V transition-metal hydrides by means of inelastic neutron scattering, Fizika Tverdogo Tela 11 (1969) 2894–2901 (in Russian) [Engl. transl.: Sov. Phys. Solid State 11 (1970) 2343–2349].

[45] J.J. Reilly, R.H. Wiswall, Higher hydrides of vanadium and niobium, Inorg. Chem. 9 (1970) 1678–1682, https://doi.org/10.1021/ic50089a013

[46] M.A. Kuzovnikov, V.E. Antonov, T. Hansen, A.S. Ivanov, A.I. Kolesnikov, V.I. Kulakov, V.D. Muzalevsky, S. Savvin, M. Tkacz, Isotopic dependence of the frequency of optical vibrations in molybdenum monohydride, J. Alloy. Compd. 893 (2021) 162299, https://doi.org/10.1016/j.jallcom.2021.162299

[47] V.E. Antonov, T.E. Antonova, V.K. Fedotov, B.A. Gnesin, A.S. Ivanov, A.I. Kolesnikov, Anharmonicity of optical hydrogen vibrations in RhH, J. Alloy. Compd. 446–447 (2007) 508–511, https://doi.org/10.1016/j.jallcom.2006.11.150

[48] J.E. Worsham, M.K. Wilkinson, C.G. Shull, Neutron-diffraction observations on the palladium-hydrogen and palladium-deuterium systems, J. Phys. Chem. Solids 3 (1957) 303–310, https://doi.org/10.1016/0022-3697(57)90033-1

[49] J.E. Shirber, B. Morosin, Lattice constants of β-PdH_x and β-PdD_x with x near 1.0, Phys. Rev. B 12 (1975) 117–118, https://doi.org/10.1103/PhysRevB.12.117

[50] D.K. Ross, V.E. Antonov, E.L. Bokhenkov, A.I. Kolesnikov, E.G. Ponyatovsky, J. Tomkinson, Strong anisotropy in the inelastic neutron scattering from PdH at high energy transfer, Phys. Rev. B 58 (1998) 2591–2595, https://doi.org/10.1103/PhysRevB.58.2591

[51] V.E. Antonov, A.I. Davydov, V.K. Fedotov, A.S. Ivanov, A.I. Kolesnikov, M.A. Kuzovnikov, Neutron spectroscopy of H impurities in PdD: covibrations of the H and D atoms, Phys. Rev. B 80 (2009) 134302, https://doi.org/10.1103/PhysRevB.80.134302

[52] W. Bronger, S. Chi-Chien, P. Müller, Die Kristallstruktur von Bariumhydrid, ermittelt über Neutronenbeugungsexperimente an BaD_2, Z. Anorg. Allg. Chem. 545 (1987) 69–74, https://doi.org/10.1002/zaac.19875450208

[53] A. Machida, M. Honda, T. Hattori, A. Sano-Furukawa, T. Watanuki, Y. Katayama, K. Aoki, K. Komatsu, H. Arima, H. Ohshita, K. Ikeda, K. Suzuya, T. Otomo, M. Tsubota, K. Doi, T. Ichikawa, Y. Kojima, D.Y. Kim, Formation of NaCl-Type monodeuteride LaD by the disproportionation reaction of LaD_2, Phys. Rev. Lett. 108 (2012) 205501, https://doi.org/10.1103/PhysRevLett.108.205501

[54] D.G. .Hunt, D.K. .Ross, Optical vibrations of hydrogen in metals, J. Less Common Met. 49 (1976) 169–191, https://doi.org/10.1016/0022-5088(76)90034-5

[55] J.-J. Didisheim, K. Yvon, P. Fischer, W. Hälg, L. Schlapbach, Neutron diffraction evidence for a structural phase transformation in stoichiometric LaD_3 at 230 K, Phys. Lett. 78A (1980) 111–114, https://doi.org/10.1016/0375-9601(80)90824-5

[56] T.J. Udovic, J.J. Rush, Q. Huang, I.S. Anderson, Neutron scattering studies of the structure and dynamics of rare-earth hydrides and deuterides, J. Alloy. Compd. 253–254 (1997) 241–247, https://doi.org/10.1016/S0925-8388(96)02885-X

[57] C.E. Holley Jr., R.N.R. Mulford, F.H. Ellinger, W.C. Koehler, W.H. Zachariasen, The crystal structure of some rare earth hydrides, J. Phys. Chem. 59 (1955) 1226–1228, https://doi.org/10.1021/j150534a010

[58] P. Vorderwisch, S. Hautecler, J. Eckert, Neutron spectroscopy of localized modes in $CeD_{2-x}H_y$, J. Alloy. Compd. 253–254 (1997) 252–254, https://doi.org/10.1016/S0925-8388(96)03084-8

[59] J. Schefer, P. Fischer, W. Halg, J. Osterwalder, L. Schlapbach, J.D. Jorgensen, Variation of the order-disorder phase transition and of the magnetic ordering with deuterium concentration in CeD_x ($2.2 \le x \le 3.0$), J. Phys. C Solid State Phys. 17 (1984) 1575–1583, https://doi.org/10.1088/0022-3719/17/9/014

[60] P. Vorderwisch, S. Hautecler, Inelastic neutron scattering by cerium hydrides I. Experimental, Phys. Stat. Sol. b 64 (1974) 495–501, https://doi.org/10.1002/pssb.2220640210

[61] P. Vajda, J.N. Daou, Rare Earths-Hydrogen, in: F.A. Lewis, A. Aladjem (Eds.), Hydrogen Metal Systems I, Switzerland: Trans Tech Publications, Solid State Phenomena 49–50, 1996, 71–158, https://doi.org/10.4028/www.scientific.net/SSP.49-50.71.

[62] P.P. Parshin, M.G. Zemlyanov, M.E. Kost, A.Y. Rumyantsev, N.A. Chernoplekov, Vibration-spectra of hydrogen in Pr-trihydrides and Nd-trihydrides, Fizika Tverdogo Tela 22 (1980) 472–476, WOS:A1980JK19000028 (in Russian) [Engl. transl.: Sov. Phys. Solid State 22 (1980) 275].

[63] T.J. Udovic, J.J. Rush, I.S. Anderson, Neutron spectroscopic comparison of β-phase rare earth hydrides, J. Alloy. Compd. 231 (1995) 138–143, https://doi.org/10.1016/0925-8388(95)01788-7

[64] B. Lebech, N.H. Andersen, S. Steenstrup, A.S. Pedersen, Neutron diffraction studies of ytterbium dihydride: the crystal structure at 300 K, Acta Cryst. C 39 (1983) 1475–1480, https://doi.org/10.1107/S010827018300894X

[65] A.J. Maeland, Vibration spectra of the orthorhombic alkaline-earth hydrides by the inelastic scattering of cold neutrons and by infrared transmission measurements, J. Chem. Phys. 52 (1970) 3952–3956, https://doi.org/10.1063/1.1673594

[66] M.A. Kuzovnikov, V.E. Antonov, A.S. Ivanov, T. Hansen, S. Savvin, V.I. Kulakov, M. Tkacz, A.I. Kolesnikov, Neutron scattering study of tantalum monohydride and monodeuteride, Int. J. Hydrog. Energy 46 (2021) 20630–20639, https://doi.org/10.1016/j.ijhydene.2021.03.149

[67] M.A. Kuzovnikov, V.E. Antonov, A.S. Ivanov, T. Hansen, S. Savvin, V.I. Kulakov, M. Tkacz, A.I. Kolesnikov, V.M. Gurev, Neutron scattering study of tantalum dihydride, Phys. Rev. B 102 (2020) 024113, https://doi.org/10.1103/PhysRevB.102.024113

[68] V.E. Antonov, V.K. Fedotov, A.I. Harkunov, A.I. Kolesnikov, N.I. Novokhatskaya, G. Grosse, F.E. Wagner, T. Hansen, A.S. Ivanov, Neutron spectroscopy of $ReH_{0.09}$, Phys. Rev. B 64 (2001) 184302, https://doi.org/10.1103/PhysRevB.64.184302

[69] M. Dietrich, W. Reichardt, H. Rietschel, Phonon densities of states of the thorium hydrides, Solid State Commun. 21 (1977) 603–605, https://doi.org/10.1016/0038-1098(77)90043-6

[70] M.H. Mueller, R.A. Beyerlein, J.D. Jorgensen, T.O. Brun, C.B. Satterthwaite, R. Caton, Structure of Th_4D_{15} from measurements at the Argonne ZING-P pulsed

neutron source, J. Appl. Cryst. 10 (1977) 79–83, https://doi.org/10.1107/S0021889877012953
[71] W. Bartscher, A. Boeuf, R. Caciuffo, J.M. Fournier, W.F. Kuhs, J. Rebizant, F. Rustichelli, Neutron diffraction study of β-UD_3 and β-UH_3, Solid State Commun. 53 (1985) 423–426, https://doi.org/10.1016/0038-1098(85)91000-2
[72] I.Y. Glagolenko, K.P. Carney, S. Kern, E.A. Goremychkin, T.J. Udovic, J.R.D. Copley, J.C. Cook, Quantitative analysis of UH_3 in U metal and UO_2 matrices by neutron vibrational spectroscopy, Appl. Phys. A 74 (2002) S1397–S1399, https://doi.org/10.1007/s003390201808
[73] J.A. Goldstone, P. Vorderwisch, B. Cort, A.C. Lawson, J.W. Ward, Optical vibration frequency distributions in neptunium hydride and deuteride, Z. Phys. Chem. 164 (1989) 1107–1112, https://doi.org/10.1524/zpch.1989.164.Part_1.1107
[74] M. Hirscher, V.A. Yartys, M. Baricco, J.B. von Colbe, D. Blanchard, R.C. Bowman Jr, D.P. Broom, C.E. Buckley, F. Chang, P. Chen, Y.W. Cho, J.-C. Crivello, F. Cuevas, W.I.F. David, P.E. de Jongh, R.V. Denys, M. Dornheim, M. Felderhoff, Y. Filinchuk, G.E. Froudakis, D.M. Grant, E.M. Gray, B.C. Hauback, T. He, T.D. Humphries, T.R. Jensen, S. Kim, Y. Kojima, M. Latroche, H.-W. Li, M.V. Lototskyy, J.W. Makepeace, K.T. Møller, L. Naheed, P. Ngene, D. Noréus, M.M. Nygård, Shin-ichi Orimo, M. Paskevicius, L. Pasquini, D.B. Ravnsbæk, M.V. Sofianos, T.J. Udovic, T. Vegge, G.S. Walker, C.J. Webb, C. Weidenthaler, C. Zlotea, Materials for hydrogen-based energy storage — past, recent progress and future outlook, J. Alloy. Compd. 827 (2020) 153548, https://doi.org/10.1016/j.jallcom.2019.153548
[75] T. Springer, Investigation of vibrations in metal hydrides by neutron spectrosciopy, in: G. Alefeld, J.Völkl (Eds.), Hydrogen in Metals I, Springer-Verlag, Berlin, 1978, pp. 75–100.
[76] D.K. Ross, Neutron scattering studies of metal hydrogen systems, in: H. Wipf (Ed.), Hydrogen in Metals III, Springer-Verlag, Berlin, 1997, pp. 153–214.
[77] Y. Fukai, The Metal-Hydrogen System, second ed., Springer-Verlag, Berlin, 2005.
[78] V.E. Antonov, A.I. Kolesnikov, Yu.E. Markushkin, A.V. Palnichenko, Y. Ren, M.K. Sakharov, Heat capacity of α-AlH_3 and α-AlD_3 at temperatures up to 1000 K, J. Phys. Condens. Matter 20 (2008) 275204, https://doi.org/10.1088/0953-8984/20/27/275204
[79] M.K. Sakharov, V.E. Antonov, Y.E. Markushkin, A.I. Kolesnikov, I. Natkaniec, The diagram of phase transformations and phase equilibria in the Al–H system at pressures up to 90 kbar, Abstracts of AIRAPT-21, Catania, Italy, September 17–21, 2007, pp. 202–203.
[80] M.W. Chase Jr., NIST–JANAF themochemical tables, fourth edition, J. Phys. Chem. Ref. Data Monogr. 9 (1998) 1–1951.
[81] L.G. Khvostantsev, V.N. Slesarev, V.V. Brazhkin, Toroid type high-pressure device: history and prospects, High Press. Res. 24 (2004) 371–383, https://doi.org/10.1080/08957950412331298761
[82] V.E. Antonov, B.M. Bulychev, V.K. Fedotov, D.I. Kapustin, V.I. Kulakov, I.A. Sholin, NH_3BH_3 as an internal hydrogen source for high pressure experiments, Int. J. Hydrog. Energy 42 (2017) 22454–22459, https://doi.org/10.1016/j.ijhydene.2017.03.121
[83] H.G. Schimmel, M.R. Johnson, G.J. Kearley, A.J. Ramirez-Cuesta, J. Huot, F.M. Mulder, The vibrational spectrum of magnesium hydride from inelastic neutron scattering and density functional theory, Mater. Sci. Eng. B 108 (2004) 38–41, https://doi.org/10.1016/j.mseb.2003.10.035
[84] A.I. Kolesnikov, I. Natkaniec, V.E. Antonov, I.T. Belash, V.K. Fedotov, J. Krawczyk, J. Mayer, E.G. Ponyatovsky, Neutron spectroscopy of $MnH_{0.86}$, $NiH_{1.05}$, $PdH_{0.99}$ and harmonic behaviour of their optical phonons, Phys. B 174 (1991) 257–261, https://doi.org/10.1016/0921-4526(91)90616-M
[85] L.D. Landau, E.M. Lifshitz, Statistical Physics Part 1, third ed., Pergamon, Oxford, 1980.
[86] L.E. Storm, The low-temperature specific heat of palladium-hydride and palladium-deuteride, PhD thesis, University of Illinois at Urbana-Champaign, 1980.
[87] D. Ohlendorf, H.G. Severin, E. Wicke, Heat-capacity measurements of pulverized metal-hydrides between 1.5°K and 15°K by means of the Cu-tabletting method, Z. Phys. Chem. N. F. 128 (1981) 137–146, https://doi.org/10.1524/zpch.1981.128.2.137; Thermochimica Acta 49, 1981 11–21, https://doi.org/10.1016/0040–6031(81)85138–6.
[88] J.F. Miller, R.H. Caton, C.B. Satterthwaite, Low-temperature heat-capacity of normal and superconducting thorium hydride and thorium deuteride, Phys. Rev. B 14 (1976) 2795–2800, https://doi.org/10.1103/PhysRevB.14.2795
[89] V.E. Antonov, I.T. Belash, E.G. Ponyatovskii, V.G. Thiessen, V.I. Shiryaev, Magnetization of iron hydride, Phys. Stat. Sol. a 65 (1981) K43–K48, https://doi.org/10.1002/pssa.2210650156
[90] I.T. Belash, B.K. V.Yu. Malyshev, E.G. Ponomarev, A.Y. Ponyatovskii, Sokolov, The magnetization of cobalt hydrides, Fiz. Tverd. Tela 28 (1986) 1317–1323 WOS:A1986C669000006 (in Russian).
[91] E.G. Ponyatovskii, V.E. Antonov, I.T. Belash, Properties of high-pressure phases in metal-hydrogen systems, Uspekhi Fizicheskikh Nauk 137 (1982) 663–705, https://doi.org/10.3367/UFNr.0137.198208c.066 (in Russian) [Engl. transl.: Sov. Phys. Usp. 25 (1982) 596–619, http://dx.doi.org/10.1070/PU1982v025n08ABEH004589].
[92] L. Gamberale, D. Garbelli, G. Piana, Measurement of heat capacity of PdHx, The 9th International Conference on Cold Fusion, Condensed Matter Nuclear Science, 2002, Beijing, China, Tsinghua Univ. Press.
[93] V.E. Antonov, Phase transformations, crystal and magnetic structures of high-pressure hydrides of d-metals, J. Alloy. Compd. 330–332 (2002) 110–116, https://doi.org/10.1016/S0925-8388(01)01532-8
[94] K. Cornell, H. Wipf, V.E. Antonov, T.E. Antonova, A.I. Kolesnikov, E.G. Ponyatovsky, B. Dorner, The inelastic neutron scattering spectrum of dhcp iron hydride, Pol. J. Chem. 71 (1997) 1792–1796 WOS:000071250800016.
[95] V.E. Antonov, V.K. Fedotov, B.A. Gnesin, G. Grosse, A.S. Ivanov, A.I. Kolesnikov, F.E. Wagner, Anisotropy in the inelastic neutron scattering from fcc NiH, Europhys. Lett. 51 (2000) 140–146, https://doi.org/10.1209/epl/i2000-00523-2
[96] B. Dorner, V.E. Antonov, I.T. Belash, E.L. Bokhenkov, E.G. Poniatovsky, L.N. Pronina, High frequency vibrations of H-atoms in transition metals and alloys measured by inelastic neutron scattering, Z. Phys. Chem. 164 (1989) 1079–1082, https://doi.org/10.1524/zpch.1989.164.Part_1.1079
[97] J.J. Rush, J.M. Rowe, D. Richter, Direct determination of the anharmonic vibrational potential for H in Pd, Z. Phys. B 55 (1984) 283–286, https://doi.org/10.1007/BF01304078
[98] C. Elsässer, H. Krimmel, M. Fähnle, S.G. Louie, C.T. Chan, *Ab initio* study of iron and iron hydride: III. Vibrational states of H isotopes in Fe, Cr and Ni, J. Phys. Condens. Matter 10 (1998) 5131–5146, https://doi.org/10.1088/0953-8984/10/23/014
[99] B. Baranowski, K. Bojarski, Formation of chromium hydride from metallic chromium and high pressure gaseous hydrogen, Rocz. Chem. 46 (1972) 525–528.
[100] Y. Fukai, M. Mizutani, Phase diagram and superabundant vacancy formation in Cr-H alloys, Mater. Trans. 43 (2002) 1079–1084, https://doi.org/10.2320/matertrans.43.1079
[101] V.E. Antonov, I.A. Sholin, Proving the contact rules for phase regions: implications to phase diagrams of metal-hydrogen systems, J. Alloy. Compd. 645 (2015) S160–S165, https://doi.org/10.1016/j.jallcom.2015.01.086
[102] B. Dorner, I.T. Belash, E.L. Bokhenkov, E.G. Ponyatovsky, V.E. Antonov, L.N. Pronina, Inelastic incoherent neutron scattering spectra from fcc $NiH_{1.05}$, hcp $CrH_{1.0}$ and hcp $MoH_{1.2}$ at 15 K, Solid State Commun. 69 (1989) 121–124, https://doi.org/10.1016/0038-1098(89)90374-8
[103] M. Tkacz, High pressure studies of the FCC chromium hydride, Pol. J. Chem. 71 (1997) 1735–1741 WOS:000071250800010.
[104] J. Poźniak-Fabrowska, B. Nowak, M. Tkacz, Magnetic properties of cubic and hexagonal chromium hydrides: a comparison of the magnetic susceptibility with the ^{53}Cr NMR Knight shift, J. Alloy. Compd. 322 (2001) 82–88, https://doi.org/10.1016/S0925-8388(01)01266-X
[105] A. Marizy, G. Geneste, P. Loubeyre, B. Guigue, G. Garbarino, Synthesis of bulk chromium hydrides under pressure of up to 120 GPa, Phys. Rev. B 97 (2018) 184103, https://doi.org/10.1103/PhysRevB.97.184103
[106] S. Yu, X. Jia, G. Frapper, D. Li, A.R. Oganov, Q. Zeng, L. Zhang, Pressure-driven formation and stabilization of superconductive chromium hydrides, Sci. Rep. 5 (2015) 17764, https://doi.org/10.1038/srep17764
[107] V.E. Antonov, I.T. Belash, A.I. Kolesnikov, J. Maier, I. Natkaniec, E.G. Ponyatovskii, V.K. Fedotov, Neutron-scattering study of the vibrational-spectrum of manganese hydride, Fizika Tverdogo Tela 33 (1991) 152–157, WOS:A1991FZ03900028 (in Russian) [Engl. transl.: Sov. Phys. Solid State 33 (1991) 87–90].
[108] V.E. Antonov, T.E. Antonova, N.A. Chirin, E.G. Ponyatovsky, M. Baier, F.E. Wagner, *T-P* phase diagram of the Mn-H system at pressures to 4.4 GPa and temperatures to 1000 °C, Scr. Mater. 34 (1996) 1331–1336, https://doi.org/10.1016/1359-6462(95)00656-7
[109] Y. Fukai, T. Haraguchi, H. Shinomiya, K. Mori, Constitution of the Mn-H system at high hydrogen pressures, Scr. Mater. 46 (2002) 679–684, https://doi.org/10.1016/S1359-6462(02)00052-0
[110] Y. Fukai, H. Ishikawa, T. Goto, J. Susaki, T. Yagi, J.L. Soubeyrox, D. Fruchart, High-pressure synthesis and magnetic-properties of cubic manganese hydride, Z. Phys. Chem. 163 (1989) 479–482, https://doi.org/10.1524/zpch.1989.163.Part_2.0479
[111] I.T. Belash, B.K. Ponomarev, V.G. Tissen, N.S. Afonokova, V.S. Shekhtman, E.G. Ponyatovskii, Ferromagnetism in the Mn-H and Mn-D systems, Fiz. Tverd. Tela 20 (1978) 422–427.
[112] A.C. Switendick, Electronic structure of transition metal hydrides, in: Transition Metal Hydrides, R. Bau (Ed.), Adv. Chem. Ser. Vol. 167, ACS, Washington, 1978, pp.264–282.
[113] A.I. Kolesnikov, V.E. Antonov, S.M. Bennington, B. Dorner, V.K. Fedotov, G. Grosse, J.C. Li, S.F. Parker, F.E. Wagner, The vibrational spectrum and giant tunnelling effect of hydrogen dissolved in α-Mn, Physica B 263–264 (1999) 421–423, https://doi.org/10.1016/S0921-4526(98)01401-X
[114] W.L. Mao, W. Sturhahn, D.L. Heinz, H.-K. Mao, J. Shu, R.J. Hemley, Nuclear resonant x-ray scattering of iron hydride at high pressure, Geophys. Res. Lett. 31 (2004) L15618, https://doi.org/10.1029/2004GL020541
[115] E.Y. Tonkov, High Pressure Phase Transformations: A Handbook, Gordon and Breach, Philadelphia, 1992, p. p.
[116] V.E. Antonov, I.T. Belash, E.G. Ponyatovsky, *T-P* phase diagram of the Fe-H system at temperatures to 450 °C and pressures to 6.7 GPa, Scr. Met. 16 (1982) 203–208, https://doi.org/10.1016/0036-9748(82)90387-8
[117] Y. Fukai, K. Mori, H. Shinomiya, The phase diagram and superabundant vacancy formation in Fe–H alloys under high hydrogen pressures, J. Alloy. Compd. 348 (2003) 105–109, https://doi.org/10.1016/S0925-8388(02)00806-X
[118] T. Hiroi, Y. Fukai, K. Mori, The phase diagram and superabundant vacancy formation in Fe–H alloys revisited, J. Alloy. Compd. 404–406 (2005) 252–255, https://doi.org/10.1016/j.jallcom.2005.02.076
[119] V.E. Antonov, V.M. Gurev, V.I. Kulakov, M.A. Kuzovnikov, I.A. Sholin, V.Y. Zuykova, Solubility of deuterium and hydrogen in fcc iron at high pressures and temperatures, Phys. Rev. Mater. 3 (2019) 113604, https://doi.org/10.1103/PhysRevMaterials.00.003600
[120] V.E. Antonov, I.T. Belash, V.F. Degtyareva, D.N. Mogilyansky, B.K. Ponomarev, V. Sh. Shekhtman, Crystal structure and magnetic properties of high-pressure phases in the Fe-H and Fe-Cr-H systems, Int. J. Hydrog. Energy 14 (1989) 371–377, https://doi.org/10.1016/0360-3199(89)90167-5

[121] J.V. Badding, R.J. Hemley, H.K. Mao, High-pressure chemistry of hydrogen in metals: In situ study of iron hydride, Science 253 (1991) 421–424, https://doi.org/10.1126/science.253.5018.421

[122] M. Yamakata, T. Yagi, W. Utsumi, Y. Fukai, In situ x-ray-observation of iron hydride under high-pressure and high-temperature, Proc. Jpn. Acad. 68B, 1992, 172–176, https://doi.org/10.2183/pjab.68.172.

[123] G. Schneider, M. Baier, R. Wordel, F.E. Wagner, V.E. Antonov, E.G. Ponyatovsky, Yu Kopilovskii, E. Makarov, Mössbauer study of hydrides and deuterides of iron and cobalt, J. Less Common Met. 172–174 (1991) 333–342, https://doi.org/10.1016/0022-5088(91)90464-F

[124] C.M. Pépin, A. Dewaele, G. Geneste, P. Loubeyre, M. Mezouar, New iron hydrides under high pressure, Phys. Rev. Lett. 113 (2014) 265504, https://doi.org/10.1103/PhysRevLett.113.265504

[125] C.M. Pépin, G. Geneste, A. Dewaele, M. Mezouar, P. Loubeyre, Synthesis of FeH_5: a layered structure with atomic hydrogen slabs, Science 357 (2017) 382–385, https://doi.org/10.1126/science.aan0961

[126] G.C. Kennedy, R.C. Newton, Solid-liquid and solid-solid phase transitions in some pure metals at high temperatures, in: W. Paul (Ed.), Solids under Pressure, 163–178 McGraw-Hill, New York, 1963, p. p.

[127] I.T. Belash, V.E. Antonov, E.G. Ponyatovskii, System Co-H under hydrogen high-pressure, Dokl. Akad. Nauk SSSR 235, 1977, 128–131, WOS:A1977DN30500033 (in Russian).

[128] Y. Fukai, S. Yokota, J. Yanagawa, The phase diagram and superabundant vacancy formation in Co-H alloys, J. Alloy. Compd. 407 (2006) 16–24, https://doi.org/10.1016/j.jallcom.2005.06.016

[129] V.E. Antonov, I.T. Belash, V.Y. Malyshev, E.G. Ponyatovskii, New high pressure phase in the cobalt-hydrogen system, Doklady Akademii Nauk SSSR 272 (1983) 1147–1150, WOS:A1983RQ31100031 (in Russian).

[130] V.E. Antonov, T.E. Antonova, M. Baier, G. Grosse, F.E. Wagner, On the isomorphous phase transformation in the solid f.c.c. solutions Co-H at high pressures, J. Alloy. Compd. 239 (1996) 198–202, https://doi.org/10.1016/0925-8388(96)02188-3

[131] V.K. Fedotov, V.E. Antonov, T.E. Antonova, E.L. Bokhenkov, B. Dorner, G. Grosse, F.E. Wagner, Atomic ordering in the hcp cobalt hydrides and deuterides, J. Alloy. Compd. 291 (1999) 1–7, https://doi.org/10.1016/S0925-8388(99)00229-7

[132] M.A. Kuzovnikov, M. Tkacz, High pressure studies of cobalt-hydrogen system by X-ray diffraction, J. Alloy. Compd. 650 (2015) 884–886, https://doi.org/10.1016/j.jallcom.2015.08.062

[133] M. Wang, J. Binns, M.-E. Donnelly, M. Peña-Alvarez, P. Dalladay-Simpson, R.T. Howie, High pressure synthesis and stability of cobalt hydrides, J. Chem. Phys. 148 (2018) 144310, https://doi.org/10.1063/1.5026535

[134] M. Peña-Alvarez, B. Li, L.C. Kelsall, J. Binns, P. Dalladay-Simpson, A. Hermann, R.T. Howie, E. Gregoryanz, Synthesis of superconducting cobalt trihydride, J. Phys. Chem. Lett. 11 (2020) 6420–6425, https://doi.org/10.1021/acs.jpclett.0c01807

[135] B. Baranowski, R. Wiśniewski, Formation of nickel hydride from nickel and gaseous hydrogen, Bull. Acad. Pol. Sci. Ser. Sci. Chim. 14 (1966) 273–276.

[136] V.E. Antonov, I.T. Belash, E.G. Poniatovskii, *T-P* phase diagrams of systems Ni-D and Ni-H at temperatures up to 375 °C and pressures up to 20 kbar, Dokl. Akad. Nauk SSSR 233 (1977) 1114–1117, WOS:A1977DF51800030 (in Russian).

[137] Y. Fukai, S. Yamamoto, S. Harada, M. Kanazawa, The phase diagram of the Ni–H system revisited, J. Alloy. Comp. 372 (2004) L4–L5, https://doi.org/10.1016/j.jallcom.2003.09.134

[138] D. Bloch, Contribution a l'etude des propertiètès magnètiques des solids sous pression hydrostatique, Ann. Phys. 1 (1966) 93–125.

[139] V.E. Antonov, I.T. Belash, O.V. Zharikov, A.V. Palnichenko, A study on superconductivities of high pressure phases in the Re-H, Ru-H, Rh-H, and Ni-H systems, Phys. Stat. Sol. b 142 (1987) K155–K159, https://doi.org/10.1002/pssb.2221420246

[140] J. Ying, H. Liu, E. Greenberg, V.B. Prakapenka, V.V. Struzhkin, Synthesis of new nickel hydrides at high pressure, Phys. Rev. Mater. 2 (2018) 085409, https://doi.org/10.1103/PhysRevMaterials.2.085409

[141] J. Binns, M.-E. Donnelly, M. Wang, A. Hermann, E. Gregoryanz, P. Dalladay-Simpson, R.T. Howie, Synthesis of Ni_2H_3 at high temperatures and pressures, Phys. Rev. B 98 (2018) 140101, https://doi.org/10.1103/PhysRevB.98.140101 (R).

[142] I.T. Belash, V.E. Antonov, E.G. Poniatovskii, Obtaining of molybdenum hydride under hydrogen high-pressure, Dokl. Akad. Nauk SSSR 235 (1977) 379–380 WOS:A1977DP66100038 (in Russian).

[143] M.A. Kuzovnikov, H. Meng, M. Tkacz, Nonstoichiometric molybdenum hydride, J. Alloy. Compd. 694 (2017) 51–54, https://doi.org/10.1016/j.jallcom.2016.09.288

[144] Y. Fukai, M. Mizutani, The phase diagram of Mo-H alloys under high hydrogen pressures, Mater. Trans. 44 (2003) 1359–1362, https://doi.org/10.2320/matertrans.44.1359

[145] S.N. Abramov, V.E. Antonov, B.M. Bulychev, V.K. Fedotov, V.I. Kulakov, D.V. Matveev, I.A. Sholin, M. Tkacz, *T-P* phase diagram of the Mo-H system revisited, J. Alloy. Compd. 672 (2016) 623–662, https://doi.org/10.1016/j.jallcom.2016.02.209

[146] X. Feng, J. Zhang, H. Liu, T. Iitaka, K. Yin, H. Wang, High pressure polyhydrides of molybdenum: a first-principles study, Solid State Commun. 239 (2016) 14–19, https://doi.org/10.1016/j.ssc.2016.03.025

[147] V.E. Antonov, I.T. Belash, O.V. Zharikov, A.I. Latynin, A.V. Palnichenko, Superconductivity of molybdenum hydride and deuteride, Fizika Tverdogo Tela 30 (1988) 598–600, WOS:A1988M520200054 (in Russian) [Engl. transl.: Sov. Phys. Solid State 30 (1988) 344–345].

[148] V.E. Antonov, I.T. Belash, V.F. Degtiareva, E.G. Poniatovskii, Production of rhodium hydride under hydrogen high-pressure, Dokl. Akad. Nauk SSSR 239 (1978) 342–343 WOS:A1978EU75900024 (in Russian).

[149] B. Li, Y. Ding, D.Y. Kim, R. Ahuja, G. Zou, H.-K. Mao, Rhodium dihydride (RhH_2) with high volumetric hydrogen density, Proc. Natl. Acad. Sci. U.S.A. 108 (2011) 18618–18621, https://doi.org/10.1073/pnas.1114680108

[150] V.E. Antonov, I.T. Belash, V.Yu. Malyshev, E.G. Ponyatovsky, The solubility of hydrogen in the platinum metals under high pressure, Int. J. Hydrogen Energy 11 (1986) 193–197, http://dx.doi.org/10.1016/0360–3199(86)90083–2 (Reprinted from: Platinum Metals Review 28, 1984, pp.158–163).

[151] M.A. Kuzovnikov, M. Tkacz, Dihydride formation in the palladium-rhodium alloys under high hydrogen pressure, Int. J. Hydrog. Energy 42 (2017) 340–346, https://doi.org/10.1016/j.ijhydene.2016.11.133

[152] D.A. Papaconstantopoulos, E.N. Economou, B.M. Klein, L.L. Boyer, Electronic structure and superconductivity in Pd-Ag-H and Pd-Rh-H alloys, Phys. Rev. B 20 (1979) 177–183, https://doi.org/10.1103/PhysRevB.20.177

[153] E. Wicke, H. Brodowsky, Hydrogen in palladium and palladium alloys, in: G. Alefeld, J. Völkl (Eds.), Hydrogen in Metals II, Springer-Verlag, Berlin, 1978, pp. 73–155.

[154] B. Baranowski, Metal-hydrogen systems at high hydrogen pressures, in: G. Alefeld, J. Völkl (Eds.), Hydrogen in Metals II, Springer-Verlag, Berlin, 1978, pp. 157–200.

[155] M.P. Pitt, E.M. Gray, Tetrahedral occupancy in the Pd-D system observed by *in situ* neutron powder diffraction, Europhys. Lett. 64 (2003) 344–350, https://doi.org/10.1209/epl/i2003-00187-x

[156] K.G. McLennan, E.M. Gray, J.F. Dobson, Deuterium occupation of tetrahedral sites in palladium, Phys. Rev. B 78 (2008) 014104, https://doi.org/10.1103/PhysRevB.78.014104

[157] J.J. Rush, J.M. Rowe, D. Richter, Dynamics of dilute H in β-phase palladium deuteride: a novel mass defect (R), Phys. Rev. B 31 (1985) 6102–6103, https://doi.org/10.1103/PhysRevB.31.6102

[158] K. Brownsberger, M. Ahart, M. Somayazulu, C. Park, S.A. Gramsch, R.J. Hemley, X-ray diffraction, lattice structure, and equation of state of PdH_X, and PdD_X to megabar pressures, J. Phys. Chem. C 121 (2017) 27327–27331, https://doi.org/10.1021/acs.jpcc.7b09290

[159] B. Guigue, G. Geneste, B. Leridon, P. Loubeyre, An x-ray study of palladium hydrides up to 100 GPa: synthesis and isotopic effects, J. Appl. Phys. 127 (2020) 075901, https://doi.org/10.1063/1.5138697

[160] R.J. Miller, T.O. Brun, C.B. Satterthwaite, Magnetic susceptibility of Pd-H and Pd-D at temperatures between 6 and 150 K, Phys. Rev. B 18 (1978) 5054–5059, https://doi.org/10.1103/PhysRevB.18.5054

[161] J.M. Rowe, J.J. Rush, H.G. Smith, M. Mostoller, H.E. Flotow, Lattice dynamics of a single crystal of $PdD_{0.63}$, Phys. Rev. Lett. 33 (1974) 1297–1300, https://doi.org/10.1103/PhysRevLett.33.1297

[162] A. Rahman, K. Sköld, C. Pelizzari, S.K. Sinha, H. Flotow, Phonon spectra of nonstoichiometric palladium hydrides, Phys. Rev. B 14 (1976) 3630–3634, https://doi.org/10.1103/PhysRevB.14.3630

[163] C. Elsässer, K.M. Ho, C.T. Chan, M. Fähnle, Vibrational states for hydrogen in palladium, Phys. Rev. B 44 (1991) 10377–10380, https://doi.org/10.1103/PhysRevB.44.10377

[164] M.A. Kuzovnikov, M. Tkacz, H. Meng, D.I. Kapustin, V.I. Kulakov, High-pressure synthesis of tantalum dihydride, Phys. Rev. B 96 (2017) 134120, https://doi.org/10.1103/PhysRevB.96.134120

[165] A. Ivanov, M. Jimenez-Ruiz, J. Kulda, IN1-LAGRANGE – the new ILL instrument to explore vibration dynamics of complex materials, J. Phys. Conf. Ser. 554 (2014) 012001, https://doi.org/10.1088/1742-6596/554/1/012001

[166] Q. Zhuang, X. Jin, T. Cui, Y. Ma, Q. Lv, Y. Li, H. Zhang, X. Meng, K. Bao, Pressure-stabilized superconductive ionic tantalum hydrides, Inorg. Chem. 56 (2017) 3901–3908, https://doi.org/10.1021/acs.inorgchem.6b02822

[167] J. Ying, X. Li, E. Greenberg, V.B. Prakapenka, H. Liu, V.V. Struzhkin, Synthesis and stability of tantalum hydride at high pressures, Phys. Rev. B 99 (2019) 224504, https://doi.org/10.1103/PhysRevB.99.224504

[168] B. Stritzker, W. Buckel, Superconductivity in the palladium-hydrogen and the palladium-deuterium systems, Z. Phys. 257 (1972) 1–8, https://doi.org/10.1007/BF01398191

[169] T. Skośkiewicz, A.W. Szafranski, W. Bujnowski, B. Baranowski, Isotope effect in the superconducting palladium-hydrogen-deuterium system, J. Phys. C Solid State Phys. 7 (1974) 2670–2676, https://doi.org/10.1088/0022-3719/7/15/015

[170] J. Bardeen, L.N. Cooper, J.R. Schrieffer, Theory of superconductivity, Phys. Rev. 108 (1957) 1175–1204, https://doi.org/10.1103/PhysRev.108.1175

[171] A.P. Drozdov, M.I. Eremets, I.A. Troyan, V. Ksenofontov, S.I. Shylin, Conventional superconductivity at 203 kelvin at high pressures in the sulfur hydride system, Nature 525 (2015) 73–76, https://doi.org/10.1038/nature14964

[172] A.P. Drozdov, P.P. Kong, V.S. Minkov, S.P. Besedin, M.A. Kuzovnikov, S. Mozaffari, L. Balicas, F. Balakirev, D. Graf, V.B. Prakapenka, E. Greenberg, D.A. Knyazev, M. Tkacz, M.I. Eremets, Superconductivity at 250 K in lanthanum hydride under high pressures, Nature 569 (2019) 528–531, https://doi.org/10.1038/s41586-019-1201-8

[173] I.A. Troyan, D.V. Semenok, A.G. Kvashnin, A.V. Sadakov, O.A. Sobolevskiy, V.M. Pudalov, A.G. Ivanova, V.B. Prakapenka, E. Greenberg, A.G. Gavriliuk, I.S. Lyubutin, V.V. Struzhkin, A. Bergara, I. Errea, R. Bianco, M. Calandra, F. Mauri, L. Monacelli, R. Akashi, A.R. Oganov, Anomalous high-temperature superconductivity in YH_6, Adv. Mater. 33 (2021) 2006832, https://doi.org/10.1002/adma.202006832

[174] P.P. Kong, V.S. Minkov, M.A. Kuzovnikov, A.P. Drozdov, S.P. Besedin, S. Mozaffari, L. Balicas, F.F. Balakirev, V.B. Prakapenka, S. Chariton, D.A. Knyazev, E. Greenberg, M.I. Eremets, Superconductivity up to 243 K in the yttrium-

hydrogen system under high pressure, Nat. Commun. 12 (2021) 5075, https://doi.org/10.1038/s41467-021-25372-2
[175] W. Chen, D.V. Semenok, X. Huang, H. Shu, X. Li, D. Duan, T. Cui, A.R. Oganov, High-temperature superconducting phases in cerium superhydride with a T_c up to 115 K below a pressure of 1 megabar, Phys. Rev. Lett. 127 (2021) 117001, https://doi.org/10.1103/PhysRevLett.127.117001
[176] C.B. Satterthwaite, I.L. Toepke, Superconductivity of hydrides and deuterides of Thorium, Phys. Rev. Lett. 25 (11) (1970) 741–743, https://doi.org/10.1103/PhysRevLett.25.741
[177] I.O. Bashkin, V.E. Antonov, E.G. Ponyatovsky, Superconductivity of high-pressure phases in the metal-hydrogen systems, in: A. Narlikar (Ed.), Studies of High Temperature Superconductors, Vol. 45: Cuprates and Some Unconventional Systems, Nova Science Publishers, New York, 2003, pp. 171–241.
[178] I. Errea, M. Calandra, F. Mauri, First-principles theory of anharmonicity and the inverse isotope effect in superconducting palladium-hydride compounds, Phys. Rev. Lett. 111 (2013) 177002, https://doi.org/10.1103/PhysRevLett.111.177002
[179] B. Stritzker, H. Wühl, Superconductivity in metal-hydrogen systems, in: G. Alefeld, J. Völkl (Eds.), Hydrogen in Metals II, Springer-Verlag, Berlin, Heidelberg, New York, 1978, pp. 243–272.
[180] A.I. Kolesnikov, A.M. Balagurov, I.O. Bashkin, A.V. Belushkin, E.G. Ponyatovsky, M. Prager, Neutron scattering studies of ordered gamma-ZrD, J. Phys. Condens. Matter 6 (1994) 8977–8988, https://doi.org/10.1088/0953-8984/6/43/004
[181] T.J. Udovic, Q. Huang, C. Karmonik, J.J. Rush, Structural ordering and dynamics of LaH_{3-x}, J. Alloy. Compd. 293–295 (1999) 113–117, https://doi.org/10.1016/S0925-8388(99)00309-6
[182] G. Zhang, X. Wang, J. Lv, Raman spectroscopy characterization of uranium hydride and deuteride, J. Nucl. Mater. 458 (2015) 376–379, https://doi.org/10.1016/j.jnucmat.2014.12.117
[183] M.G. Zemlyanov, E.G. Brovman, N.A. Chernoplekov, Yu.L. Shitikov. Study of the dynamics of lithium hydride and deuteride in the inelastic scattering of cold neutrons. In: Proceedings of the Symposium on Inelastic Scattering of Neutrons, Bombay (India), 15–19 December 1964, Vol. 2 (IAEA, Vienna, 1965), pp. 431–451 (in Russian).
[184] J.J. Rush, N.F. Berk, A. Magerl, J.M. Rowe, J.L. Provo, Anomalous vibrations of hydrogen isotopes in β-phase vanadium hydride, Phys. Rev. B 37 (13) (1988) 7901–7903, https://doi.org/10.1103/physrevb.37.7901
[185] B.N. Ganguly, High frequency local modes, superconductivity and anomalous isotope effect in PdH(D) systems, Z. Phys. 265 (1973) 433–439, https://doi.org/10.1007/BF01391800
[186] B. Baranowski, M. Tkacz, W. Bujnowski, Determination of absorption-desorption isotherms in metal-hydrogen system in high-pressure region, Rocz. Chem. 49 (1975) 437–439 WOS:A1975W050600025.
[187] V.E. Antonov, A.I. Latynin, M. Tkacz, *T–P* phase diagrams and isotope effects in the Mo-H/D systems, J. Phys. Condens. Matter 16 (2004) 8387–8398, https://doi.org/10.1088/0953-8984/16/46/024
[188] Z. Liao, C. Liu, Y. Zhang, Y. Guo, X. Ke, First-principles study on crystal structures and superconductivity of molybdenum hydrides under high pressure, J. Appl. Phys. 128 (2020) 105901, https://doi.org/10.1063/5.0005873
[189] T. Sato, S. Orimo, Hydrogen vibration in hydrogen storage materials investigated by inelastic neutron scattering, Top. Catal. 64 (2021) 614–621, https://doi.org/10.1007/s11244-021-01421-4
[190] S.F. Parker, Spectroscopy and bonding in ternary metal hydride complexes—potential hydrogen storage media, Coord. Chem. Rev. 254 (2010) 215–234, https://doi.org/10.1016/j.ccr.2009.06.016
[191] X. Zhang, Y. Sun, G. Xia, X. Yu, Light-weight solid-state hydrogen storage materials characterized by neutron scattering, J. Alloy. Compd. 899 (2022) 163254, https://doi.org/10.1016/j.jallcom.2021.163254
[192] S.F. Parker, K.P.J. Williams, T. Smith, M. Bortz, B. Bertheville, K. Yvon, Vibrational spectroscopy of tetrahedral ternary metal hydrides: Mg_2NiH_4, Rb_3ZnH_5 and their deuterides, Phys. Chem. Chem. Phys. 4 (2002) 1732–1737, https://doi.org/10.1039/b109975b
[193] T. Sato, A.J. Ramirez-Cuesta, L. Daemen, Y.-Q. Cheng, K. Tomiyasu, S. Takagia, S. Orimo, Hydrogen release reactions of Al-based complex hydrides enhanced by vibrational dynamics and valences of metal cations, Chem. Commun. 52 (2016) 11807–11810, https://doi.org/10.1039/c6cc05199e
[194] V.A. Yartys, R. Denys, B. Hauback, H. Fjellvåg, I. Bulyk, A. Riabov, Y.M. Kalychak, Short hydrogen–hydrogen separations in novel intermetallic hydrides, $RE_3Ni_3In_3D_4$ (RE=La, Ce and Nd), J. Alloy. Compd. 330 (2002) 132–140, https://doi.org/10.1016/s0925-8388(01)01638-3
[195] R.A. Klein, R. Balderas-Xicohténcatl, J.P. Maehlen, T.J. Udovic, C.M. Brown, R. Delaplane, Y. Cheng, R.V. Denys, A.J. Ramirez-Cuesta, V.A. Yartys, Neutron vibrational spectroscopic evidence for short H···H contacts in the $RNiInH_{1.4;\ 1.6}$ (R = Ce, La) metal hydrides, J. Alloy. Compd. 894 (2022) 162381, https://doi.org/10.1016/j.jallcom.2021.162381
[196] A.I. Kolesnikov, V.E. Antonov, A.M. Balagurov, S. Bennington, M. Prager, J. Tomkinson, Neutron scattering studies of ordered PdCuH and PdAgH prepared under a high hydrogen pressure, High Press. Res. 14 (1995) 81–89, https://doi.org/10.1080/08957959508200906
[197] A.V. Irodova, V.P. Glazkov, V.A. Somenkov, V.E. Antonov, E.G. Ponyatovsky, Hydrogen caused ordering in PdAg alloy, Z. Phys. Chem. 163 (1989) 53–57, https://doi.org/10.1524/zpch.1989.163.Part_1.0053
[198] V.E. Antonov, A.V. Bazhenov, I.O. Bashkin, L.V. Zorina, A.I. Kolesnikov, S.S. Khasanov, V.K. Fedotov, T.N. Fursova, High-pressure hydrofullerites, J. Surface Investigation 14 (2020) 995–1002, https://doi.org/10.1134/S1027451020050237 [Poverkhnost' 10 (2020) 3–11, https://doi.org/10.31857/S1028096020100027 (in Russian)].
[199] A.I. Kolesnikov, V.E. Antonov, I.O. Bashkin, G. Grosse, A.P. Moravsky, E.G. A.Yu. Muzychka, F.E. Ponyatovsky, Wagner, Neutron spectroscopy of C_{60} fullerite hydrogenated under high pressure; evidence for interstitial molecular hydrogen, J. Phys. Condens. Matter 9 (1997) 2831–2838, https://doi.org/10.1088/0953-8984/9/13/022
[200] A.I. Kolesnikov, I.O. Bashkin, V.E. Antonov, D. Colognesi, J. Mayers, A.P. Moravsky, Neutron spectroscopy study of single-walled carbon nanotubes hydrogenated under high pressure, J. Alloy. Compd. 446–447 (2007) 389–392, https://doi.org/10.1016/j.jallcom.2006.11.207
[201] V.E. Antonov, I.O. Bashkin, A.V. Bazhenov, B.M. Bulychev, V.K. Fedotov, T.N. Fursova, A.I. Kolesnikov, V.I. Kulakov, R.V. Lukashev, D.V. Matveev, M.K. Sakharov, Y.M. Shulga, Multilayer graphane synthesized under high hydrogen pressure, Carbon 100 (2016) 465–473, https://doi.org/10.1016/j.carbon.2015.12.051
[202] M.A. Kuzovnikov, M. Tkacz, High-pressure synthesis of novel polyhydrides of Zr and Hf with a Th_4H_{15}-type structure, J. Phys. Chem. C 123 (2019) 30059–30066, https://doi.org/10.1021/acs.jpcc.9b07918
[203] I.A. Kruglov, A.G. Kvashnin, A.F. Goncharov, A.R. Oganov, S. Lobanov, N. Holtgrewe, S. Jiang, V.B. Prakapenka, E. Greenberg, A.V. Yanilkin, Uranium polyhydrides at moderate pressures: prediction, synthesis, and expected superconductivity, Sci. Adv. 4 (2018) eaat9776, https://doi.org/10.1126/sciadv.aat9776
[204] A. Shamp, J. Hooper, E. Zurek, Compressed cesium polyhydrides: Cs^+ sublattices and H_3^- three-connected nets, Inorg. Chem. 51 (2012) 9333–9342, https://doi.org/10.1021/ic301045v
[205] J. Hooper, E. Zurek, Rubidium polyhydrides under pressure: emergence of the linear H_3^- species, Chem. Eur. J. 18 (2012) 5013–5021, https://doi.org/10.1002/chem.201103205